THERMAL MANAGEMENT OF ELECTRONICS CABINET AND EFFECTS OF DIFFERENT FRONT COVER PATTERNS

A THESIS SUBMITTED TO
THE GRADUATE SCHOOL OF NATURAL AND APPLIED SCIENCES
OF
MIDDLE EAST TECHNICAL UNIVERSITY

BY

YANKI ÇOBANOĞLU

IN PARTIAL FULFILLMENT OF THE REQUIREMENTS
FOR
THE DEGREE OF MASTER OF SCIENCE
IN
MECHANICAL ENGINEERING

OCTOBER 2019

Approval of the thesis:

THERMAL MANAGEMENT OF ELECTRONICS CABINET AND EFFECTS OF DIFFERENT FRONT COVER PATTERNS

submitted by **YANKI ÇOBANOĞLU** in partial fulfillment of the requirements for the degree of **Master of Science in Mechanical Engineering Department, Middle East Technical University** by,

Prof. Dr. Halil Kalıpçılar
Dean, Graduate School of **Natural and Applied Sciences** _____

Prof. Dr. M. A. Sahir Arıkan
Head of Department, **Mechanical Engineering** _____

Prof. Dr. İlker Tarı
Supervisor, **Mechanical Engineering, METU** _____

Prof. Dr. Derek K. Baker
Co-Supervisor, **Mechanical Engineering, METU** _____

Examining Committee Members:

Prof. Dr. Tuba Okutucu Özyurt
Mechanical Engineering, METU _____

Prof. Dr. İlker Tarı
Mechanical Engineering, METU _____

Assist. Prof. Dr. Özgür Bayer
Mechanical Engineering, METU _____

Prof. Dr. Murat Köksal
Mechanical Engineering, Hacettepe University _____

Prof. Dr. Cemil Kocar
Nuclear Engineering, Hacettepe University _____

Date: 16.10.2019

I hereby declare that all information in this document has been obtained and presented in accordance with academic rules and ethical conduct. I also declare that, as required by these rules and conduct, I have fully cited and referenced all material and results that are not original to this work.

Name, Surname: Yankı Çobanoğlu

Signature:

ABSTRACT

THERMAL MANAGEMENT OF ELECTRONICS CABINET AND EFFECTS OF DIFFERENT FRONT COVER PATTERNS

Çobanoğlu, Yankı
Master of Science, Mechanical Engineering
Supervisor: Prof. Dr. İlker Tarı
Co-Supervisor: Prof. Dr. Derek K. Baker

October 2019, 110 pages

An electronics cabinet populated with different components such as workstations, uninterrupted power supply, etc. is experimentally and numerically investigated. Experimental temperature measurements were taken on different locations surrounding the components using type-K thermocouples and a data logger over a period of 8 hours in which the cabinet was in steady-state. These measurements were then used to validate the numerical model created in commercially available computational fluid dynamics software ANSYS Icepak. First, the model for the Workstation – 1, one of the components inside the cabinet, is presented, since most of the information on its thermal behavior is available. Mesh independence analysis were done, and conservation of mass and energy were checked. Next, whole cabinet was modeled which consists of other components and rack frame within a domain of the size of a room. Steady-state Navier-Stokes equations were solved along with k-ε turbulence equations with variable material properties to account for natural convection effects. A grid-independent solution is obtained and validated using experimental measurements. The validated model used for investigating different front cover patterns with different openness ratios and solutions to prevent limit excess. Results show that blanking panels are viable solutions to prevent leakages,

85% open front cover can be used whereas 25% cannot be, and variable free-area ratio cover can be used only together with a blanking panel that prevents leakage from PDU outlet.

Keywords: Electronics Cabinet, Thermal Management, Computational Fluid Dynamics

ÖZ

ELEKTRONİK KABİNLERİNİN ISIL YÖNETİMİ VE FARKLI ÖN KAPAK MODELLERİNİN ETKİSİ

Çobanoğlu, Yankı
Yüksek Lisans, Makina Mühendisliği
Tez Danışmanı: Prof. Dr. İlker Tarı
Ortak Tez Danışmanı: Prof. Dr. Derek K. Baker

Ekim 2019, 110 sayfa

İş istasyonu, kesintisiz güç kaynağı vb. bileşenlerden oluşan bir elektronik kabinin deneysel ve hesaplamalı analizi yapılmıştır. Deneysel veriler, bileşenlerin etrafındaki farklı noktalardan, K-tipi termokupllarla, kabinin denge durumunda olduğu 8 saat boyunca toplanmış ve bu veri hesaplamalı analizin doğrulanmasında kullanılmıştır. Hesaplamalı analiz, ANSYS Icepak adlı ticari hesaplamalı akışkanlar dinamiği yazılımında yapılmıştır. Öncelikle, İş istasyonu – 1 adlı bileşen modellenmiştir. Bunun için, bileşen içinde bulunan fan, ısı kuyusu, işlemci gibi parçalar, ısıl özellikleri de göz onunda bulundurularak modellenmiştir. Sayısal ağdan bağımsız bir çözüm elde edilmiş, ve kütle ve enerjinin korunumu yasaları kontrol edilmiştir. İçindeki tüm bileşenlerle birlikte bütün kabin, ve bir oda büyüklüğündeki etrafı modellenmiştir. Navier-Stokes denklemleri denge durumunda ve k-ε türbülans denklemleriyle birlikte, doğal konveksiyon etkilerini de açıklamak için, değişken materyal özellikleriyle çözülmüştür. Sayısal ağdan bağımsız bir sonuç elde edilmiş, ve bu model değişik ön kapak desenlerinin etkilerinin incelenmesinde kullanılmıştır. Sonuçlar incelendiğinde, %25 açıklığa sahip ön kapağın sıcaklık sınırlarını aştığı ve dolayısıyla kullanılamayacağı, %85 açıklığa sahip ön kapağın ise sınırları aşmadığı ve dolayısıyla kullanılabileceği, boşluk panellerinin ısı sızıntılarını önlemede başarılı oldukları, ve

değişken açıklığa sahip ön kapağın ancak bir boşluk paneliyle birlikte kullanılabileceği görülmüştür.

Anahtar Kelimeler: Elektronik Kabini, Isıl Yönetim, Hesaplamalı Akışkanlar Dinamiği

To my family…

ACKNOWLEDGMENTS

I would like to thank my advisor Prof. İlker Tarı for his guidance and wisdom throughout my graduate years. I would also like to thank my co-advisor Prof. Derek K. Baker who was always helpful and patient with me. I am grateful for the valuable feedback of the jury members of my thesis defense.

I would like to thank my colleagues at Philips Healthcare for contributing to my professional development and career.

I would also like to thank my family and friends for supporting me in every way.

Last but not least, I would like to thank my love, Dilge, for being there for me, believing in me and making me a better person.

TABLE OF CONTENTS

APPENDICES

LIST OF TABLES

TABLES

LIST OF FIGURES

FIGURES

LIST OF ABBREVIATIONS

ABBREVIATIONS

CFD	Computational Fluid Dynamics
CFM	Cubic Feet Per Minute
CPU	Central Processing Unit
GPU	Graphics Processing Unit
HDD	Hard Disk Drive
PCIe	Peripheral Component Interconnect Express
PDU	Power Distribution Unit
PIV	Particle Image Velocimetry
RAM	Random Access Memory
RPM	Revolutions Per Minute
SSD	Solid State Drive
SIMPLE	Semi-Implicit Method for Pressure Linked Equations
UPS	Uninterruptible Power Source
WS	Workstation

LIST OF SYMBOLS

SYMBOLS

A	Free-area ratio
α	Thermal diffusivity
β	Coefficient of volumetric expansion
c	Centroid
C	Turbulence model constant
C_p	Specific heat capacity
$\vec{f}$	Normal vector
$\vec{F}$	External body forces
$\vec{g}$	Gravitational acceleration
G	Generation of turbulence kinetic energy
Gr	Grashof number
h	Sensible enthalpy
I	Unit tensor
I_c	Pressure loss coefficient
k	Thermal conductivity
L	Characteristic length
m	Mass flow rate
μ	Dynamic Viscosity

p	Pressure
Pr	Prandtl number
ρ	Density
Q	Volumetric flow rate
$\dot{Q}_{gen}$	Heat generation
Re	Reynolds number
S_h	Volumetric heat source
σ	Turbulent Prandtl number
T	Temperature
t	Time
τ	Stress tensor
θ_t	Dimensionless temperature
$\vec{v}$	Velocity

CHAPTER 1

INTRODUCTION

1.1. Motivation

Thermal management of electronic components and cabinets, or “racks”, that house these components has become an important issue with the ever-increasing heat dissipation of electronic products. This issue mainly emanates from the increasing need for data processing and storage in the age of digitalization. This means not only individual electronic products can dissipate higher levels of heat thanks to the miniaturization of semiconductors, but also racks housing these products have higher heat density. This situation may lead to hotspots inside the rack which in turn may lead to poor performance, failure or decreased product lifetime. These hotspots occur as heat dissipated by an electronic component affects one another and causes to heat build-up. To prevent such a scenario, precautions must be taken to ensure that all electronic products inside the rack stay below their temperature limits. One such precaution is to make sure that outflow from electronics carrying heat does not affect other components. Therefore, rack cooling both on electronics-level and rack-level plays an important role.

On electronics-level, heat-generating components are Central Processing Unit (CPU), Graphics Processing Unit (GPU), Random Access Memory (RAM), Hard Disk Drive (HDD) and other media such as power supply, miscellaneous cards, etc. The long-established method for cooling such components is forced convection air-cooling using fans, heat-sinks, heat pipes, etc. Other cooling methods are also used such as water-cooling, two-phase cooling, etc. which have different benefits and drawbacks.

On rack-level, every component inside the rack and how they are placed plays an important role in temperature variation throughout the rack. Common scenarios that

lead to failure of one or more components are blockage of hot airflow coming out of a component, placement of components with higher heat dissipation close to each other, etc. These cases may lead to hotspots with temperatures higher than the requirement of a component inside the rack, leading to failure of the component.

One method used in thermal management of electronics racks is Computational Fluid Dynamics, or CFD. In a CFD analysis, governing equations of fluid flow and heat transfer, namely conservation of mass, momentum, and energy equations, are solved by numerical methods.

In this thesis, an electronics cabinet housing a Power Dissipation Unit (PDU), an Uninterruptible Power Supply (UPS) with a controller and battery, two computers (or workstations), an ethernet switch and four custom-made electronic components for different processes is investigated. The cabinet is a 19-inch (referring to the width of the front panel of each component) industry-standard server rack that is 42 U tall, where 1 U, or 1 rack unit, is 44.5 mm. A front view of the cabinet with the units inside can be found in Figure 1.1.

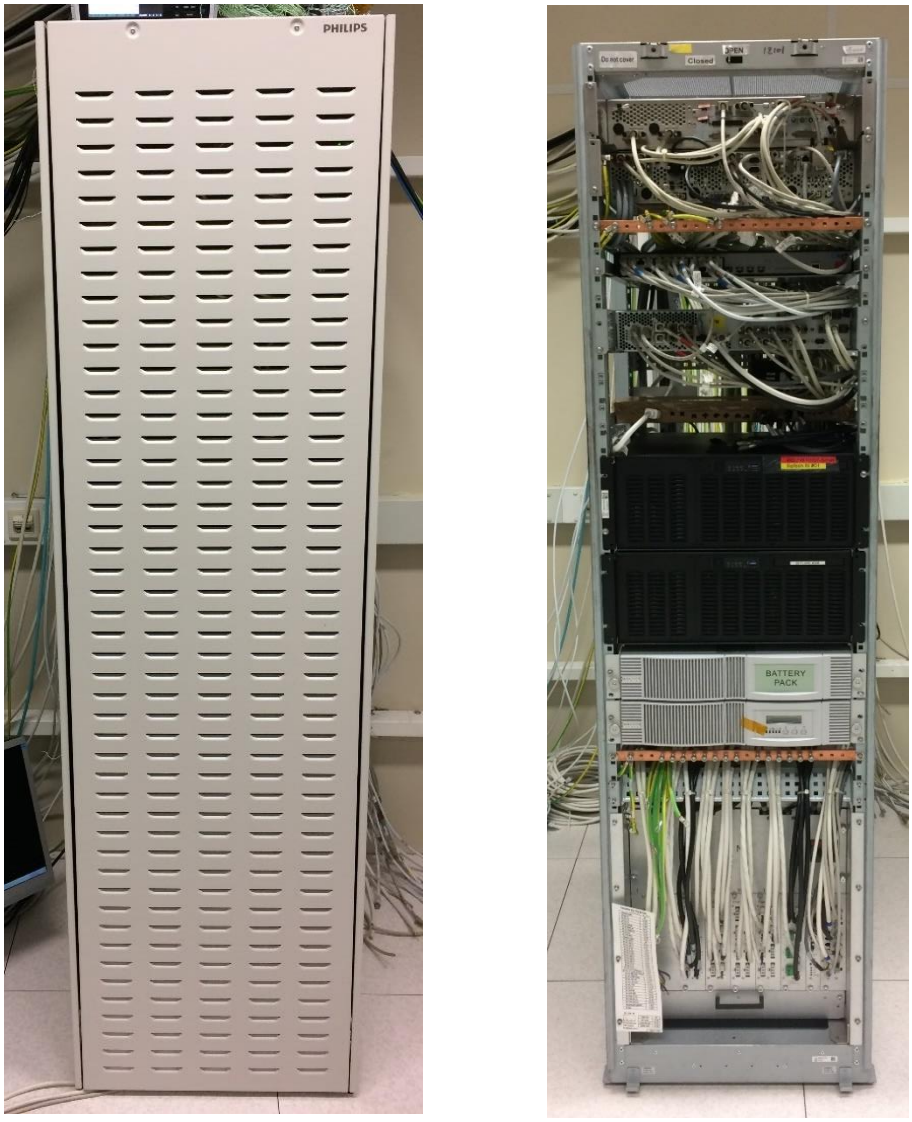

Figure 1.1. Front-view of electronics cabinet with and without a front cover

This cabinet is the part of various X-ray machines manufactured by Philips Healthcare. Every component inside it has a temperature limit for healthy operation. Although components are individually tested to check whether they operate below this limit, they also need to be tested inside the rack to make sure they are still below the limit with all the other heat-dissipating components. Also, adding a front cover to the cabinet significantly alters the airflow and temperatures inside it. Therefore, different

front cover opening ratios should be tested, too. For this purpose, experimental temperature measurements are done inside and also outside of the rack.

Then, a numerical model is created to better understand the temperature distribution and airflow inside and outside. The first numerical model is created without a front cover to observe the effects of having one. This model is validated using the experimental measurements. Building upon this base model, different front cover patterns with openness ratios of 25% and 85% and their effects are analyzed.

To summarize, the objective of this thesis is to first experimentally analyze the cabinet without a front cover to see whether all the components comply with their corresponding temperature limits, and then numerically model it to see the effects of having a front cover and re-check the temperature compliance. Lastly, a theoretical front cover model is proposed that has variable free-area ratio depending on the velocity component normal to the cover plane.

This thesis comprises of 6 chapters. In the first chapter, an introduction to the subject and description of the system in question are given along with the literature survey. The second chapter presents the experimental measurements done on the cabinet. In the third chapter, details of Workstation – 1, one of the components inside the cabinet, are given. The fourth chapter presents the details of the numerical model created for the whole cabinet. In the fifth chapter, different cover patterns are analyzed and compared. The thesis ends with a discussion of the results.

1.2. Literature Survey

Most of the rack-cooling studies in the literature are done on data-centers, a room that contains multiple racks full of servers, motivated by the fact that data-centers consume significant amounts of electricity. These studies can be divided into different categories depending on their length-scale, ranging from chip-level to room-level, or on their preferred method of analysis, whether experimental or numerical or both. A similarity between these studies and current study can be drawn, since both deal with similar geometries and physical phenomena, such as heat dissipation due to electronic

components and thermal management of racks housing them. However, studies that include more than one rack in the same room are out of the scope of this thesis. Therefore, only directly relevant parts of these studies are presented.

Rack cooling studies can be divided into three different length scales, which are server-level, rack-level and room-level. Although there are multi-scale studies in the literature, to the authors knowledge, there are no studies that includes chip-level modelling of servers together with room-level modelling of the whole cabinet, without simplifying the geometries of servers, or workstations. This thesis concerns with all the length scales, as from the chip of a workstation to the walls of a room are all modeled. Therefore, studies concerning different length scales are presented.

Another categorization of the literature can be made according to the cooling method chosen. Liquid-cooling and two-phase cooling solutions are omitted since they are out of scope of this study. Therefore, only air-cooling methods are presented. One such method of cooling is using a Computer Room Air Conditioning unit, or CRAC. In this method, an air conditioning unit is used to monitor and regulate the temperature and humidity inside the room by circulating hot and cold air through. This method is not suitable for this study since it needs an under-floor plenum, a space underneath the cabinet floor, to circulate cold air. The rooms in which cabinet under investigation is situated does not have such a space or raised floor. Therefore, in this study, no standalone cooling unit is deployed, and cooling is provided only by the fans of units themselves. To the authors knowledge, there are no studies that investigate the usage of individual fans as only method of cooling in an electronics rack.

Lastly, geometries and heat dissipations of components inside the cabinet differ from those of studies in literature. As mentioned, data-centers consume large amounts of energy; therefore, a lot of studies are present focusing on optimization of energy consumption through geometric standardization of components. This means that most of the studies in the literature investigate racks populated by the same or similar components regarding their geometries and heat dissipations. However, this study

investigates a cabinet that is populated by different components; therefore, different geometries and heat dissipations.

Gao et al. (2015) investigated the airflow inside a typical datacenter and optimized it. They used CFD simulations to do so and validated their base model with measurements that are taken from an actual data-center. To optimize the airflow pattern, they investigated three more cases with different measures, that are using blanking partitions to block airflow, adding vertical partitions to prevent the mixture of hot and cold air and partly enclosing certain areas. They found that measures taken prevented hot and cold air mixing; therefore, lower inlet temperatures.

Nelson (2007) developed a simplified compact model of an electronics enclosure based on server simulators that had variable heat dissipation and airflow. Since the system contains varying length-scales, some of the complicated geometries inside the server simulators, such as fans, grilles, and heat sinks, were simplified as shown in Figure 1.2. Fan performance curves and pressure-drop characteristics of grilles and heat sinks were obtained via experimental analysis by measuring temperatures and velocities using grids of thermocouples and Particle Image Velocimetry (PIV), respectively. These values and relationships then were used as inputs for the compact CFD model developed. Experimental measurements were used to validate the model, although some discrepancies were present for certain configurations of heat load and airflow rate. Possible reasons for these discrepancies were presented. Results show that, even though some physical simplifications may lead to discrepancies, once these are resolved, compact server models are viable options for rack-level studies. Also, this study shows that fans should be modeled as circular faces rather than square ones, and with a hub, for realistic results, as the author compares these different cases. Therefore, in this study, fans are modeled as circular fans with a hub.

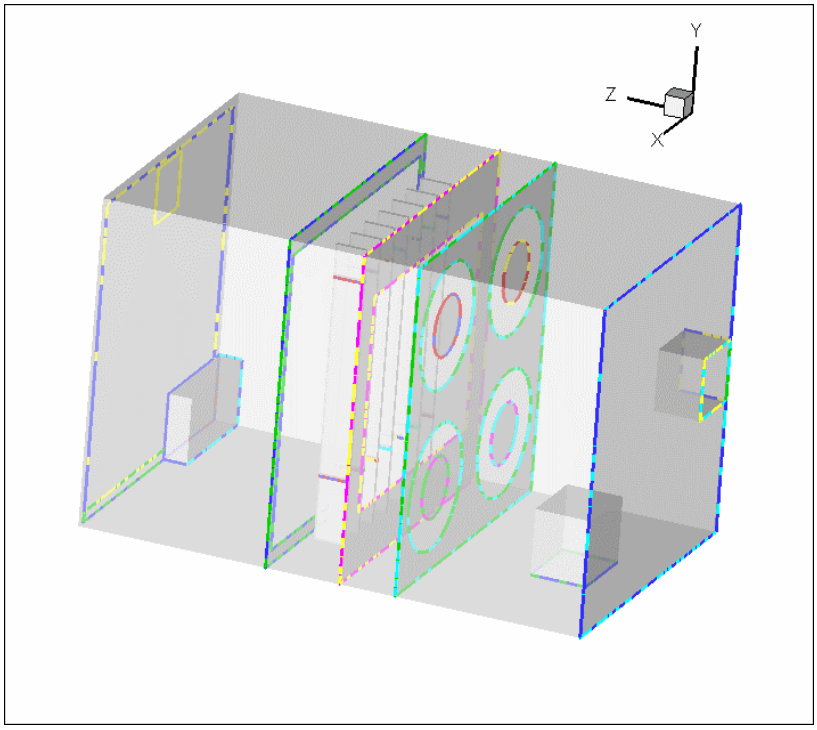

Figure 1.2. Compact model of a single server simulator. Adapted from Nelson (2007).

Zhang et al. (2008) investigated the effect of rack detail on the numerical results of a data-center. Their models ranged from a simple black box to very detailed rack and component representation, as shown in Figure 1.3. Temperature and airflow measurements were done on a test rack using server simulators. For the numerical part, they used commercial CFD software Flovent and compared different turbulence models. Furthermore, they compared measured data with CFD models of varying detail. Their results show that in certain applications where local cooling, in which smaller air conditioning units are deployed near the racks, is dominant over raised-floor cooling, rack detail has a considerable effect on the numerical results.

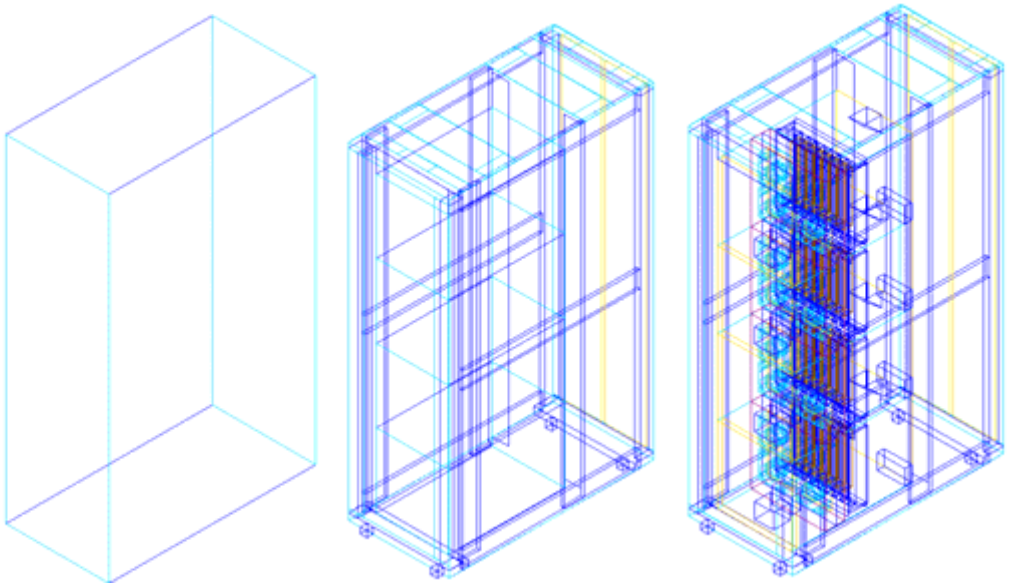

Figure 1.3. Different levels of rack detail. Adapted from Zhang et al. (2008).

Radmehr et al. (2007) analyzed the airflow distribution across a server rack. Their primary focus was on high-velocity vertical jet occurring in front of the rack, discharged from perforated tiles (which is a cooling method for data-centers in which cold air flows through the floor with perforated tiles and goes through the rack to cool it down), and its effect on airflow taken by the servers at various heights along the rack. They modeled airflow through the rack using commercial CFD software COMPACT. Two cases were studied; in the first case, a server rack from a row of racks was considered with symmetrical boundary conditions, and in the second case, a single server rack alone in a room was considered with asymmetrical boundary conditions. Both cases are shown in Figure 1.4. Their server models included fans and flow resistances. Results show that Case – 1 is more critical regarding the airflow drop, and in Case – 1, high-velocity jet leads to a 15% reduction in airflow for bottom servers, which experience the highest drop.

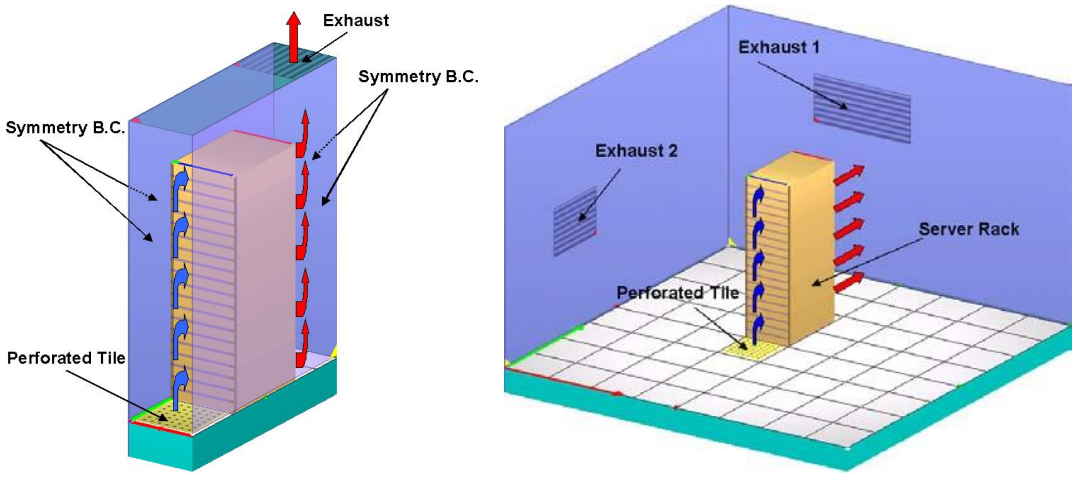

Figure 1.4. Case-1 and Case-2, respectively. Adapted from Radmehr et al. (2007).

Tan et al. (2007) studied airflow and heat transfer interaction of servers and racks. They used Icepak for numerical modeling of servers and rack, separately. For servers, they included fans and grilles and distributed the heat load throughout the volume of the server. The mass flow rate through the server was determined by examining the pressure profiles at the inlets and outlets. This mass flow rate was then used as input for the rack model. For the rack, the model included servers as hollow blocks with recirculating openings to ensure mass flow continuity. Utilizing an iterative scheme, they coupled two models by extracting pressure data from the rack model and substituting back into the server model until two models are converged. They validated their model with experimental temperature measurements. Their results show that decoupling of server and rack models, which leads to a lesser computational expense and compatible length scales, is possible.

Dang et al. (2017) proposed a rack cooling system that has a rear door with a heat pipe and a novel inner duct for airflow management. They numerically modeled the rack with four servers that only have CPUs and axial fans, as shown in Figure 1.5. Geometric model, mesh and server detail can be seen in Figure 1.6. In their model, they set the convective heat transfer coefficient for outer surfaces of servers to 25 $W/(m^2 \cdot K)$, which is an important detail for this study. The numerical model was

validated with experimental temperature and velocity measurements and good agreement between the two was shown. They investigated the effect of total rack heating power, chilled air temperature and rack fan pressure on CPU temperatures, and effect of the inner duct on temperature distribution inside the rack. Results show that the proposed inner duct decreases the air temperature inside the rack as well as removing some hotspots, and heat pipe can transfer more heat with increasing total rack heating power.

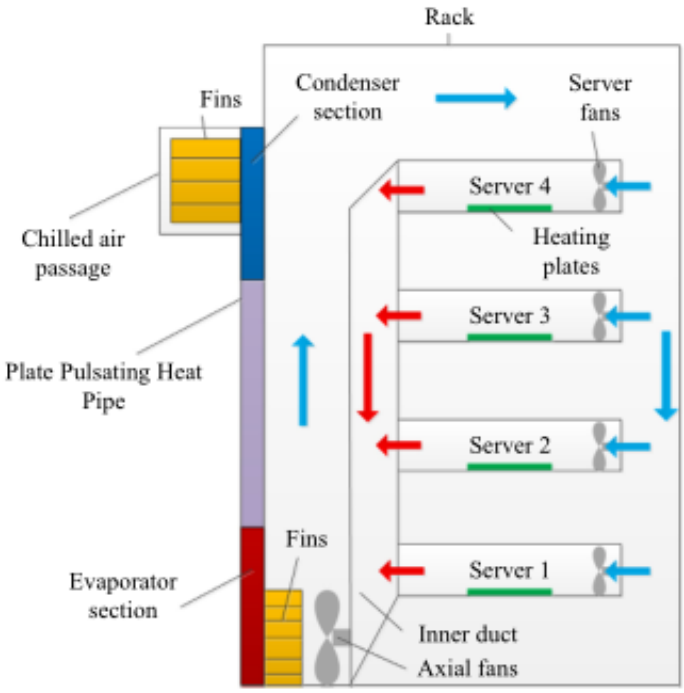

Figure 1.5. Side view of the rack. Adapted from Dang et al. (2017).

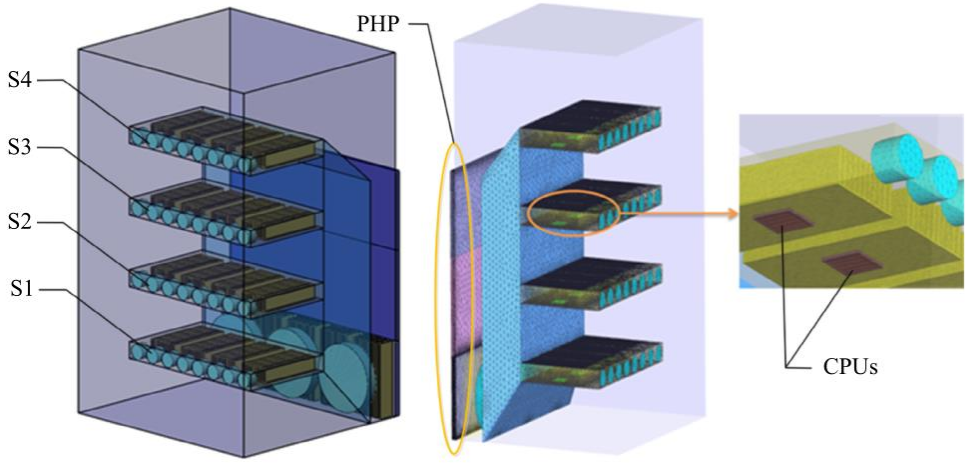

Figure 1.6. Geometric model, mesh and server detail, respectively. Adapted from Dang et al. (2017).

Rambo & Joshi (2005) studied a data processing cabinet stacked with 1 U and "blade servers", meaning a series of vertically stacked servers. Their focus was on the arrangement of these servers inside the cabinet and its effect on system-level cooling. They investigated six configurations with different server placements inside the cabinet, changing the place of blade servers and their arrangement relative to each other. They developed CFD models of both servers using Fluent. Server models were simplified to provide temperature rise and flow resistance with only CPUs, fans and screens or vents being modeled. Rest of the components such as RAMs, power supply, etc. are modeled as solid objects that block airflow. An example of 1 U server model is shown in Figure 1.7. Results show that an arrangement that spreads out high-powered blade servers had the best thermal performance and an arrangement that puts them together in the middle section of the cabinet has the worst thermal performance.

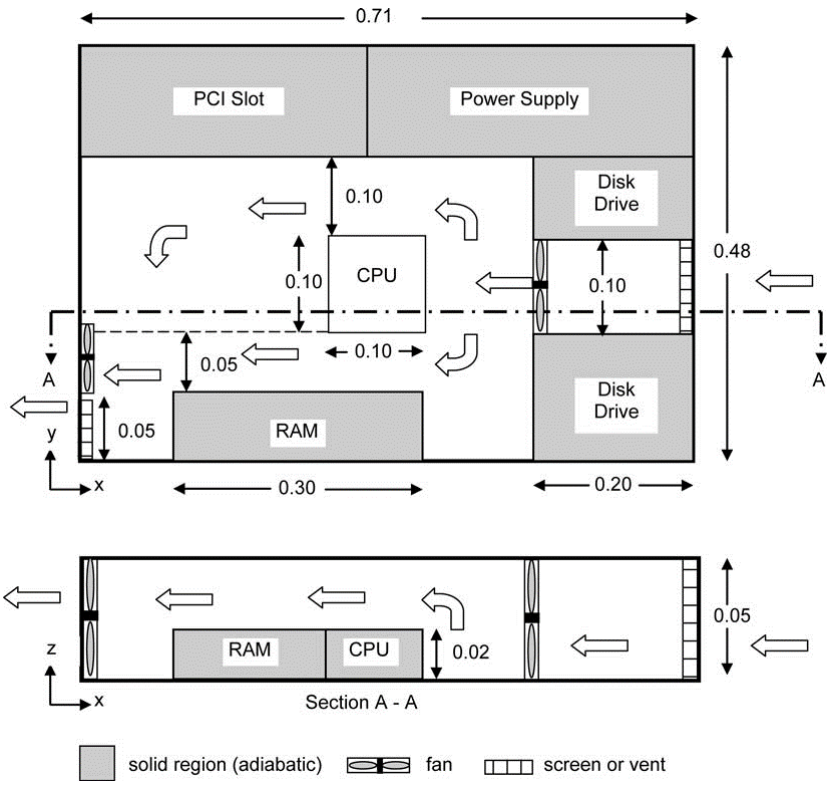

Figure 1.7. 1U server model. Adapted from Rambo & Joshi (2005).

Choi et al. (2007) developed a CFD-based tool called ThermoStat to bridge the gap between server-level and rack-level models. They used Phoenics as their CFD software for its simplicity and wide-range availability among academic institutions. They modeled servers in component-level (CPUs, disks, etc.) and a rack with 20 of these servers. They neglected the wires and guiding components on the back of the rack as they found out these do not significantly affect the outcome. The CFD model was validated with experimental temperature measurements and thermal camera readings. Results show that the tool developed is capable of obtaining thermal profiles of servers with varying load conditions and can be used to arrange servers inside the rack or for thermal optimization studies.

Ghosh et al. (2012) studied the effect of server population and how they are arranged inside a rack on surrounding air temperatures in a data center. The experimental part

of their study included an isolated test rack fully populated by blade servers. The rack was cooled by cold air supplied through perforated tiles on the floor and hot air was disposed of through the ceiling. Figure 1.8 shows the schematic of the rack, cold aisle where the cold air is supplied, and the hot aisle where the exhaust air is disposed of through the ceiling. Temperatures were measured using a grid structure consisting of 21 type-T thermocouples. Measured values were then used to validate the CFD analysis. Figure 1.9 shows that significant recirculation occurs near the head node (void on top of the rack) and affects the temperature field. Lastly, the location of server clusters inside the rack was investigated by placing 12 servers on the bottom, middle, and top portion of the rack as shown in Figure 1.10. CPU temperatures and fan speeds were observed for each configuration. Results indicate that top configuration has the lowest CPU temperatures and average fan speeds for all servers. These results have significant implications for the thermal management of electronics racks.

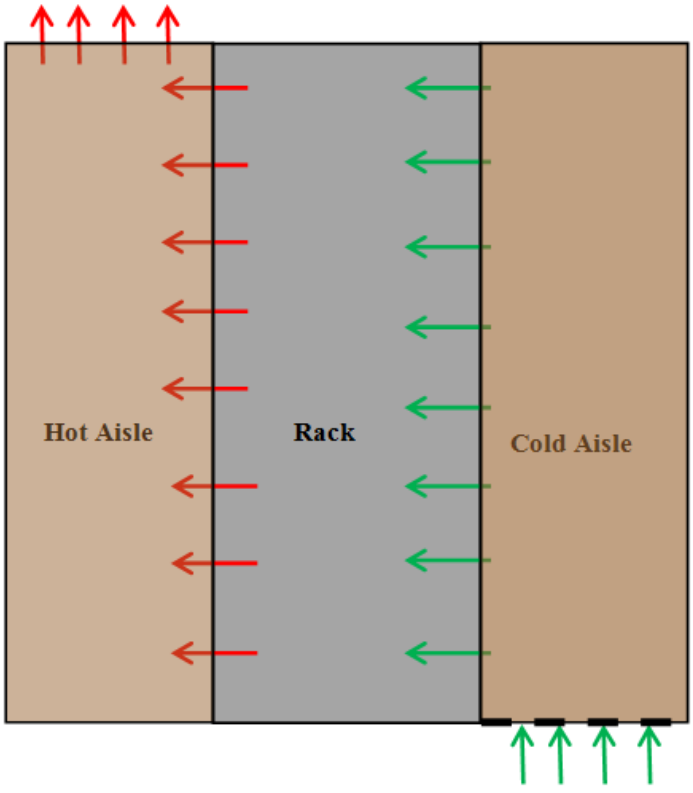

Figure 1.8. Schematic of the isolated rack. Adapted from Ghosh et al. (2012).

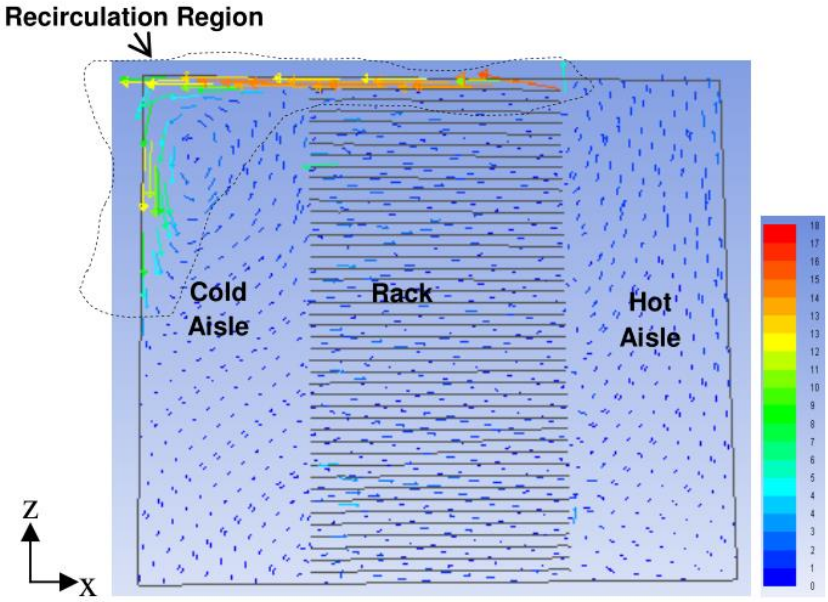

Figure 1.9. Airflow field visualized. Adapted from Ghosh et al. (2012).

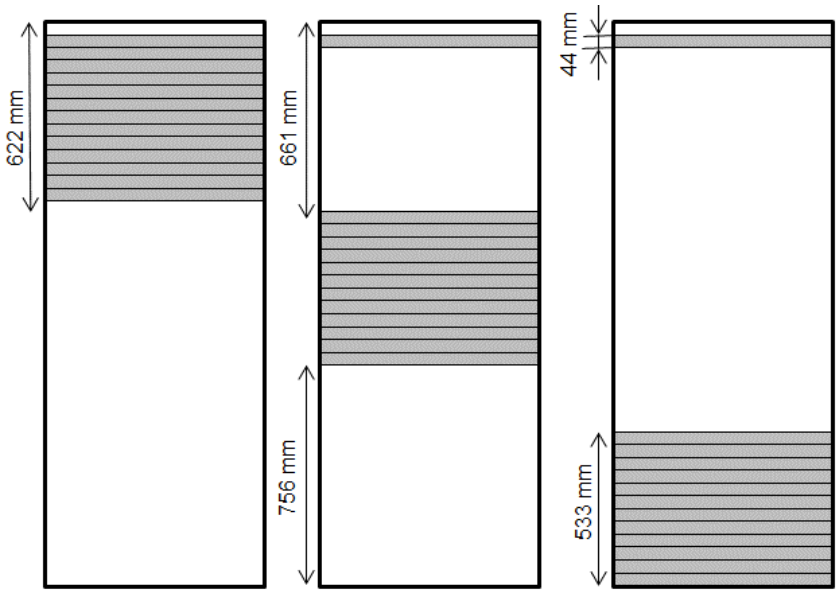

Figure 1.10. Different server population configurations; top, middle, and bottom, respectively. Adapted from Ghosh et al. (2012).

As mentioned, datacenter cooling studies in literature include rack-cooling objectives, which is a common point with this study. This thesis builds upon the previous rack-cooling or datacenter studies by filling the gap of multiple length-scale analysis that includes everything from chip to the room. Furthermore, as datacenters are fairly optimized structures, datacenter studies investigate components with similar geometries and heat dissipation values. However, not all racks are in datacenters and in need of optimization, as electronics cabinets are widely used in every industry for different purposes. This differentiation from datacenters means components inside these racks may have different geometries and heat dissipation values, as is the case in this thesis. This gap is filled by modelling all components true to their geometries and heat dissipation values.

In this chapter, an introduction to the subject of this study and its structure is presented. Previous studies in the literature are investigated and similarities and differences are drawn. Objectives of this study and its relation to the previous studies and its addition to the literature are stated.

CHAPTER 2

EXPERIMENTAL MEASUREMENTS

2.1. Experimental Setup and Results

As mentioned in the previous chapter, there are temperature limits for each component when they are all running inside the cabinet. Therefore, experimental measurements are done on the cabinet running on full power without a front cover. Table 2.1 lists the temperature limits of each component.

Table 2.1. *Temperature limits of each component*

Location	Temperature Limit (℃)
PDU inlet	30
UPS inlet	30
Workstation – 1 inlet	40
Workstation – 2 inlet	40
Interface – 1 inlet	35
Interface – 2 inlet	35
Managed Switch inlet	35
Box – 1 inlet	35
Box – 2 inlet	35
All outlets	60

These limits are for specific locations around the components where the measurements are done, not for hotspots. These locations are selected according to the company precedents.

For experiments, type-K thermocouples are used to read temperatures at specific points, as the company chose to use them for their availability. Graphtec midi logger GL800 data logger is used to record data. Figure 2.1 shows a thermocouple and the data logger.

Figure 2.1. Type-K thermocouple and Graphtec data logger

19 thermocouples were used to measure temperatures. The points, where the thermocouples are placed, are decided according to precedent company procedures. 9 thermocouples are placed on “inlet” of each component, where inlet indicates the front-facing surface of the component. Another 9 thermocouples are placed on the “outlet” of the components, where outlet indicates the surface with outward airflow, and the last one is placed on the side cover. Figure 2.2 shows how the inlet thermocouples are placed for Workstation – 1 and Workstation – 2 as an example.

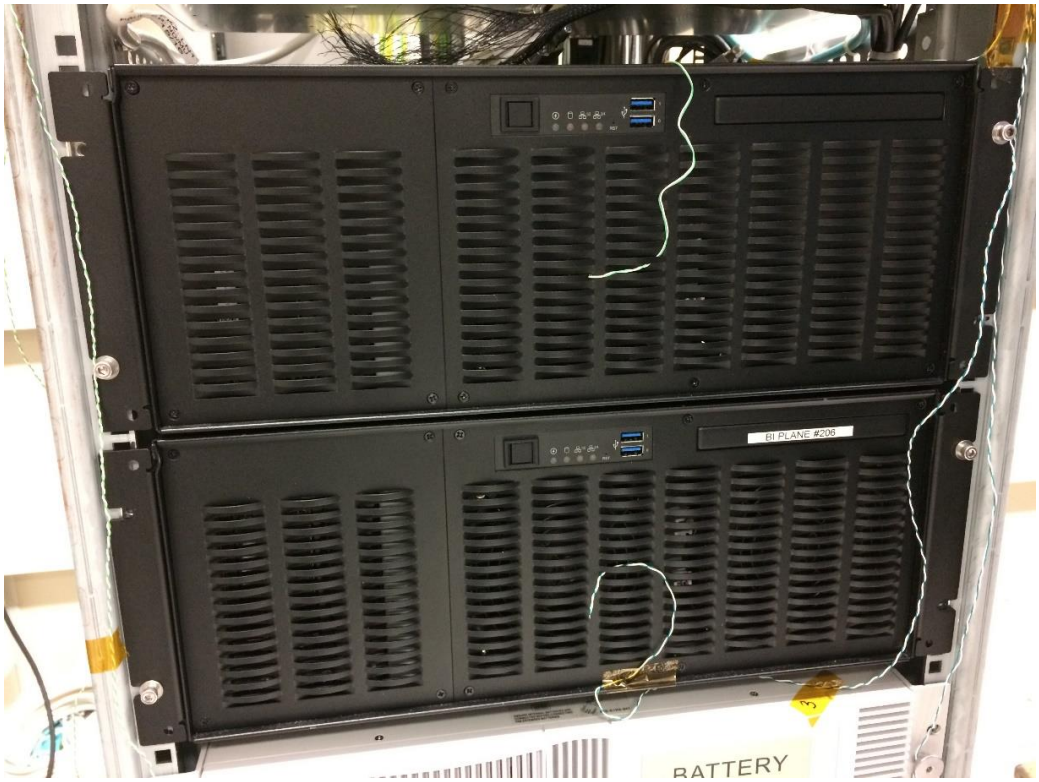

Figure 2.2. Inlet thermocouples on Workstation – 1 and Workstation – 2

Figure 2.3 shows the placement of one of the outlet thermocouples for Workstation – 2. Note that each workstation has two outlet thermocouples, one on the grill and another on the power supply fan.

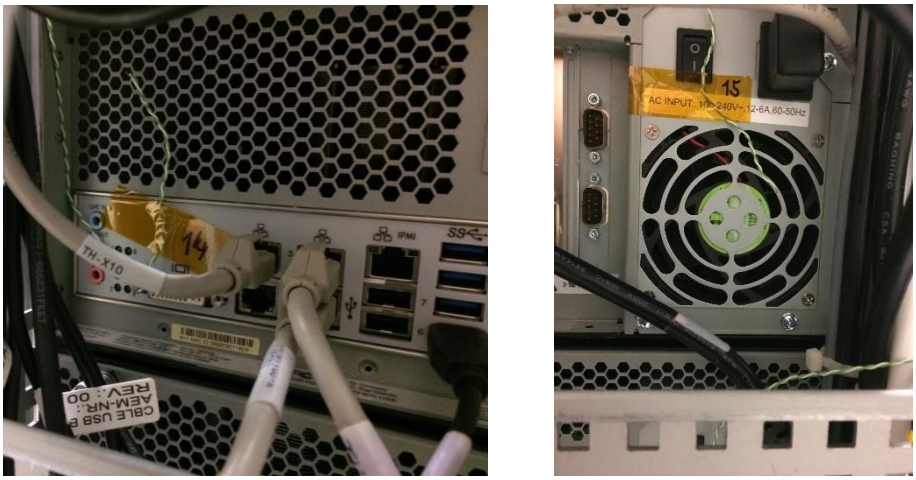

Figure 2.3. Outlet thermocouples for Workstation – 2

Figure 2.4 shows the approximate location of each thermocouple. Note that thermocouples 1-9 are located on the front side of the cabinet whereas thermocouples 9-18 are on the back of it.

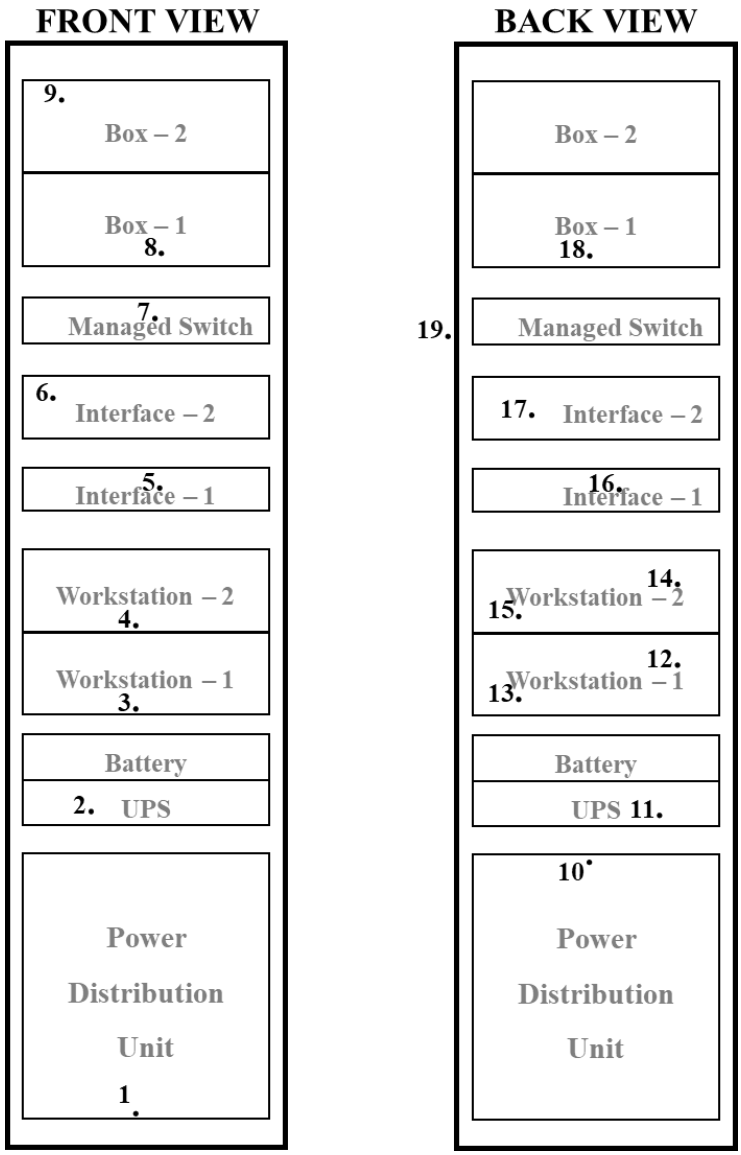

Figure 2.4. Locations of thermocouples on front and back of the cabinet, respectively.

Thermocouple locations are also summarized in Table 2.2.

Table 2.2. *Thermocouple locations*

Thermocouple Number	Location
1	PDU inlet
2	UPS inlet
3	Workstation – 1 inlet
4	Workstation – 2 inlet
5	Interface – 1 inlet
6	Interface – 2 inlet
7	Managed Switch inlet
8	Box – 1 inlet
9	Box – 2 inlet
10	PDU outlet
11	UPS outlet
12	Workstation – 1 outlet #1
13	Workstation – 1 outlet #2
14	Workstation – 2 outlet #1
15	Workstation – 2 outlet #2
16	Interface – 1 outlet
17	Interface – 2 outlet
18	Box – 1 outlet
19	Side Cover

In a real-life environment, there are other cabinets that are powered by the one under investigation, since the PDU responsible for providing power to all the cabinets, is in this one. To simulate this situation, a power supply is used to power the whole cabinet, as seen in Figure 2.5. The power supply provides approximately 8 kW through the PDU.

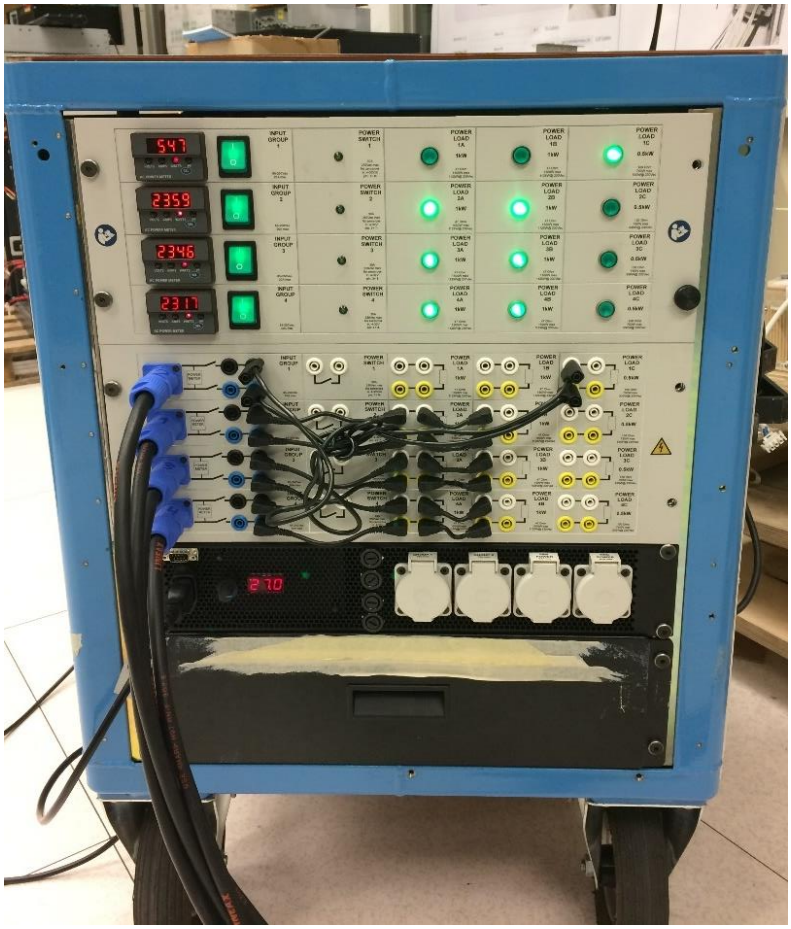

Figure 2.5. Power supply used during the experiments

Both workstations are loaded using “Burn-in” software that loads the electronic parts inside them to simulate maximum heat dissipation. Other components cannot be loaded the same way since they do not have an interface to run such a software; however, managed switch is loaded by connecting 20 ethernet cables to increase the traffic.

Cabinet is left to run overnight to stabilize the temperatures, which takes around 8 hours. After that, measurements are taken and averaged over the course of 3 hours. Table 2.3 presents the temperature values obtained.

Table 2.3. *Temperature measurements*

Thermocouple Number	Temperature (℃)	Standard Deviation
1	26.8	0.16
2	26.0	0.40
3	25.9	0.25
4	25.9	0.27
5	28.2	0.34
6	27.0	0.67
7	31.5	1.01
8	30.8	0.67
9	29.1	0.86
10	51.8	0.52
11	37.0	0.23
12	41.8	0.16
13	33.0	0.20
14	31.5	0.14
15	32.7	0.24
16	31.9	0.30
17	31.6	0.29
18	32.2	0.28
19	26.7	0.32

Measurements show that all of the components operate below their allowable maximum temperature limits both on inlets and outlets. However, components such as PDU, UPS and Managed Switch, operate around 3 to 4 ℃ below their limits (see Table 2.1) on their inlets. This justifies the need to analyze effects of front covers, as a front cover may increase the temperatures inside.

The outlets of the components are on the safer side than the inlets, as PDU outlet, which seems to be the most critical one, operates around 9 ℃ below the limit.

These measurements will also be used to validate the numerical model in the following chapters.

2.2. Data Acquisition System Error Analysis

It is important to address the uncertainty associated with the experimentally obtained data, as it is a matter of how accurate the model validated with these data will be.

All the temperature measurements in this study were done using type-K thermocouples and a data acquisition system. An issue that needs to be addressed is calibration of the measurement equipment. Thermocouples and the data-logger are calibrated twice a year by the provider, according to the company policy. The last calibration date of the equipment was almost two months before the measurements and no usage took place in between. Therefore, it is assumed that the equipment is calibrated properly. Nonetheless, there may still be some error associated with the calibration; hence, upper limit error of ± 2.2 ℃ is used since, type-K thermocouples have an accuracy of ±2.2 ℃ or ±0.75%, whichever is larger. The data acquisition system, Graphtec GL800, has a measurement accuracy of ± (0.05% of reading + 1.0 ℃) for type-K thermocouples, according to the manufacturers datasheet.

Thermocouple and data acquisition errors are added together by taking their root sum squares, which is,

$$\sqrt{(2.2)^2 + \left(\frac{0.05}{100} * T + 1\right)^2}$$

where T is the measurement in ℃. For example, for Thermocouple 1, experimental measurement is 26.8 ℃; therefore, the error associated with this measurement is,

$$\sqrt{(2.2)^2 + \left(\frac{0.05}{100} * 26.8 + 1\right)^2} = 2.42\ ℃$$

CHAPTER 3

WORKSTATION – 1

3.1. Geometry

One of the components inside the cabinet is designated as Workstation – 1 that is intended for parallel processing. The purpose of this chapter is to create a model for this component as most of the information on it, such as details of parts inside, are known as opposed to all the other components inside the cabinet.

Specifications of this component are shown in Table 3.1.

Table 3.1. *Workstation – 1 part models*

Part Name	Model
CPU	Intel Xeon E5-2618L v3 (×2)
GPU	Nvidia Quadro K620 (×3)
Heatsink	Tower Active Heatsinks (×2)
Fans	4 Different Fans, Total of 8

Dimensions of the parts modeled in this component are presented in Table 3.2 and Table 3.3.

Table 3.2. *Workstation – 1 part dimensions*

Part Name	Dimensions (H × W × D) (mm)
Chassis	174.2 × 431.8 × 497.8
Motherboard	1.000 × 311.8 × 362.8
Heat Sink	112.0 × 92.00 × 70.00
HDD & SSDs	110.0 × 28.00 × 140.0
Power Supply	146.0 × 90.00 × 159.0

Table 3.3. *Workstation – 1 part dimensions continued*

Part Name	Dimensions (W × D) (mm)
CPU	525.00 × 450.00
GPU	68.91 × 160.02
Fans	119.00 × 38.00 92.00 × 25.40 80.00 × 25.00 50.00 × 50.00

3.2. Modeling Methodology

A CFD analysis can be divided into three parts; pre-processing, solver execution and post-processing. In pre-processing, geometry or "domain" is defined and divided into cells or control volumes, comprising a grid, or "mesh". In solver execution, governing equations, boundary and initial conditions, and algorithms used are presented. In post-processing, relevant results are presented.

There are different types of objects, as they are called, in Icepak to represent different types of electronic parts, such as blocks, openings, fans, heat sinks, etc. Details of the parts modeled are presented in this section.

Chassis: Computational domain of the Workstation – 1 is the chassis of it. By default, a "Cabinet" is defined in Icepak, which represents the chassis using walls. Non-slip

wall condition is specified with default thermal specification of adiabatic wall. Material of the cabinet is left as default, which is steel-oxidized.

Fans: Icepak has a "Fan" object with 2D and 3D options. For all the fans inside the Workstation – 1, a 3D circular fan object is used (Nelson, 2007). To create a more realistic model, fan swirl was incorporated in the model with an RPM value taken from corresponding datasheet.

Table 3.4 shows volumetric flow rates and RPM values assigned to each fan. Note that volumetric flow rates are in CFM since this is the unit used in datasheets. Details of fan modelling are presented in Appendix-A.

Table 3.4. *Fan specifications*

Fan Number	Volumetric Flow Rate (CFM)	RPM
WS Fan-1	70.00	3200
WS Fan-2	102.59	4800
WS Fan-3	63.57	3600
WS Fan-4	30.00	2500

CPU and GPUs: For heat-dissipating objects such as CPU and GPUs, a 2D rectangular "Source" object is used. For all CPU and GPUs inside Workstation – 1, constant heat dissipation rate of 75 W and 45 W, respectively, is specified, which is taken from the manufacturers datasheet. Maximum power dissipation is assumed since burn-in software was run on Workstation – 1. This software stresses CPUs and GPUs to represent a critical situation with high heat load.

Heat Sinks: Both CPUs have identical heat sinks on them, which were modeled using the "Heat Sink" object. Extruded fin heat sinks without a base thickness were used since Icepak does not have an option for tower-type heat sinks, an example of which is shown in Figure 3.1. Exact model and specification of heat sinks are unknown since

manufacturer does not provide the necessary information. Hence, fin thickness and spacing were approximated. Extruded aluminum was specified as material for heat sinks.

Figure 3.1. Example tower-type heat sink. Adapted from www.fudzilla.com/home/item/24581

Heat Pipes: Heat sinks in the Workstation – 1 also include heat pipes made of copper. Since these heat pipes have highly irregular shapes, they are approximated using solid prisms of "Block" objects. A material with an isotropic conductivity of 390 W/(m·K) is assigned to heat pipes. Thermal resistance of 0.13 ℃/W (Liang & Hung, 2010) is specified on surfaces of heat pipes where fins are extruded to simulate thermal contact resistance.

Motherboard: The motherboard inside the Workstation – 1 is also modeled using solid prism of "Block" object. A material with a conductivity of 40 W/(m·K) is assigned to it. Although Icepak has another object type of "Printed Circuit Boards", inputs needed for this object such as trace parameters, coverage, etc. are not known. Therefore, motherboard is simplified as a solid rectangular prism.

Power Supply: Workstation – 1 has a power supply that has its own fan. This component is modeled using "Plate" object. For the heat source inside the power supply, a rectangular prismatic "Source" object is created. Power output of Workstation – 1 is 346 W, which means with an assumed efficiency of 95% (Pandiyan, 2012), it dissipates 17.5 W of heat, which is rounded for easiness. Therefore, source object has a total power of 17.5 W.

Perforated Plates: Workstation – 1 has perforated plates on the front and back of its chassis, and around the power supply, all of which are modeled using "Grille" object. Free area ratio of 0.8 is assigned with a resistance type of "Perforated thin vent" for grilles around power supply, a free are ratio of 0.6 is assigned to grilles on the front and 0.65 is assigned to grilles on the back with same resistance type. Icepak calculates pressure drop resulting from these resistances using relations from Idel'chik, (1960).

HDD and SSDs: There are a total of 3 disks inside Workstation – 1. All these parts are modeled using "Block" objects; however, HDDs are modeled as heat-dissipating solids with 7 W total power, whereas SSDs are modeled as hollow blocks, since they do not have any heat dissipation and only act as a barrier to the air flow.

RAMs and PCIe Boards: There are 8 RAMs with 6 W of heat dissipation each and 2 PCIe boards, both with 3 W of heat dissipation, inside Workstation – 1. These parts are also modeled using 2D source objects.

Other parts: A thin plastic part inside Workstation – 1 directs the airflow coming from front fans to RAMs and GPUs, and it is modeled using "Wall" objects instead of "Plate" or "Block" objects, since it does not have any heat dissipation.

Some of the parts of Workstation – 1 such as ports, sockets, internal cables, etc. are not included in the model since they have negligible thermal significance compared to other parts and do not affect air flow inside significantly. Figure 3.2 shows the model created for Workstation – 1.

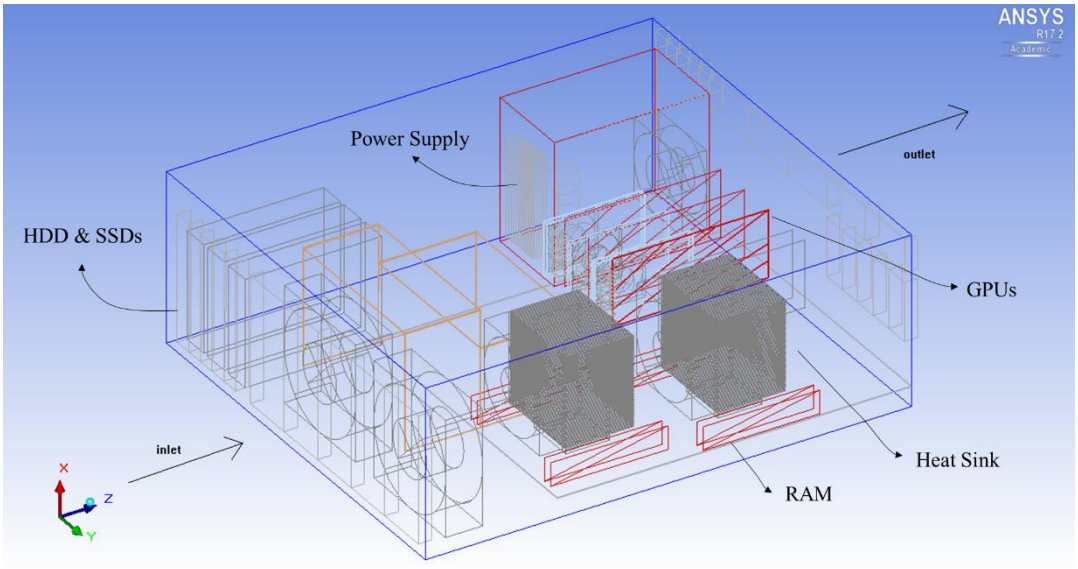

Figure 3.2. Workstation – 1 model

Details of CPU package and GPUs can be found in Appendix-A.

3.3. Meshing

Icepak offers two different mesh generators, hex-dominant, which is the default option, and hexahedral mesher. Hex-dominant is an unstructured mesh generator and uses pyramidal and triangular cells in addition to hexahedral cells, allowing it to be used for a wide-range of shapes and sizes. Icepak User's Guide (ANSYS, 2012) recommends using hex-dominant mesh generator for most applications, since it can do everything that can be done by hexahedral mesh generator. Therefore, in this analysis, hex-dominant mesh generator, or namely Mesher-HD, is used.

Icepak offers the ability to create non-conformal mesh structures using "Assembly" option. Different objects can be grouped together in the same assembly and these assemblies can be assigned mesh parameters different than the rest of the domain. This allows the user to generate finer mesh inside and around assemblies, which is most needed in case of temperature and velocity fluctuations, and a coarse mesh in areas where less resolution is sufficient. This way, total element count can be decreased

without affecting the results. Assemblies also prevent what is called “Mesh bleeding”, a phenomenon shown in Figure 3.3. Mesh bleeding occurs when different parts of the model is assigned different mesh densities, and higher density mesh effects other parts of the model.

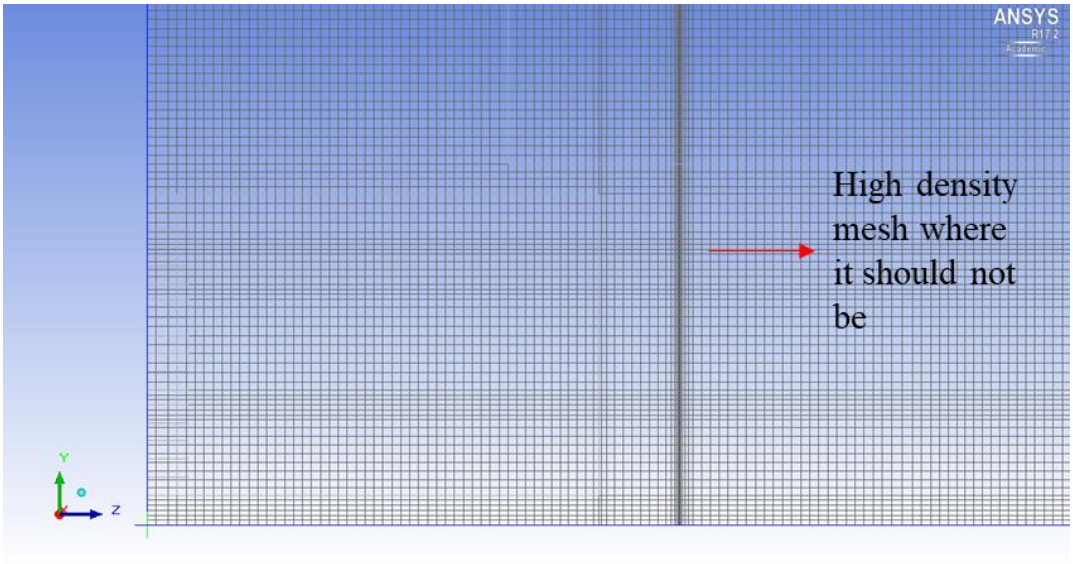

Figure 3.3. Mesh bleeding example

When creating an assembly, Icepak offers an option called “Slack” to make the assembly bigger than the objects it contains. This way, a different mesh density can be created not only on the object, but also around it. This also allows to resolve the areas where heat transfer occurs; therefore, finer mesh is needed.

Every fan inside the Workstation – 1 is put in an assembly since velocity fluctuations are present on the inlets and the wakes of fans. Two fans on the inlet of Workstation – 1 are in the same assembly, to prevent mesh bleeding from occurring in the gap between them with two different assemblies.

By default, Icepak creates O-grid mesh structure on fans and a fine mesh in their wake, as shown in Figure 3.4.

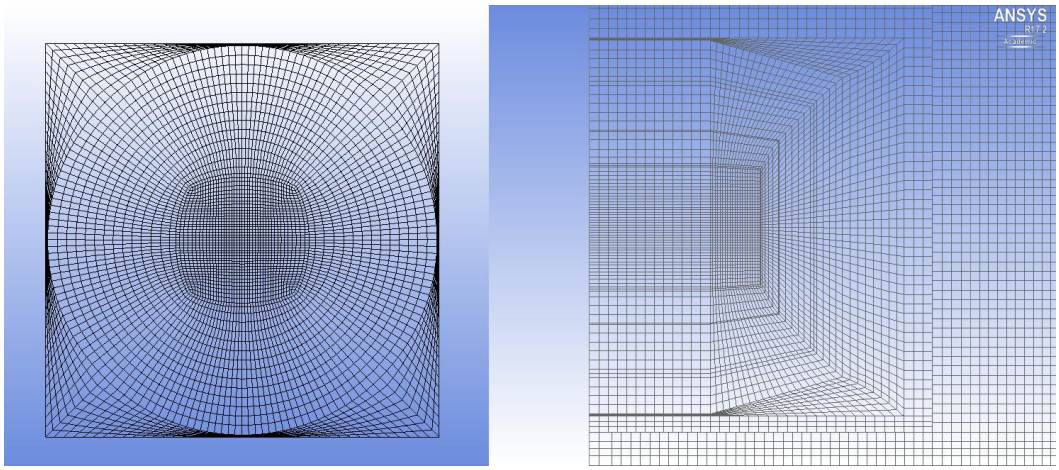

Figure 3.4. Example O-grid mesh on fan and fine mesh in its wake from top view

This structure is needed to resolve the velocity fluctuations in the wake of the fan. However, fans on the CPU packages are adjacent to the heat-sinks, making it impossible to have a finer mesh in their wake. Therefore, these fans are modeled without an O-grid structure.

CPU packages inside the Workstation – 1 have the finest mesh since heat-sink fin gaps are significantly small compared to other distances between objects. All the components in a CPU package, namely CPU, heat-sink and heat-pipes, are placed in the same assembly which is meshed separately. Maximum element size of 2 mm is assigned for y and z directions, whereas 0.5 mm element size is assigned for x-direction. For minimum gap, 5.10^{-5} m is assigned in x-direction considering the distance between two consecutive fins.

GPUs and PCIe boards are placed inside different assemblies with maximum element size of 3 mm so that temperature fluctuations around heat generating parts can be sufficiently resolved.

Motherboard is not included in any assembly since the mesh generated without an assembly is adequate to resolve temperature gradients inside it. However, it should be

noted that an assembly created for a part that lies on the motherboard, such as CPU and GPUs, protrudes the part of the motherboard it is placed on. This causes motherboard to have different areas with different mesh densities and some mesh bleeding. To counter this, most of the components are placed in an assembly. Surface mesh for motherboard can be seen in Figure 3.5.

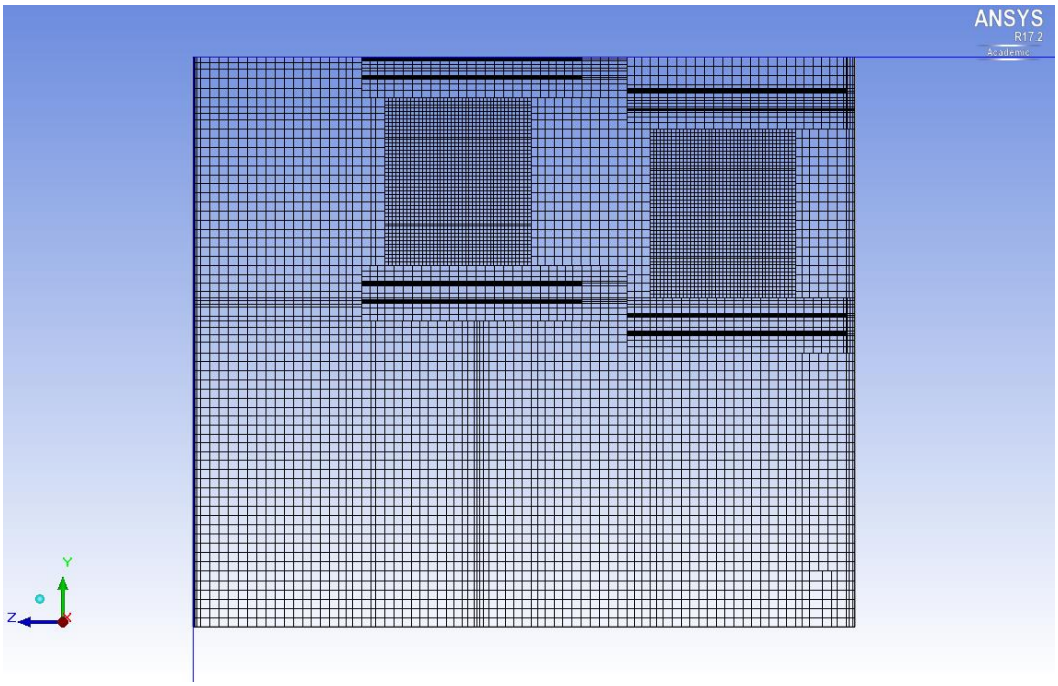

Figure 3.5. Motherboard Mesh

A coarser mesh is generated for the rest of the Workstation – 1 with maximum element size of 5 mm. All in all, total mesh count for Workstation – 1 is 2907812. Figure 3.6 shows the mesh in *yz* mid-plane.

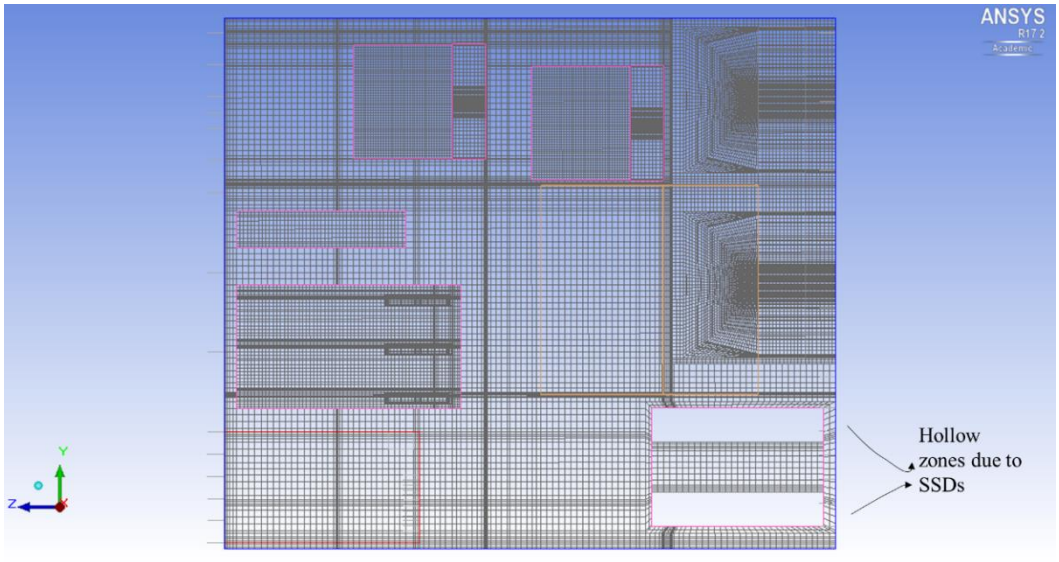

Figure 3.6. Mesh on yz mid-plane at x=0.085m

Another mesh parameter that should be considered is mesh quality. A high mesh count does not guarantee an accurate solution without a high-quality mesh. There are a few parameters that can be used to determine mesh quality such as skewness, aspect ratio, etc. In Icepak, skewness of a cell is defined as difference between the cell shape and the shape of an equilateral cell with equivalent volume. Therefore, in contrast to Fluent, a cell with low skewness, such as 0.05, may cause instabilities in the solution, therefore, should be avoided. Aspect ratio, on the other hand, is how much a cell is stretched. A sudden change in aspect ratio between two cells may decrease the accuracy and lead to divergence.

Icepak automatically calculates mesh quality by using skewness and face alignment, which is calculated as shown in Eq – 3.1.

$$face\ alignment\ index = \overrightarrow{c_0 c_1}.\vec{f} \tag{3.1}$$

where c_0 and c_1 are the centroid of two adjacent elements, and $\vec{f}$ is the normal vector between the two elements, according to Icepak User's Guide (ANSYS, 2012).

The mesh generated for Workstation – 1 has a minimum skewness value of 0.16 and face alignment of 0.31 for a small number of elements. The reason for this poor quality in certain places is the circular shape of the fans.

3.4. Solver Execution

Fluid flow inside Workstation – 1 is modeled as steady-state, turbulent, single-phase flow. Icepak uses Fluent as solver; therefore, governing equations are taken from Fluent Theory Guide (ANSYS, 2016). For pressure-velocity coupling, SIMPLE algorithm is chosen. Standard scheme is chosen for pressure interpolation. Both momentum and energy equations are discretized using second order schemes. Natural convection is neglected since dominant cooling method is forced-convection.

Conservation of mass equation is given as;

$$\frac{\partial \rho}{\partial t} + \nabla \cdot (\rho \vec{v}) = 0 \tag{3.2}$$

where ρ is density. For an incompressible fluid, Eq – 3.2 reduces to,

$$\nabla \cdot \vec{v} = 0 \tag{3.3}$$

Eq – 3.4 shows the Conservation of Momentum equation. Stress tensor τ is given in Eq – 3.5 as;

$$\frac{\partial}{\partial t} (\rho \vec{v}) + \nabla \cdot (\rho \vec{v} \vec{v}) = -\nabla p + \nabla \cdot \left(\bar{\bar{\tau}} \right) + \rho \vec{g} + \vec{F} \tag{3.4}$$

$$\bar{\bar{\tau}} = (\mu + \mu_t) \left[(\nabla \vec{v} + \nabla \vec{v}^T) - \frac{2}{3} \nabla \cdot \vec{v} I \right] \tag{3.5}$$

where $\rho \vec{g}$ and $\vec{F}$ are the gravitational body force and external body forces, respectively, μ is molecular viscosity, μ_t is turbulent viscosity computed from $\mu_t = \rho C_\mu \frac{k^2}{\epsilon}$, I is the unit tensor.

Energy equation is given as;

$$\frac{\partial}{\partial t}(\rho h) + \nabla \cdot (\rho h \vec{v}) = \nabla \cdot ((k + k_t)\nabla T) + S_h \quad (3.6)$$

where h is sensible enthalpy, k is the thermal conductivity, k_t is the conductivity due to turbulent transport defined as $k_t = C_p \mu_t / \mathrm{Pr}_t$, and S_h is volumetric heat source.

Standard $k - \varepsilon$ turbulence model is chosen for this simulation (Rambo & Joshi, 2005), which adds two more equations;

$$\frac{\partial}{\partial t}(\rho k) + \frac{\partial}{\partial x_i}(\rho k u_i) = \frac{\partial}{\partial x_j}\left[\left(\mu + \frac{\mu_t}{\sigma_k}\right)\frac{\partial k}{\partial x_j}\right] + G_k + G_b - \rho\varepsilon \quad (3.7)$$

$$\frac{\partial}{\partial t}(\rho \varepsilon) + \frac{\partial}{\partial x_i}(\rho \varepsilon u_i) = \frac{\partial}{\partial x_j}\left[\left(\mu + \frac{\mu_t}{\sigma_\varepsilon}\right)\frac{\partial \varepsilon}{\partial x_j}\right] + C_{1\varepsilon}\frac{\varepsilon}{k}(G_k + C_{3\varepsilon}G_b) - C_{2\varepsilon}\rho\frac{\varepsilon^2}{k} \quad (3.8)$$

where G_k is the generation of turbulence kinetic energy due to mean velocity gradients, computed from $G_k = -\rho\overline{u_\iota{}' u_J{}'}\frac{\partial \mathrm{u_j}}{\partial x_i}$, G_b is the generation of turbulence kinetic energy due to buoyancy, computed from $G_b = \beta g_i \frac{\mu_t}{Pr_t}\frac{\partial T}{\partial x_i}$, $C_{1\varepsilon}$,$C_{2\varepsilon}$ and C_μ are constants taken as 1.44, 1.92 and 0.09, respectively, and σ_k and σ_ε are the turbulent Prandtl numbers for k and ε, taken as 1.0 and 1.3, respectively.

Regarding the boundary conditions, no-slip condition is specified on the walls of chassis, meaning that all velocity components are zero at these surfaces. Sources due to heat dissipations in the model are specified in the previous section and summarized in Table 3.5.

Table 3.5. *Workstation – 1 energy sources*

Part	Heat Dissipation (W)
CPU (x2)	75
GPU (x3)	45
PCIe (x2)	3
HDD	7
RAM (x8)	6
Power Supply	17.5

Other boundary conditions include the fans inside Workstation – 1. There is a total of 8 fans all of which are modeled as 3D circular "Fan" objects. A fan object is a "Fan Boundary Condition" in Fluent, which creates discontinuous pressure rise across itself according to the fan curve input. A fan curve shows the relationship between pressure rise and velocity, and it can be linear, polynomial, piece-wise linear, piece-wise polynomial or a user-defined function. This fan curve is usually provided by the manufacturer, but it also can be obtained by experiments. In this thesis, all fan curves are taken from manufacturers datasheet (Hermansen, 2011). From the system pressure, operating point of the fan is calculated. All fan curves for Workstation – 1 are taken as piece-wise linear relationships.

Fluent offers two precision options, single-precision and double-precision. Although double precision considers more digits after decimal point, it is also supposed to increase the solution time and computational expense. However, when two solutions with same parameters but different precision settings are compared, it can be seen that there is an insignificant difference between them. Furthermore, using single precision solver leads to a decrease in solution time. For the temperature range of this work, single precision is deemed sufficient. Note that preliminary comparisons on single and double precision showed no significant difference between the two settings, since when results are analyzed, they truncated after 3 decimal points for both settings.

A first-cut analysis is done using first-order scheme, and then solution is continued with second-order scheme. Although second-order scheme may yield more accurate results, it also increases the computational time of the solution and may lead to problems in convergence. To counter this effect, under-relaxation factors for pressure, momentum, k and ε are lowered to 0.1, 0.3, 0.8 and 0.8 respectively. Rest of the solver parameters are the same for both solutions. Figure 3.7 shows the temperature values along the reference line on CPU-1, which is presented in Figure 3.8.

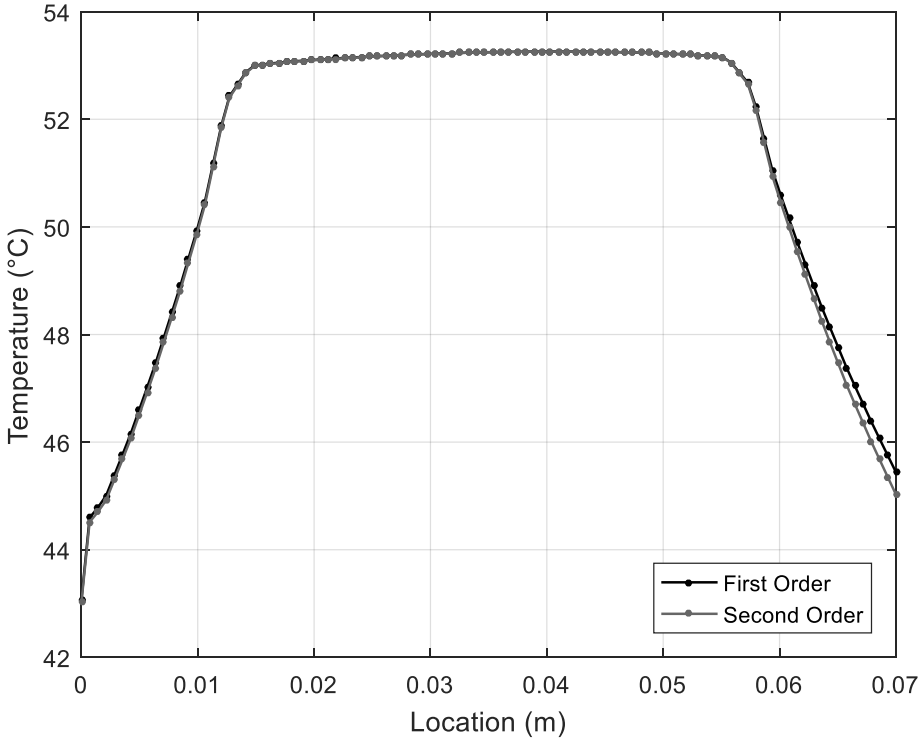

Figure 3.7. First Order vs Second Order Scheme

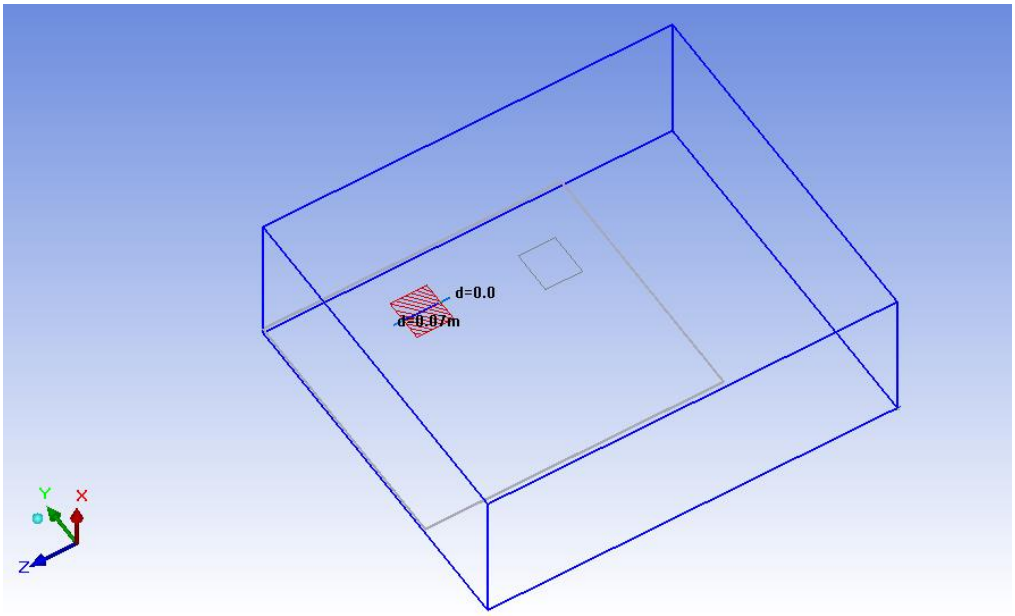

Figure 3.8. Reference line on CPU

Maximum difference occurs on the right end point of the reference line. Table 3.6 shows the temperatures for selected locations for first-order and second-order solutions.

Table 3.6. *Order of Scheme Comparison*

Location	First-Order Temperatures (°C)	Second-Order Temperatures (°C)
CPU-1	46.8	46.8
CPU-2	51.6	51.6
GPU-1	54.6	54.4
GPU-2	50.7	49.8
PCIe	37.0	35.2
Fan Outlet	30.1	30.1
Grille Outlet	32.4	32.7

As can be seen, largest difference occurs in PCIe with a difference around 1.8 ℃. Although this difference may be high, temperatures on fan and grille outlets are very close, which means that first-order scheme fails to resolve temperature gradients around heat-dissipating units; however, it is sufficient for measuring outlet temperatures. Therefore, first-order scheme is deemed sufficient for this model.

3.5. Mass and Energy Balance

Workstation – 1 has one inlet; grilles on the front fans, and five outlets; three grilles on the back, one grille on the front and fan outlet itself. For a system at steady-state, mass flow rate balance becomes;

$$m_i - m_o = 0 \tag{3.9}$$

$$m_i - (m_{o1} + m_{o2} + m_{o3} + m_{o4} + m_{o5}) = 0 \tag{3.10}$$

With constant density, Eq – 3.10 reduces to;

$$Q_i - (Q_{o1} + Q_{o2} + Q_{o3} + Q_{o4} + Q_{o5}) = 0 \tag{3.11}$$

where volumetric flow rates calculated in Icepak are given in Table 3.7 as;

Table 3.7. *Volumetric flow rates*

Location	Volumetric Flow Rate (m^3/s)
Q_i	0.0661812
Q_{o1}	0.0189681
Q_{o2}	0.0243895
Q_{o3}	0.0027774
Q_{o4}	0.0137978
Q_{o5}	0.0046247
Difference	5.72×10^{-6}

A difference of 5.72×10^{-6} is acceptable; therefore, conservation of mass upholds.

Next, energy balance is calculated. For a system at steady state, conservation of energy comes down to;

$$\dot{Q} - \dot{W} + \sum_{i} \dot{m}_i \left(h_i + \frac{v_i^2}{2} + g z_i \right) - \sum_{o} \dot{m}_o \left(h_o + \frac{v_o^2}{2} + g z_o \right) = 0 \qquad (3.12)$$

Neglecting the kinetic and potential energy terms, assuming that no energy is transferred by work across the boundary, and, for an ideal gas, substituting $dh = c_p(T) * dT$ and $\dot{m}_i = \dot{m}_o = (m_{o1} + m_{o2} + m_{o3} + m_{o4} + m_{o5})$, Eq – 3.12 can be written as;

$$\dot{Q}_{gen} + \dot{m}_{o1} * c_p * (T_i - T_{o1}) + \dot{m}_{o2} * c_p * (T_i - T_{o2}) + \dot{m}_{o3} * c_p * (T_i - T_{o3}) + \dot{m}_{o4} * c_p * (T_i - T_{o4}) = 0 \qquad (3.13)$$

where heat generation inside Workstation – 1 is 363.5 W, T's are area averaged temperature values at designated locations, mass flow rates are calculated using volumetric flow rate values in Table 3.7 and constant air density at 30 ℃ which is 1.164 kg/m^{-3}, and c_p is assumed constant at 1006 J/(kg·K^{-1}).

When all values are substituted into Eq – 3.13, summation comes up as -0.561 W, which is acceptable considering averaged temperature values and material properties assumption. When energy balance is checked in Icepak's own results page, summation comes up as -0.044 W. Therefore, Workstation – 1 model upholds the conservation of energy. Workstation – 1 model cannot be verified with experimental data, as the measurements were done while it was inside the cabinet. Therefore, this model is kept as is and used in the cabinet model in next chapter.

CHAPTER 4

CABINET MODEL

4.1. Cabinet Geometry and Mesh Details

In this chapter, cabinet model together with all the components inside is presented. Workstation – 1 model is kept the same as the one in the previous chapter, except for a few changes such as “Plate” objects instead of “Wall” objects for the chassis, since workstation is not on the boundary of the domain anymore.

Following sections present the details of the components, such as their dimensions, elements inside them, etc., their physical conditions and the details of the mesh created for cabinet model.

4.1.1. Workstation – 2

Workstation – 2 is identical to Workstation – 1 in geometry and material. Workstation – 2 has only one CPU, GPU and SSD, each. Although GPU and SSD models are the same for both workstations, CPU inside Workstation – 2 is different than that of Workstation – 1, which has a thermal design power of 85 W according to specification sheet provided by the manufacturer. Also, one of the PCIe boards dissipates 1 W, instead of 3 W. The rest of the parts inside Workstation – 2, motherboard, heat-sink, fans and grilles, are identical to Workstation – 1. Therefore, similar procedures for mesh and solver are followed for both workstations.

4.1.2. Interface – 1

Interface – 1 is a component that is responsible for device-to-device communication, and it is one of the custom-made components inside the cabinet, meaning that it is manufactured according to the company specifications. However, since the manufacturing is outsourced, most of the information about this component such as

parts used inside, etc. lies within the intellectual property of the manufacturer. Therefore, some assumptions are necessary for geometry and specifications.

Interface – 1 has a geometry of 0.040 × 0.438 × 0.150 m (H × W × D) with a distance of 0.012 m from the cabinet opening. It has one fan on its back and grilles on the front. Model created in Icepak for Interface – 1 can be seen in Figure 4.1.

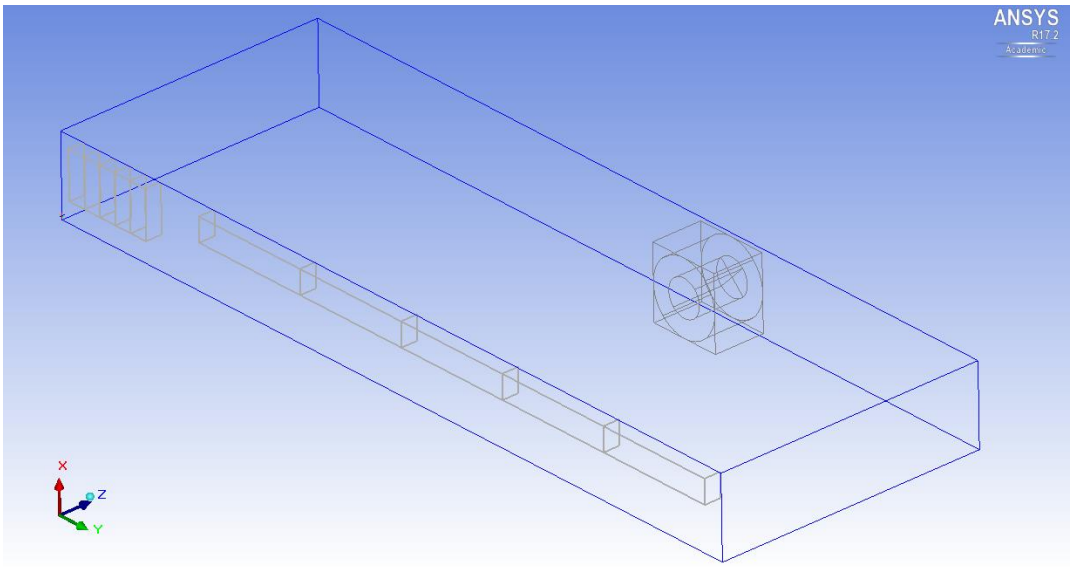

Figure 4.1. Interface – 1 model

Power dissipation of Interface – 1 is known as 20 W. A source object that covers the whole volume of Interface – 1 with 20 W total power is created. Fan inside Interface – 1 is modeled using a 3D circular fan object with maximum airflow of 0.32 m^3/min and maximum static pressure of 102.9 Pa. For grilles, 80% open area ratio is specified.

Meshing of Interface – 1 is similar to previous components. There are only two objects, a fan, which is in an assembly, and the source. Fan assembly has sufficient slack values to capture the wake of the fan.

4.1.3. Interface – 2

Interface – 2 is another interface used for communication between components inside the rack and outside of it, and it is custom-made, too. Its geometry is shown in Figure 4.2.

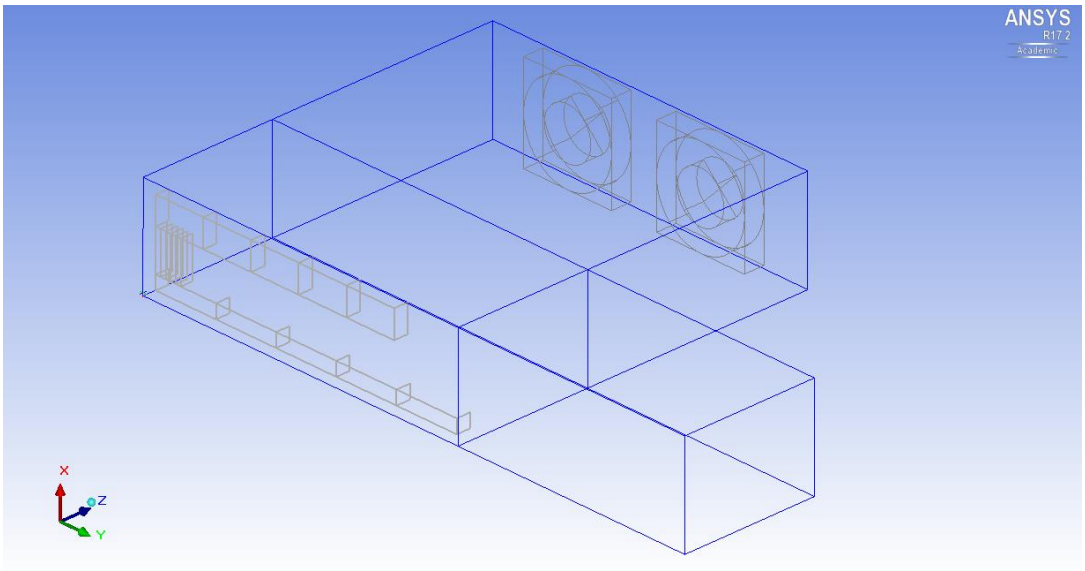

Figure 4.2. Interface – 2 model

Interface – 2 has two fans on the back that has maximum airflow of 0.4666 m^3/min and maximum static pressure of 25 Pa. For heat-dissipation, 25 W is specified which is known beforehand. For grilles on front, 80% open are ratio is specified.

4.1.4. Managed Switch

Managed switch is another off-the-shelf component inside the rack that is used to provide ethernet connection. Its dimensions are 0.044 × 0.44 × 0.173 m (H × W × D) as provided by the manufacturer.

A solid block with total power of 19.3 W, which is taken from manufacturers datasheet, is created inside the rack to represent Managed Switch. Since it does not

have any fans for forced convection and grilles it has are on the side, airflow inside Managed Switch is assumed to be negligible. Only its effect on heat-dissipation and airflow inside the rack is considered.

4.1.5. Box – 1 and Box – 2

Box – 1 and Box – 2 are two custom-made components used for providing necessary input/output features. Their dimensions are 0.095 × 0.444 × 0.110 m (H × W × D) for Box – 1, and 0.092 × 0.444 × 0.342 m (H × W × D) for Box – 2.

Neither of these products have fans for forced convection, therefore, they are modeled as hollow blocks similar to Managed Switch, but with grilles. Box – 1 and Box – 2 both have 5 W heat dissipations.

4.1.6. UPS

UPS is the component responsible for providing power in case of a power cut. Therefore, it is in idle mode, or “On-line Mode” as the manufacturer states, during all the operations detailed in this study. Dimensions of UPS are 0.0840 × 0.428 × 0.4260 m (H × W × D) as provided by the manufacturer. The model created for this component is shown in Figure 4.3.

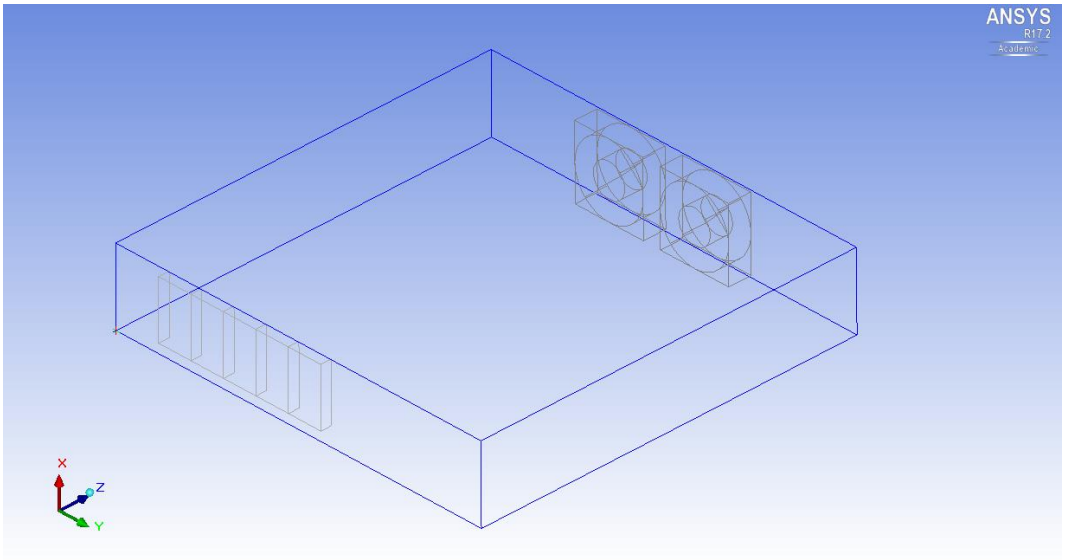

Figure 4.3. UPS model

Note that UPS has two parts, namely controller and battery. Controller is the one with two fans on the back and grilles on the front with an open area ratio of 70%. Heat dissipation of battery is assumed to be negligible during idle mode, therefore, it is modeled as hollow block (Caceres et al., 2018). It solely serves as a blockage to the air flow. For controller, a heat source of 168 W is created. This value is calculated from the manufacturers datasheet which states that the efficiency is 88% in this mode. Fans on the back have maximum airflow of 1.32 m^3/min and maximum static pressure of 66.489 Pa.

4.1.7. PDU

PDU is a custom-made component at the bottom of the rack with dimensions of 0.450 × 0.454 × 0.500 m (H × W × D). It is responsible for distributing the power to components inside the rack. The model created for PDU can be seen in Figure 4.4.

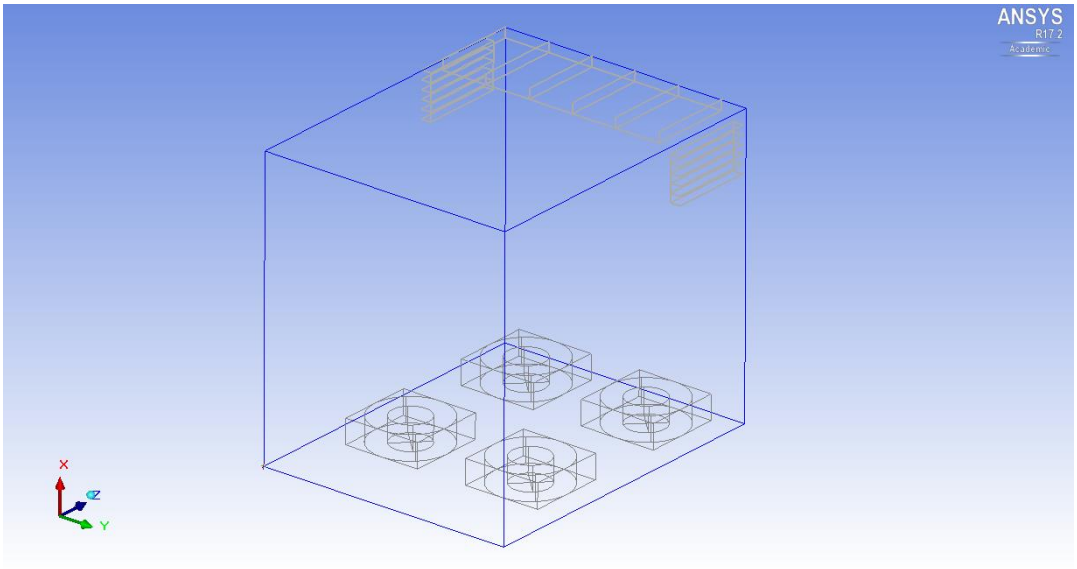

Figure 4.4. PDU model

PDU has 4 fans on the bottom, facing positive-X direction, unlike any other fan inside the rack. These fans are responsible for the vertical air movement inside. They are specified a maximum airflow of 3.88 m^3/min and maximum static pressure of 137 Pa. Grilles on top of the PDU has 80% open area ratio and heat dissipation of PDU is known as 1500 W.

4.1.8. Rack Enclosure and Cables

The rack enclosure has dimensions of 1.940 × 0.510 × 0.656 m (H × W × D) and it is responsible of housing all the components inside the rack. It is modeled using “Plate” objects for the covers and its frame is modeled using solid “Block” objects. Note that some parts of the rack frame are not modeled such as horizontal support brackets for components, holes for bolts, etc. (Choi et al., 2007).

Rack has grilles on top with an open area ratio of 70%. This surface acts as an outlet for the whole cabinet as most of the hot air exits the cabinet here. In an ideal case, all of the air should leave cabinet from this plane.

Some of the cables that significantly affect the airflow are modeled using solid block objects. Figure 4.5 shows the cables on the outlet of the PDU and, Figure 4.6 shows their model. Note that whole purpose of these models is to alter the airflow.

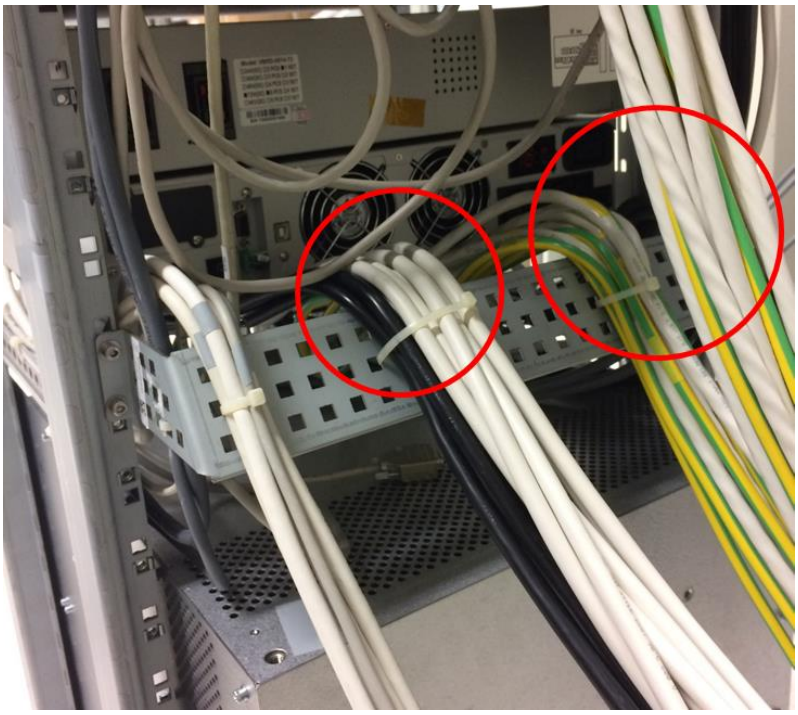

Figure 4.5. Cables on the outlet of the PDU

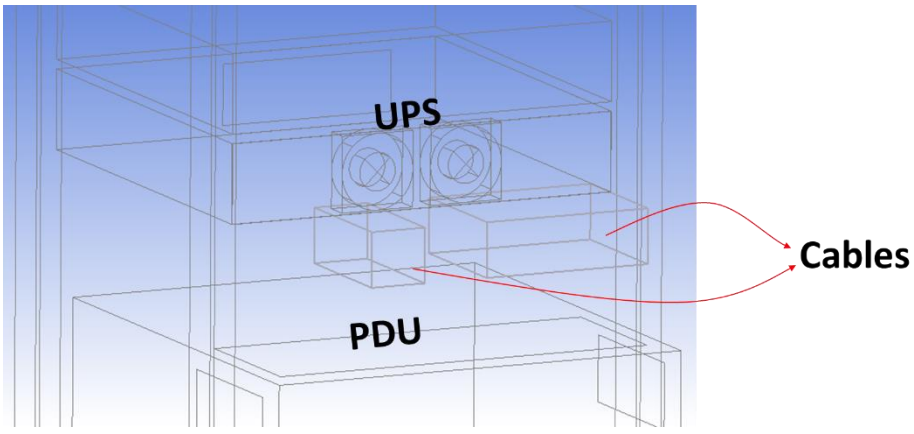

Figure 4.6. Model for cables on the outlet of the PDU

There are also cables on top of the PDU that cover the space in between PDU and UPS. Figure 4.7 shows these cables and Figure 4.8 presents the model created for them.

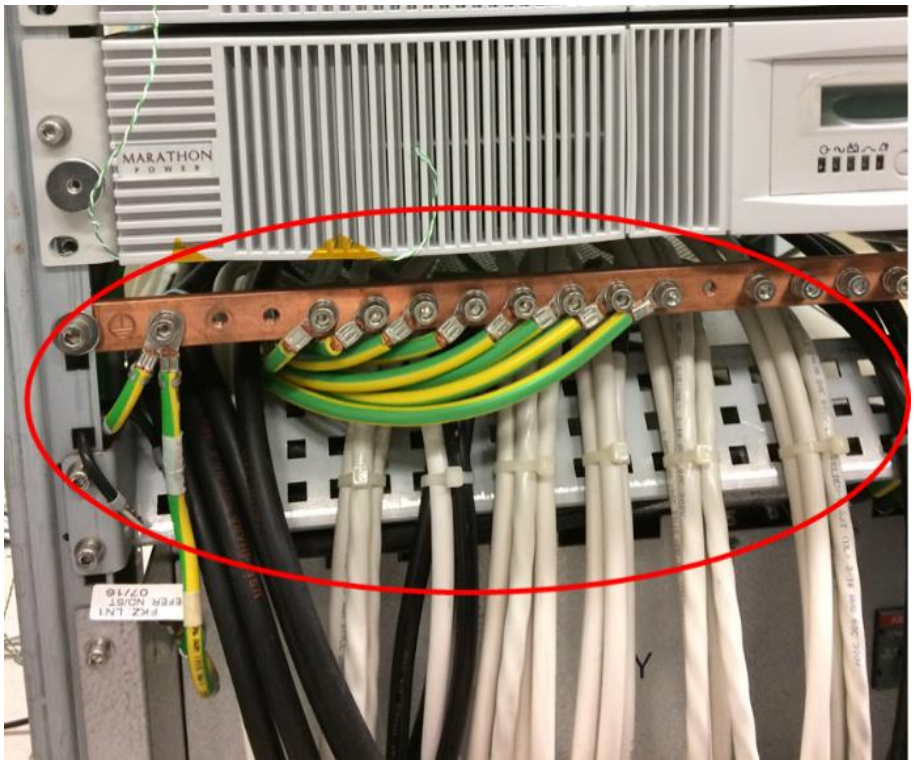

Figure 4.7. Cables in between PDU and UPS

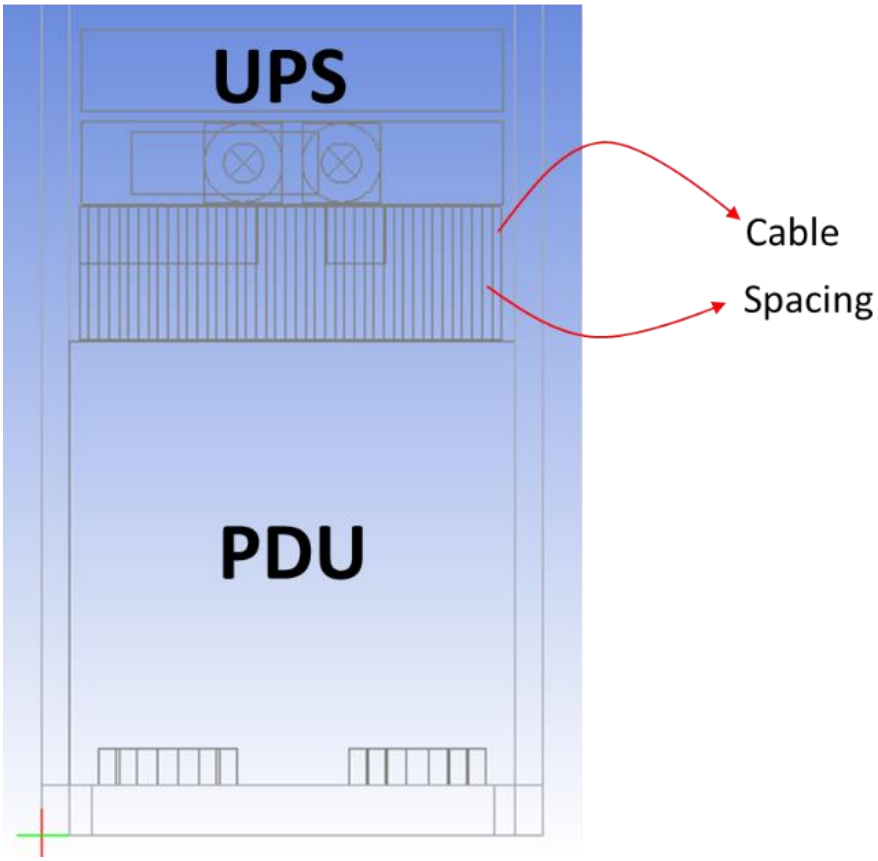

Figure 4.8. Model for cables in between PDU and UPS

As Figure 4.7 shows, there are some openings in between the cable bundles, which are specified in Figure 4.8. These cables are also modeled using solid blocks.

Rest of the modeled cables cover the spacings in between Interface – 1, Interface – 2, Managed Switch and Box – 1. These cables are shown in Figure 4.9 and modeled versions are presented in Figure 4.10

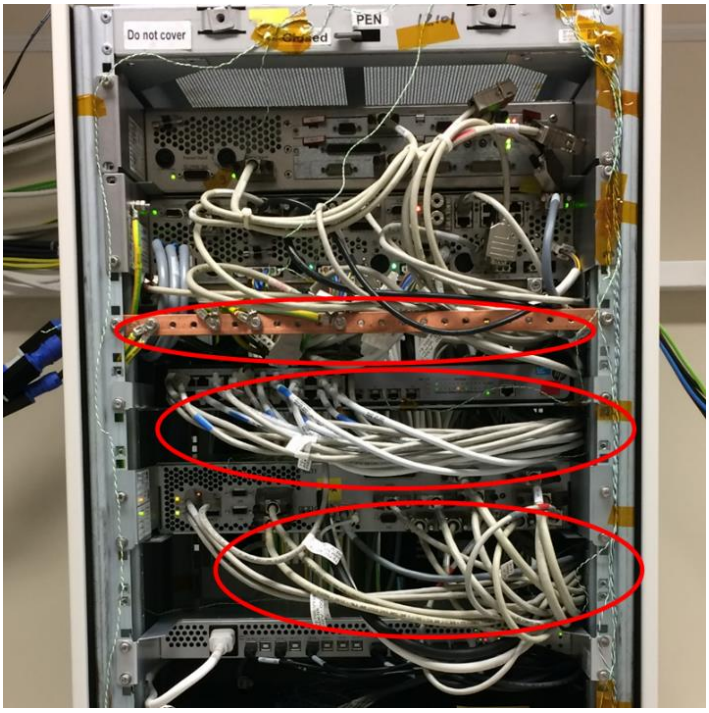

Figure 4.9. Cables in between interfaces, Managed Switch and Box – 1

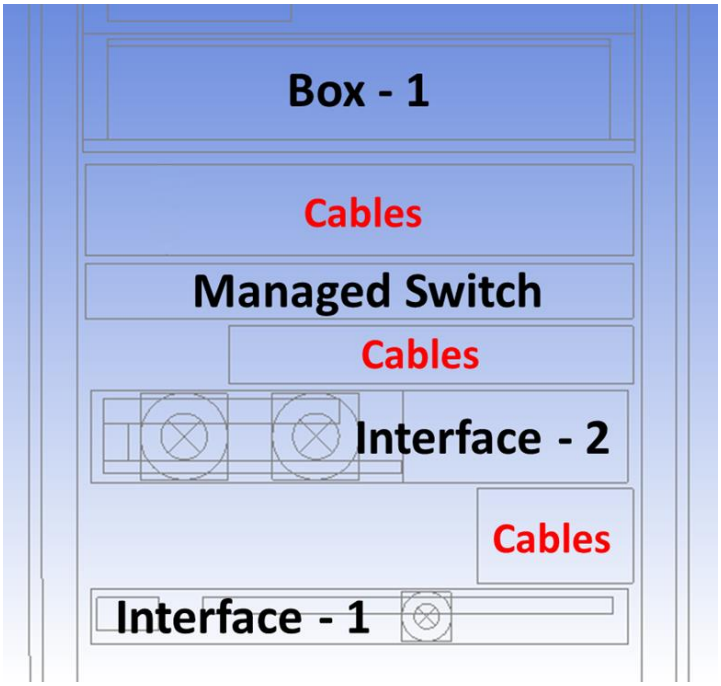

Figure 4.10. Modeled cables in between interfaces, Managed Switch and Box – 1

After each component and rack enclosure is modeled, components are placed inside the cabinet. Figure 4.11 shows the cabinet with all components inside. An assembly is created for the cabinet so that a non-conformal mesh can be created outside the cabinet where velocity and temperature fluctuations are comparatively small. This assembly is given a maximum element size of 0.007 m, and 0.02 m slack on y and z-directions. Another assembly covers vicinity of the cabinet and is given coarser mesh compared to cabinet assembly. From this assembly towards the boundaries, mesh gets coarser and coarser. At domain boundaries, finer mesh is created to capture temperature gradients due to boundary condition.

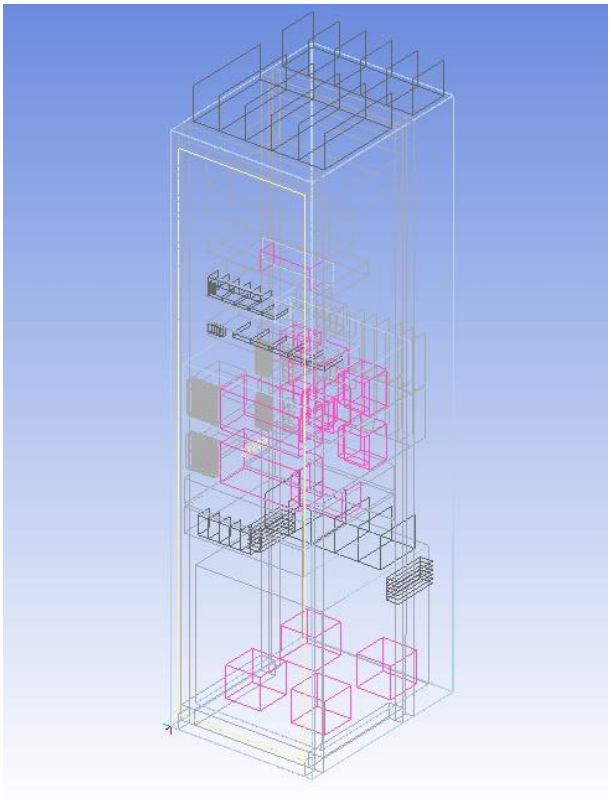

Figure 4.11. Whole rack model

Solution domain has dimensions of 2.50 m, 3.51 m and 2.656 m in x, y and z directions, respectively. Figure 4.12 shows the domain with cabinet in an assembly for clarity.

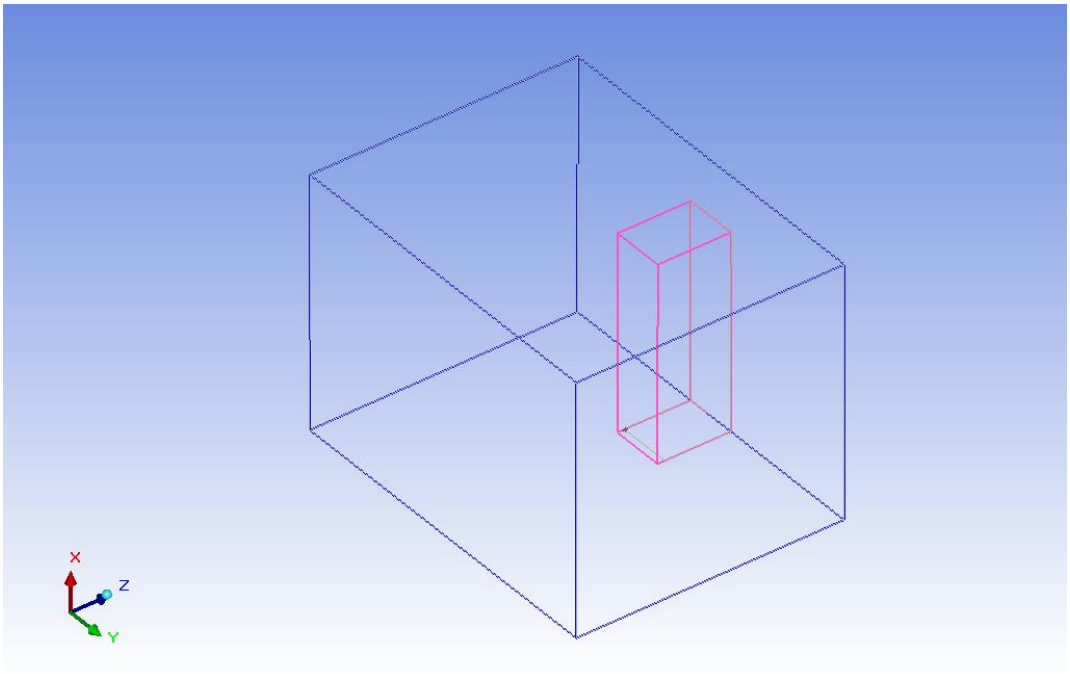

Figure 4.12. Domain with cabinet

All in all, mesh created for the whole cabinet has 10861148 elements with a minimum skewness of 0.159. These low-quality meshes are again on certain fans where surfaces are circular, and they do not adversely affect the solution since average skewness is 0.83. Figure 4.13 shows the top view of the mesh created for whole domain.

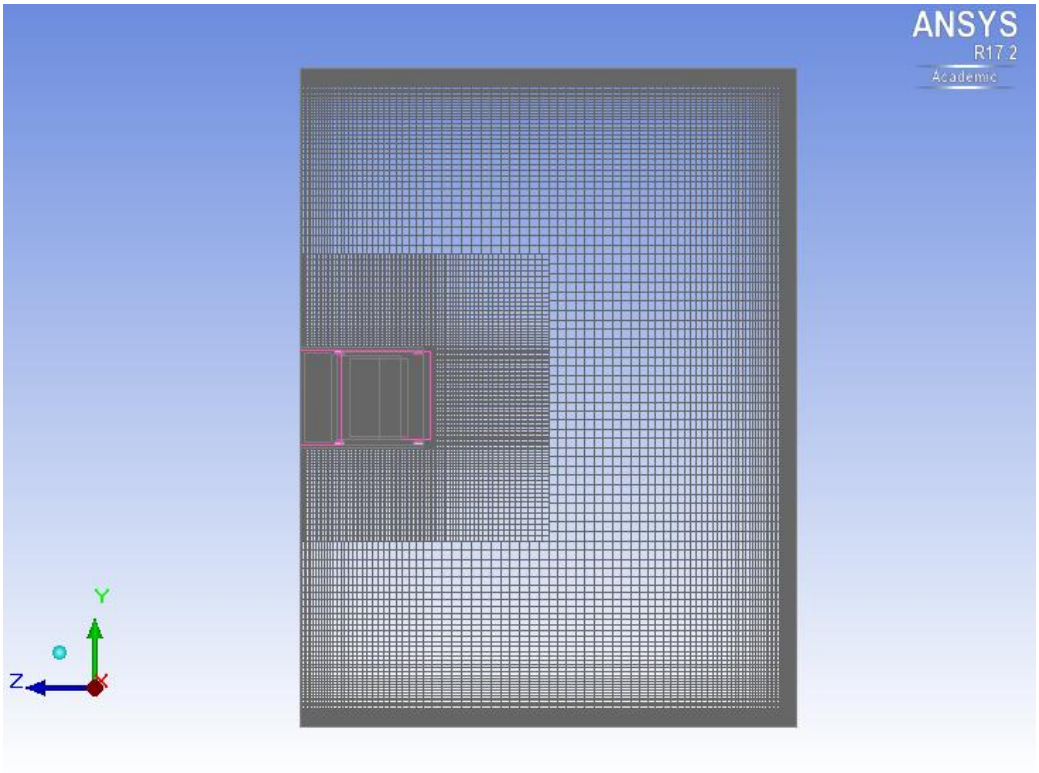

Figure 4.13. Top view of mesh

4.2. Solver Details

Governing equations of fluid flow and heat transfer are presented in previous chapter and omitted here for clarity. Similar to Workstation – 1, numerical model created for whole cabinet is steady-state, turbulent, incompressible and single-phase fluid flow in which natural convections effects are accounted for with a gravitational acceleration (g) of 9.81 m/s^2. Turbulence model used in this numerical model is also $k-\varepsilon$. SIMPLE algorithm is used for pressure-velocity coupling, whereas Standard scheme is chosen for pressure interpolation. Second-order discretization is used for spatial discretization after a first-cut solution is obtained using first-order discretization. For natural-convection effects, Boussinesq model with input density of 1.614 kg/m^3 and operating pressure of 101325 N/m^2 is used, which is;

$$(\rho - \rho_0) \cong -\rho_0 \beta (T - T_0)$$

where ρ_0 is the constant density of the flow and T_0 is the operating temperature. Radiation is neglected as models with radiation not neglected did not produce significantly different results.

Non-slip wall with a constant temperature of 20 ℃ is applied for all boundaries of the room. Fan boundary condition is used for every fan inside the cabinet and all fan curves are taken as piece-wise linear relationships. Figure 4.14 shows an example fan curve taken from the manufacturer's datasheet and digitized version of that same curve side by side. Note that "mmH_2O" is used since this is the unit provided by the manufacturer.

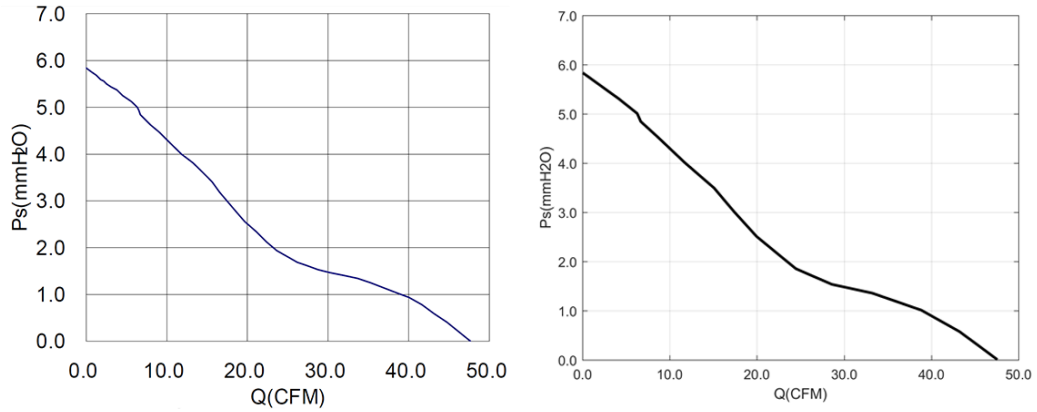

Figure 4.14. Fan Curve Digitization Example

This piece-wise linear fan curve along with swirl magnitude and flow direction are the inputs for the fan boundary condition. Then, FLUENT applies a pressure jump to the surface of the fan by calculating pressure rise across it according to the input fan curve relationship.

For grilles, a porous jump boundary condition is created with pressure-jump coefficient calculated from open-area ratio input, as mentioned in previous sections. Most components other than workstations have the same grille pattern with an open-

area ratio of 80%; therefore, all grilles in these components are assumed to have the same ratio for simplicity.

For volumetric heat generations, cell-zones with energy source terms are used according to the heat generation of the component. These sources are assumed to cover the whole volume of the fluid inside the component.

4.3. Material Properties

Variable thermophysical fluid properties are used in the cabinet model. A new fluid material is created in Icepak with piece-wise linear properties of air, namely thermal conductivity k (W/(m·K), thermal diffusivity α (m^2/s), which is equal to $\frac{k}{\rho C_p}$, and dynamic viscosity μ (kg/(m·s)) taken from Cengel, (2003). A total of 17 data points ranging from 0 ℃ to 120 ℃ are used to be on the conservative side, although the temperatures inside the cabinet never reach these extremes. Specific heat, c_p (J/kg·K) is taken constant at 1005 J/(kg·K) since its variation in this temperature range is insignificant. Density and volumetric expansion coefficient inputs for Boussinesq approximation are 1.614 kg/m^3 and 0.00333 1/K, respectively. These properties are defined for the default fluid of the model.

Table 4.1 shows the property values used.

Table 4.1. *Properties of air (at 1 atm), taken from Cengel, (2003)*

Temperature, T, (°C)	Thermal Conductivity k (W/(m·K)	Thermal Diffusivity $\alpha \times 10^{-5}$ (m^2/s)	Dynamic Viscosity $\mu \times 10^{-5}$ (kg/(m·s))
0	0.02364	1.818	1.729
5	0.02401	1.880	1.754
10	0.02439	1.944	1.778
15	0.02476	2.009	1.802
20	0.02514	2.074	1.825
25	0.02551	2.141	1.849
30	0.02588	2.208	1.872
35	0.02625	2.277	1.895
40	0.02662	2.346	1.918
45	0.02699	2.416	1.941
50	0.02735	2.487	1.963
60	0.02808	2.632	2.008
70	0.02881	2.780	2.052
80	0.02953	2.931	2.096
90	0.03024	3.086	2.139
100	0.03095	3.243	2.181
120	0.03235	3.565	2.264

4.4. Mesh Independence Analysis

Three different mesh configurations are compared to get a mesh independent solution. These configurations have total element number of 8781955, 9688728 and 10861148. A reference line is chosen that goes along the back of the cabinet in x-direction, as temperature gradients are high in this area. Figure 4.15 shows the reference line.

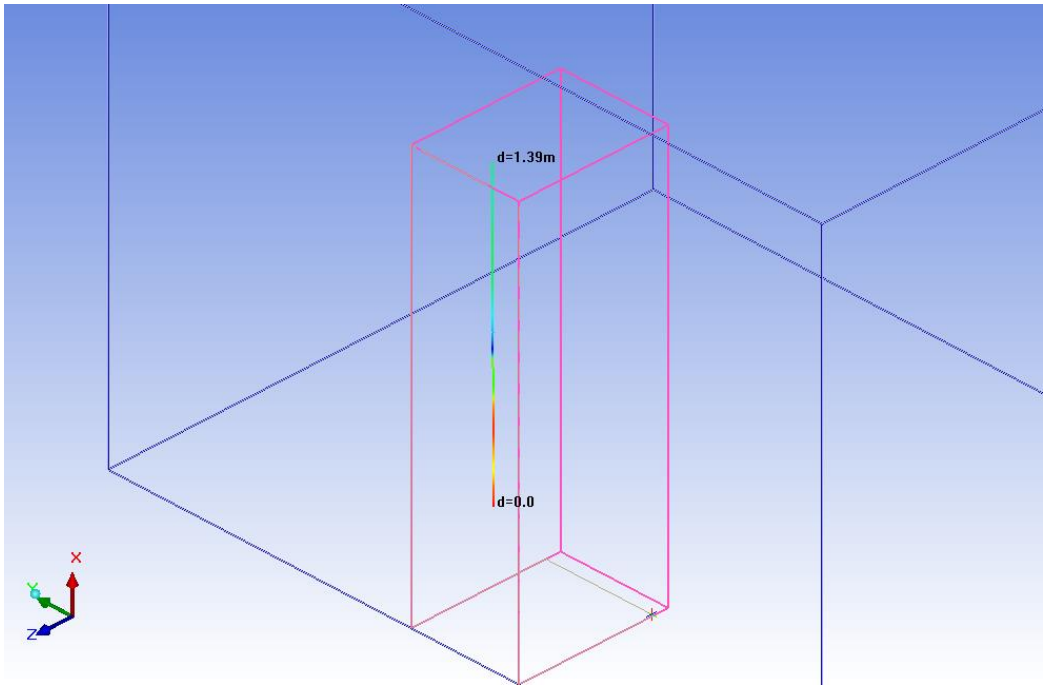

Figure 4.15. Reference line for cabinet, z = 0.6m, y = 0.255m, starting at x = 0.55m

100 computational temperature results are taken along this line and compared to each other in Figure 4.16.

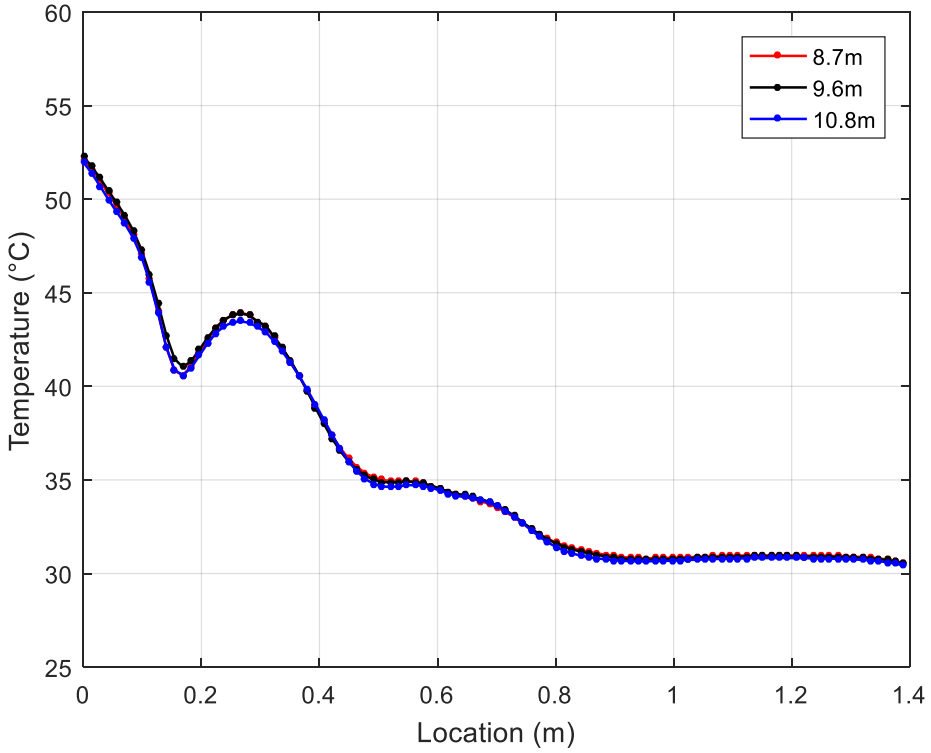

Figure 4.16. Temperatures along the reference line

As it can be seen, three mesh configurations are almost the same except for a few locations. The reason for such a close result for different mesh configurations is the number of assemblies, where the mesh is refined. As the mesh is locally refined in these regions, increasing the number of mesh in the rest of the system, where fluctuations are not significant, hence there is no assembly, does not affect the results. Therefore, mesh is deemed to be independent and the rest of the models are created using 10m mesh configuration.

4.5. Results and Discussion

Figure 4.17, Figure 4.18 and Figure 4.19 show the temperature distribution on xy, yz and xz planes, respectively.

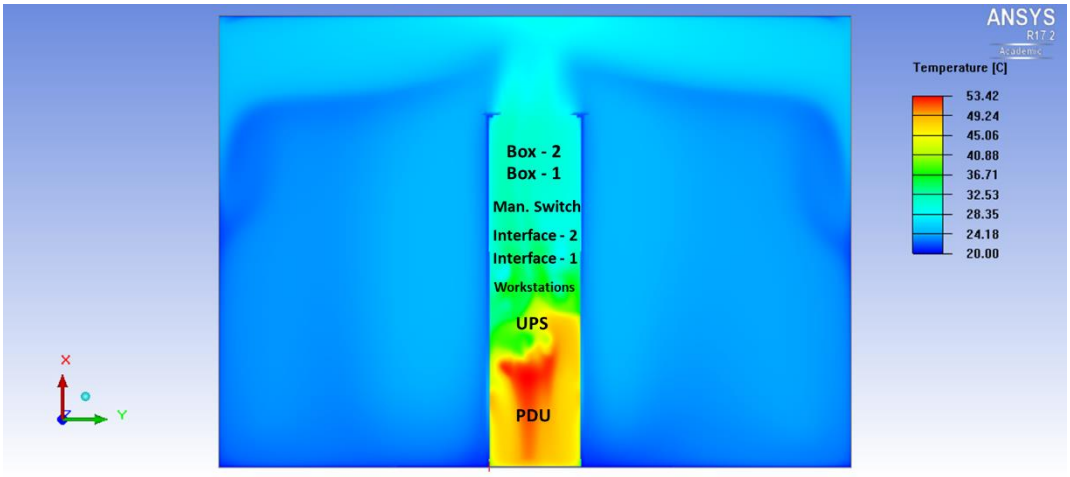

Figure 4.17. Temperature distribution on cabinet back plane (z = 0.6m)

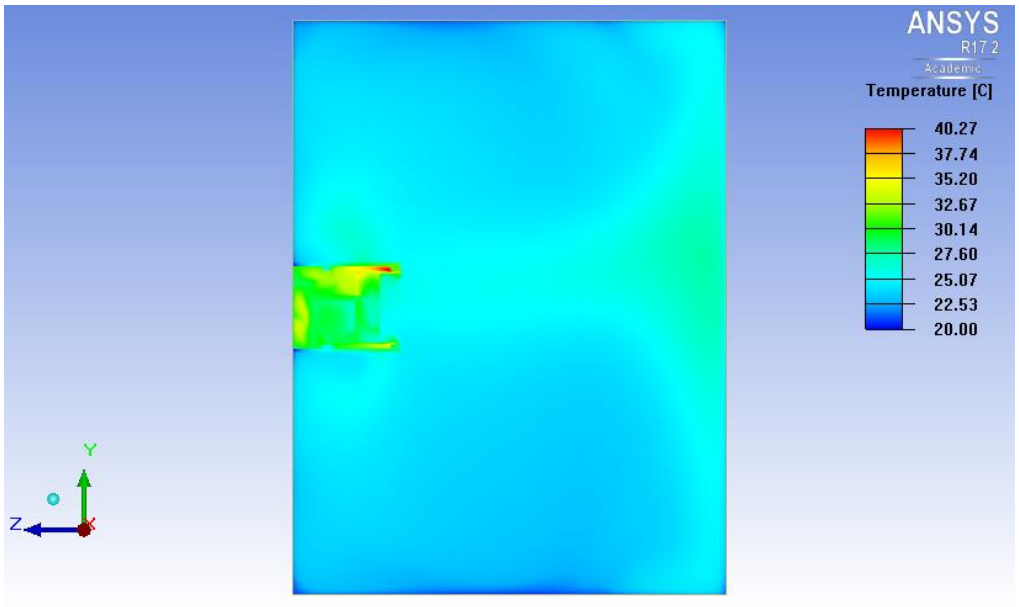

Figure 4.18. Temperature distribution on room center plane (x = 1.25m)

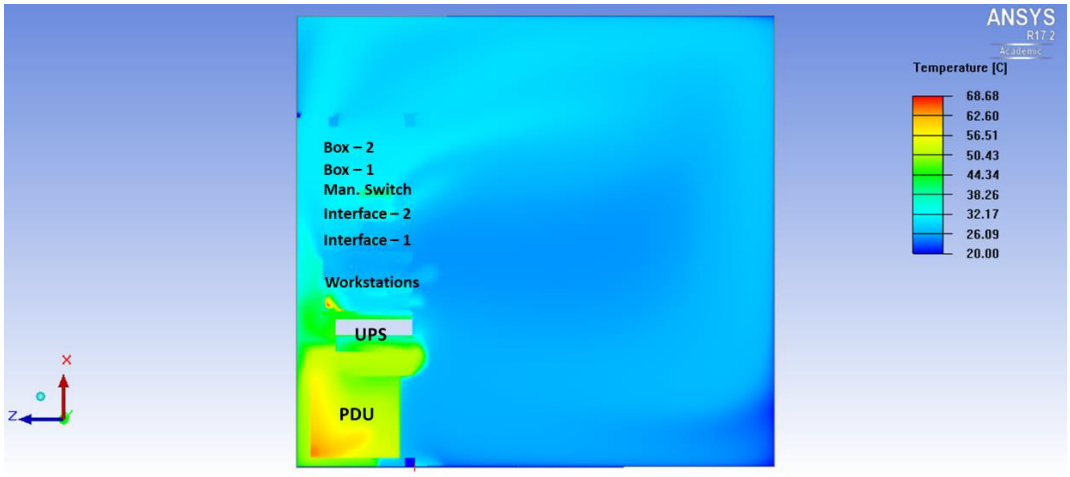

Figure 4.19. Temperature distribution on cabinet center plane (y = 0.255m)

From these figures it can be concluded that largest hotspots occur near Workstation – 1 and PDU as these two components are the largest heat dissipaters. Hot spot in Figure 4.19 occurs inside the Workstation – 1 near GPU's.

Figure 4.17 shows that hot air leaving the cabinet on top grilles gets cooled down by the top and side walls and heats up whole domain, as expected. Figure 4.20 shows the temperature distribution on bottom right corner of *yz* plane in detail.

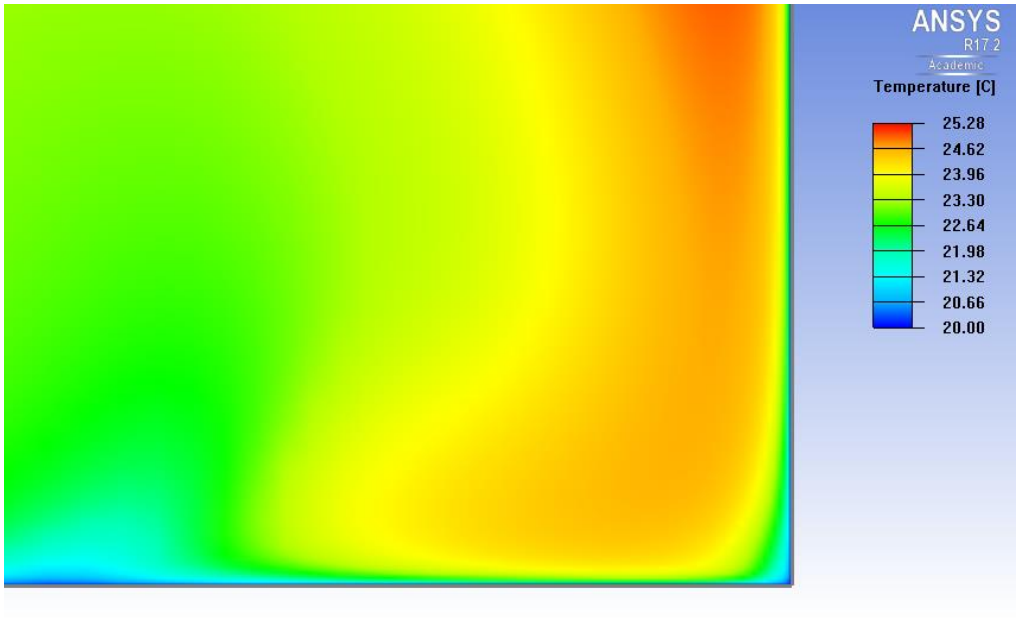

Figure 4.20. Detail of temperature distribution on bottom right corner of yz plane (x = 1.25m)

To compare with experimental data and validate the model, 19 computational temperature results are taken on locations same as experimental part. Figure 4.21 shows the experimental and numerical data with error bars calculated in Section 2.2.

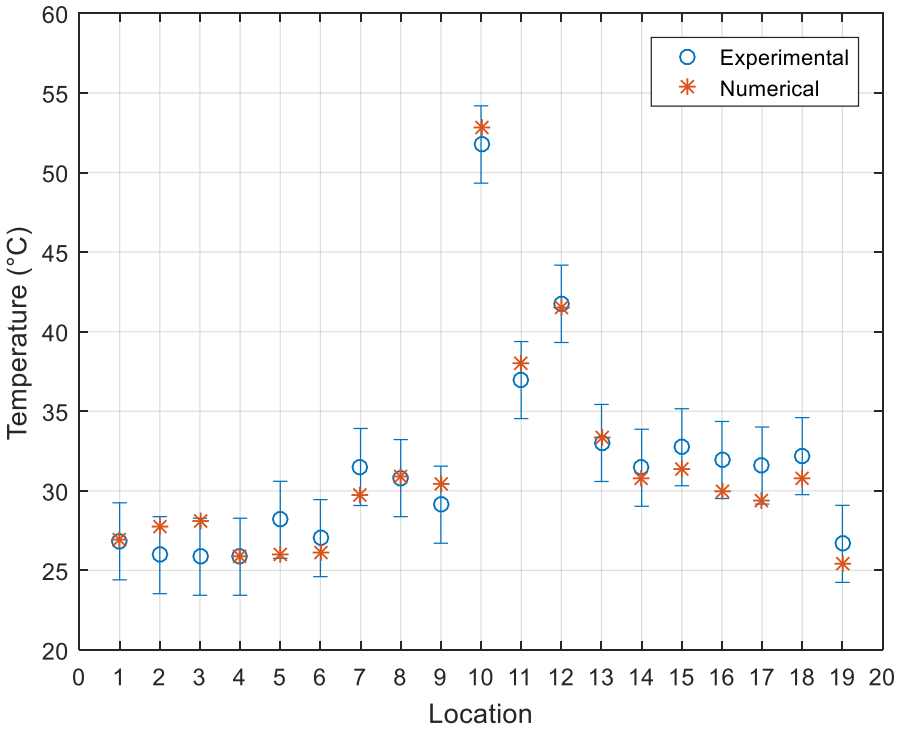

Figure 4.21. Comparison of experimental and numerical temperature results

Since all computational temperature measurements are inside error range, computational model Is deemed validated. Future models will be built upon this base model.

Maximum temperatures of parts inside Workstations of computational model are checked again to make sure they operate under the limit. Table 4.2 presents the maximum temperatures and operating limits of corresponding parts.

Table 4.2. *Maximum temperatures and operating temperature limits*

Part	WS-1 (°C)	WS-2 (°C)	Maximum Limit (°C)
CPU-1	57.25	-	87
CPU-2	53.23	54.91	87
GPU-1	68.93	-	95
GPU-2	69.25	-	95
GPU-3	92.37	48.95	95
PCIe-1	43.39	32.07	60
PCIe-2	50.16	33.32	60
HDD	38.76	27.09	60
RAM	69.02	63.38	95

As it can be seen, all parts operate under their temperature limits without a front cover. For verification of the model, a simple energy balance between domain wall boundaries and air inside is conducted. For this purpose, heat flow from every wall to the fluid inside the domain is calculated through Icepak. Table 4.3 presents heat flow values along with total heat generation in the domain.

Table 4.3. *Energy Balance*

Boundary	Heat Flow (W)
Q_{x1}	402.51
Q_{x2}	514.20
Q_{y1}	110.80
Q_{y2}	89.92
Q_{z1}	940.08
Q_{z2}	214.98
Q_{total}	2272.49
Q_{gen}	2272.00

There is a 0.49 W difference; therefore, it is assumed that energy balance upholds, and the numerical model is verified.

The effects of modeling the Workstations with as much detail as possible is investigated by comparing the base numerical model with one that does not have any workstation details. This model, called “Lumped model” only has fans and heat sources in its workstation models. Figure 4.22 shows the comparison of temperatures.

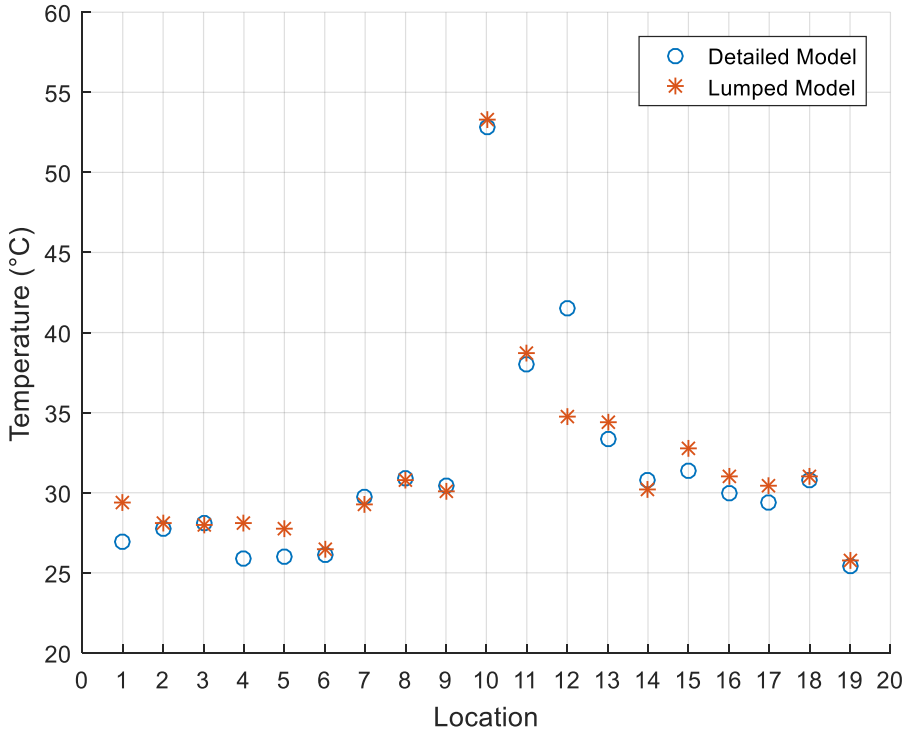

Figure 4.22. Comparison of detailed model and lumped model

Note that the detailed model is the same as the validated model. As the figure shows, lumped model misses the temperature at location 12 greatly, as this location is one of the Workstation – 1 outlets. This shows that modeling the workstations as detailed as possible is important since temperatures at Workstation – 1 outlet vary greatly.

The effects of natural convection are investigated by turning it off. Figure 4.23 shows the 19 computational temperature measurements for validated model and model without natural convection.

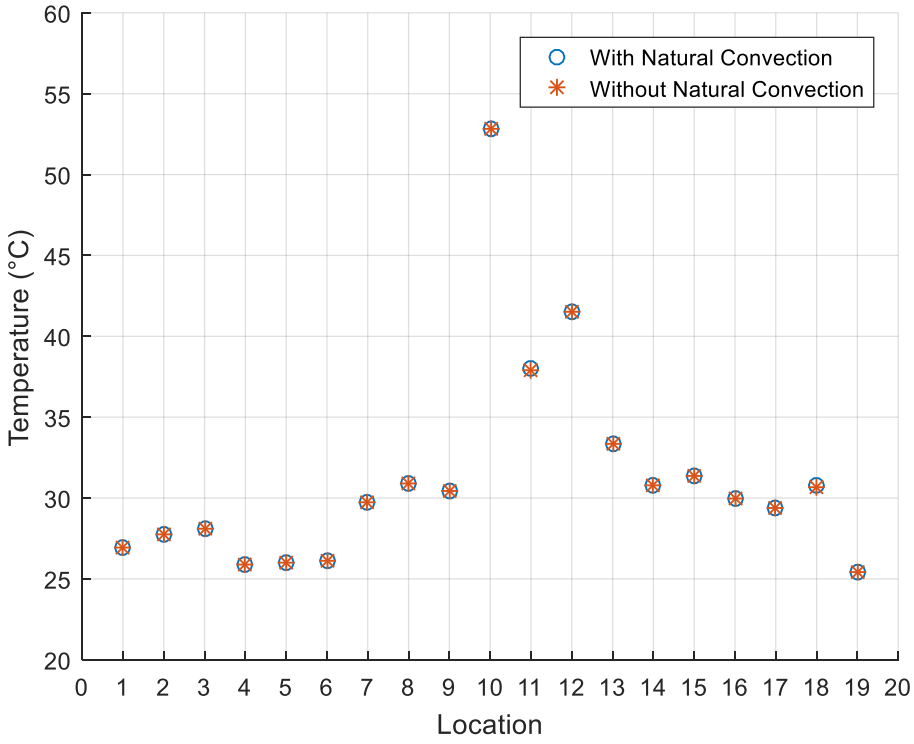

Figure 4.23. Comparison of models with and without natural convection

As figure shows, there is no difference between the two models with biggest difference being 0.05 °C. This shows that forced convection is the dominant cooling mechanism inside the cabinet. As most of the components have their own fans for cooling, these results are expected can be supported by comparing the effects of forced and natural convection by calculating Gr_L/Re_L^2, where Gr_L is the Grashof number, indicating the ratio of buoyancy forces to viscous forces acting on the fluid, and Re_L is the Reynolds

number, indicating the ratio of inertial forces to viscous forces (Bergman et al., 2011). Therefore, the ratio becomes;

$$Gr_L/Re_L^2 = \frac{g\beta(\Delta T)L}{v^2}$$

where L is the characteristic length and v is the velocity. Natural convection effects can be neglected when $Gr_L/Re_L^2 \ll 1$. When this ratio is calculated for upper horizontal plate of the Workstation – 1, where the largest hot spots occur, it becomes,

$$Gr_L/Re_L^2 = \frac{g\beta(\Delta T)L}{v^2} = 0.043$$

where ΔT is taken as 20 °C, the difference between maximum allowable temperature for inlet of Workstation – 1, 40 °C, and ambient temperature of 20 °C, L is the length of the plate, 0.497 m, and v is taken as the half of the maximum velocity inside the workstation, which is 2.75 m/s and occurs on the inlet fans. Since the ratio is fairly smaller than 1, natural convection effects are very insignificant as found in the comparison.

4.5.1. Model without Cables

The same model without any cables is modeled to investigate a scenario in which cables do not interfere with the heat and airflow. This scenario may occur in real life when cables are bundled and positioned so that they do not block airflow and result in a different temperature field. Figure 4.24 shows the comparison of temperatures for validated model and the model without any cables.

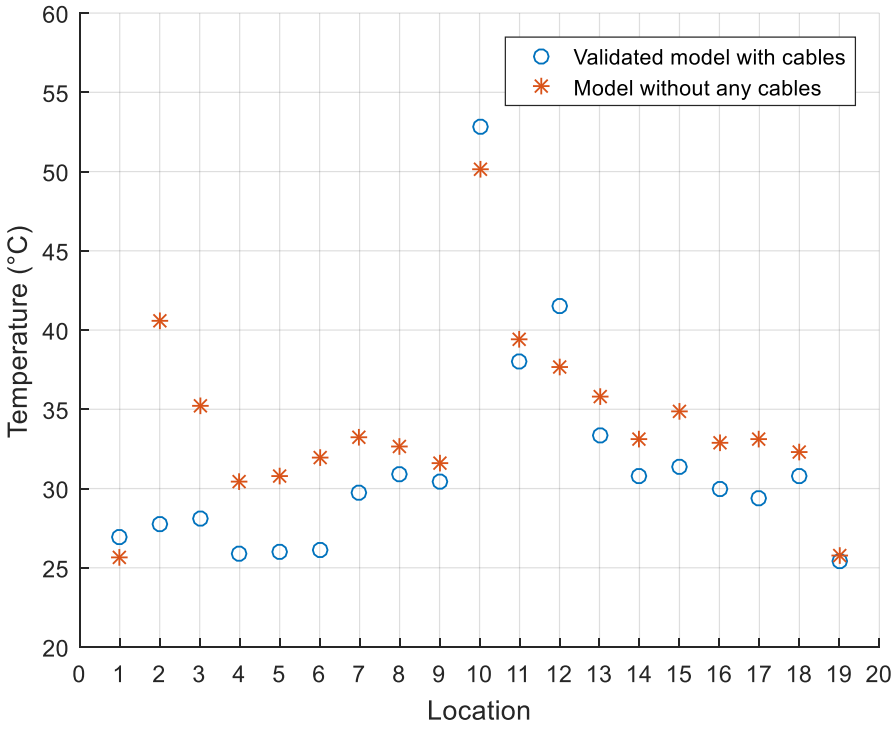

Figure 4.24. Effects of modelling cables

As can be seen, locations 2 and 3 have two highest absolute differences with 12.80 ℃ and 7.19 ℃, respectively, where temperature at location 2 is way over the limit of 30 ℃. These differences occur as hot air leaving PDU goes to the front plane of the cabinet rather than to the outlet and heats up the inlets of the components. In validated model in which cables are modeled, this leakage is prevented by cables. Figure 4.25 shows the cables on the outlet of PDU.

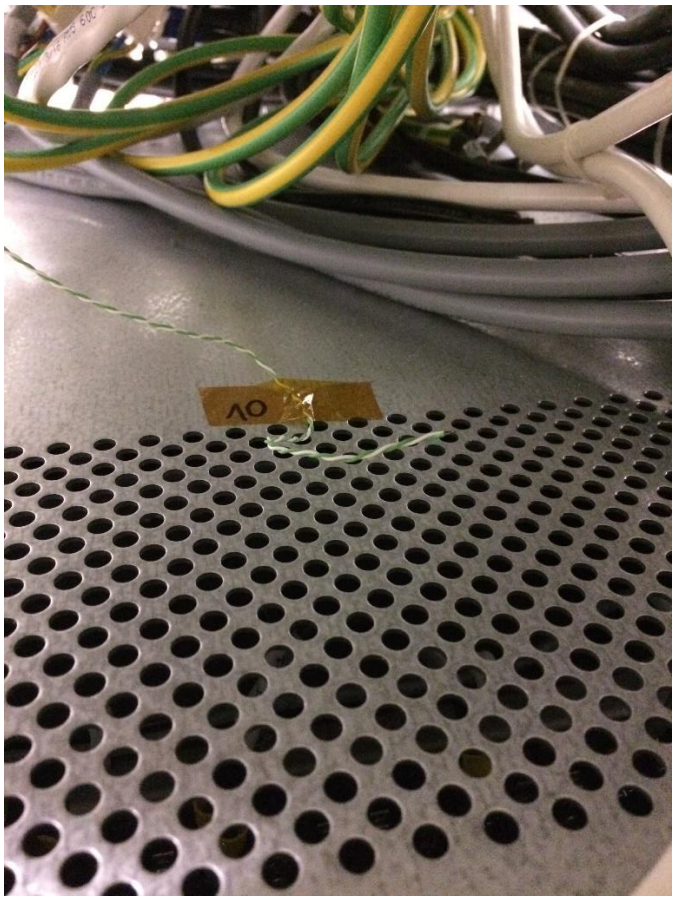

Figure 4.25. Cables on outlet of PDU

These cables lead to a hotspot around the outlet of the PDU, and block some of the airflow and redirect it. This is also the reason for high outlet temperatures for PDU and Workstation – 1, or locations 10 and 12, in model with cables compared to model without. This shows the importance of modeling cables as they significantly affect the temperature field. fIt should also be noted that in the leakage model, UPS and Workstation – 1 inlets are above the temperature limits, 30 ℃ and 40 ℃, respectively. This means that a cabinet with cables perfectly taken out of the way of the airflow cannot be operated without providing any solutions for the air leakage and hot air recirculation.

4.5.2. Blanking Panels

Blanking panels are widely used in the industry as an answer to hot air recirculation. These panels block the airflow through gaps inside the cabinet and prevent overheating (Rasmussen, 2009). Strong et al. (2009) investigated the effects of blanking panels in a server cabinet using CFD and found out that blanking panels reduced the amount of hot air recirculation significantly. Figure 4.26 shows their results.

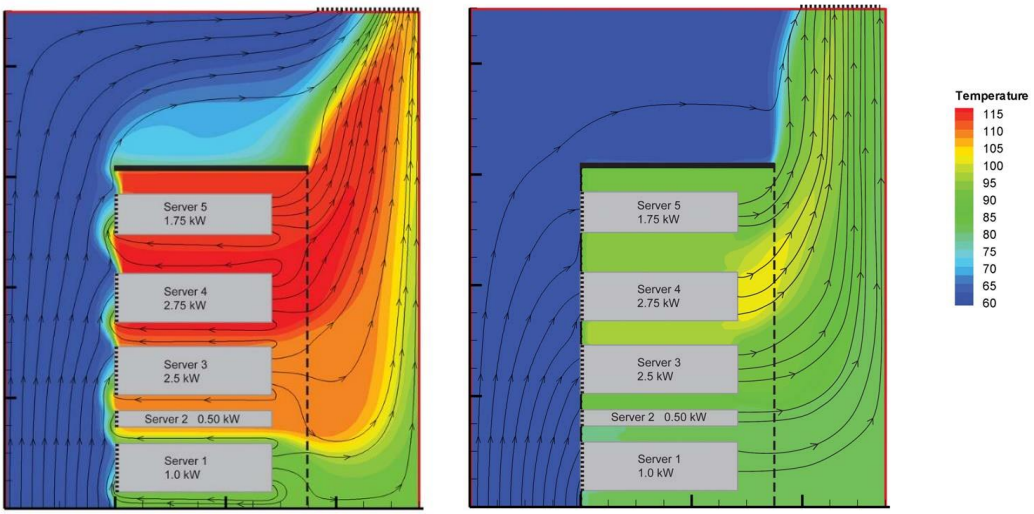

Figure 4.26. Temperature field without blanking panels and with blanking panels. Adapted from Strong et al. (2009)

In this study, effects of blanking panels are investigated by placing thin plates in between the components to prevent leakage through front plane that occurred in the previous model. Figure 4.27 shows an example blanking panel used in between Interface – 1 and 2.

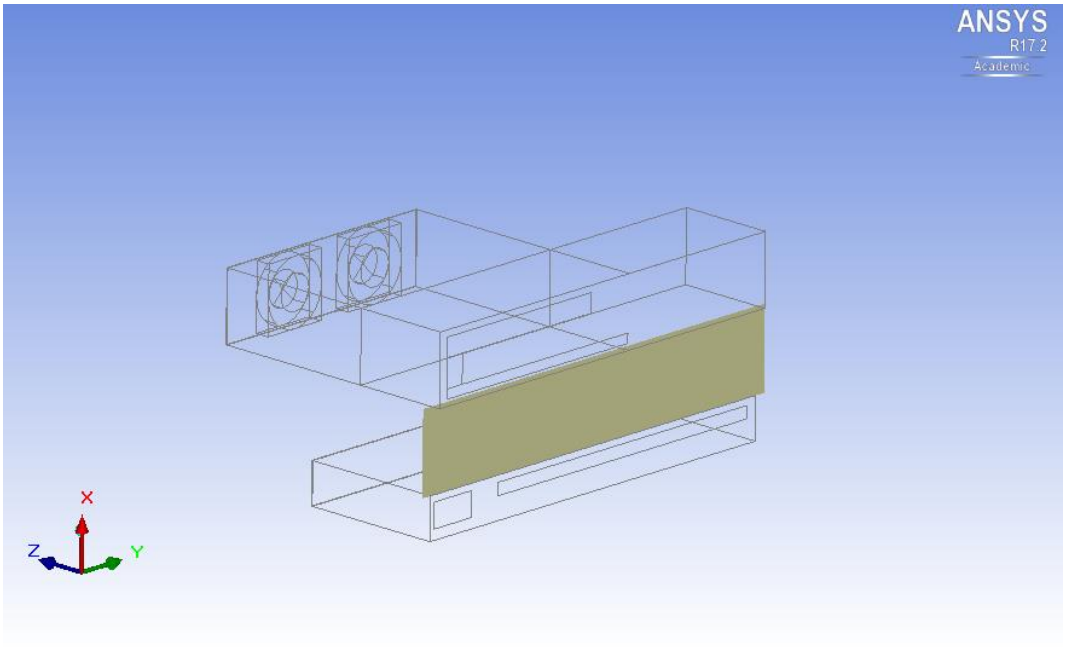

Figure 4.27. Example blanking panel. Other components are omitted for clarity.

The rest of the model and solver parameters are left as they were in the previous model without any cables. Figure 4.28, Figure 4.29 and Figure 4.30 show the temperature fields obtained.

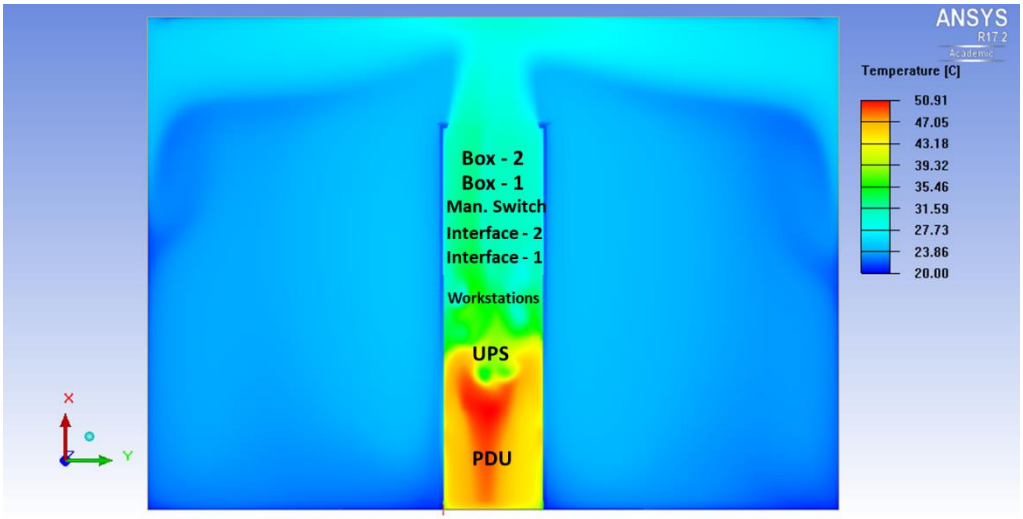

Figure 4.28. Temperature distribution on cabinet back plane, with blanking panels (z = 0.6m)

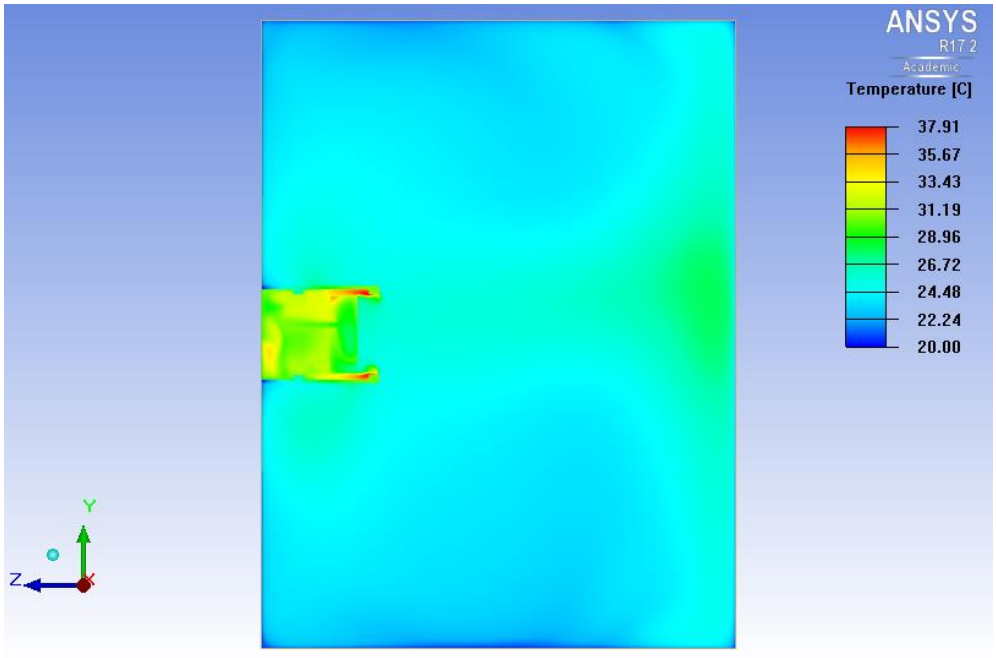

Figure 4.29. Temperature distribution on room center plane, with blanking panels (x = 1.25m)

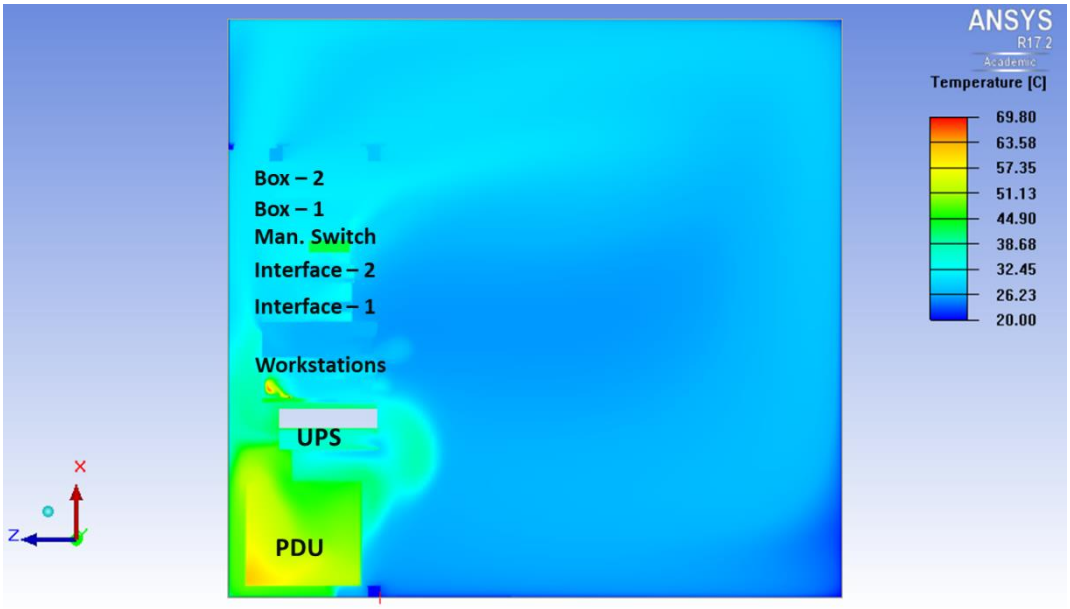

Figure 4.30. Temperature distribution on cabinet center plane, with blanking panels (y = 0.255m)

The figures show that there is still some leakage through the front plane due to the components themselves, rather than the openings in between them. This leakage cannot be prevented by using blanking panels as it would block the inlets. Figure 4.31 compares the temperatures of models with and without blanking panels.

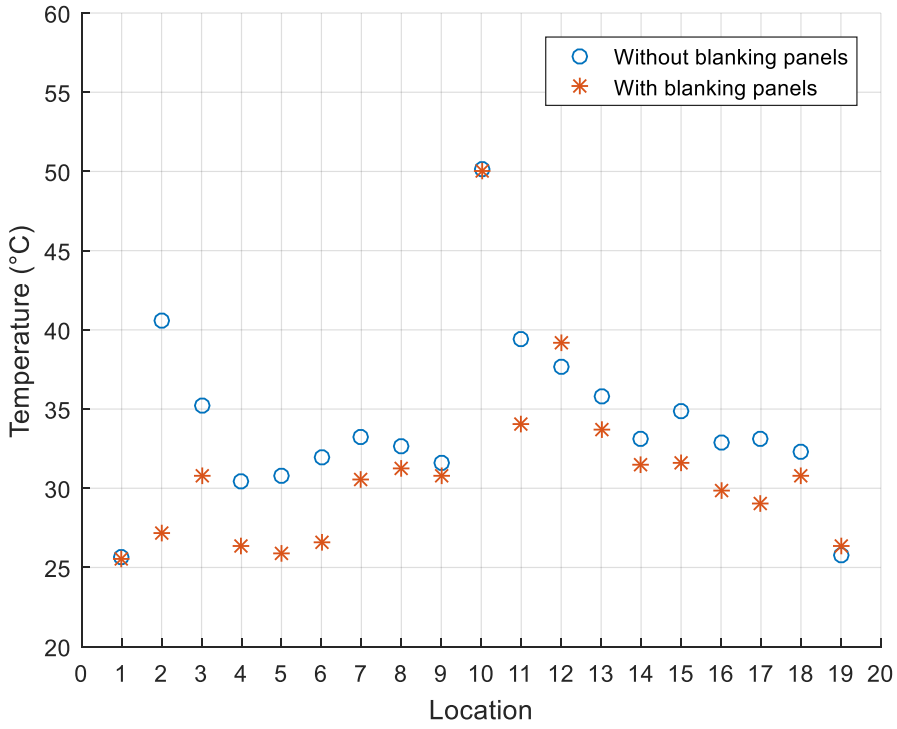

Figure 4.31. Effects of blanking panels

As figure shows, using blanking panels leads to decreased temperatures on all locations except for 12 and 19, where the differences are still very small. Therefore, it can be concluded that blanking panels are effective solutions for preventing leakages for this cabinet.

Figure 4.32 shows the particle traces in xz-plane to see the effect of blanking panels on airflow.

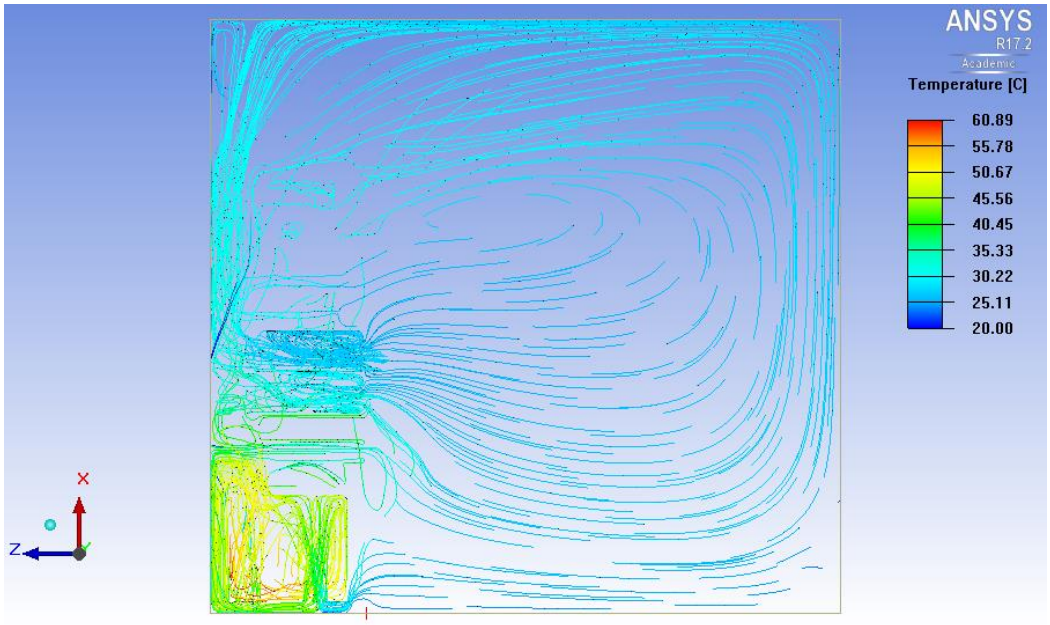

Figure 4.32. Airflow distribution on cabinet center plane with blanking panels (y = 0.255m)

Figure 4.32 shows a more uniform airflow distribution on the front plane of the cabinet as expected. Figure 4.33 and Figure 4.34 show the lower and upper part of the cabinet in detail.

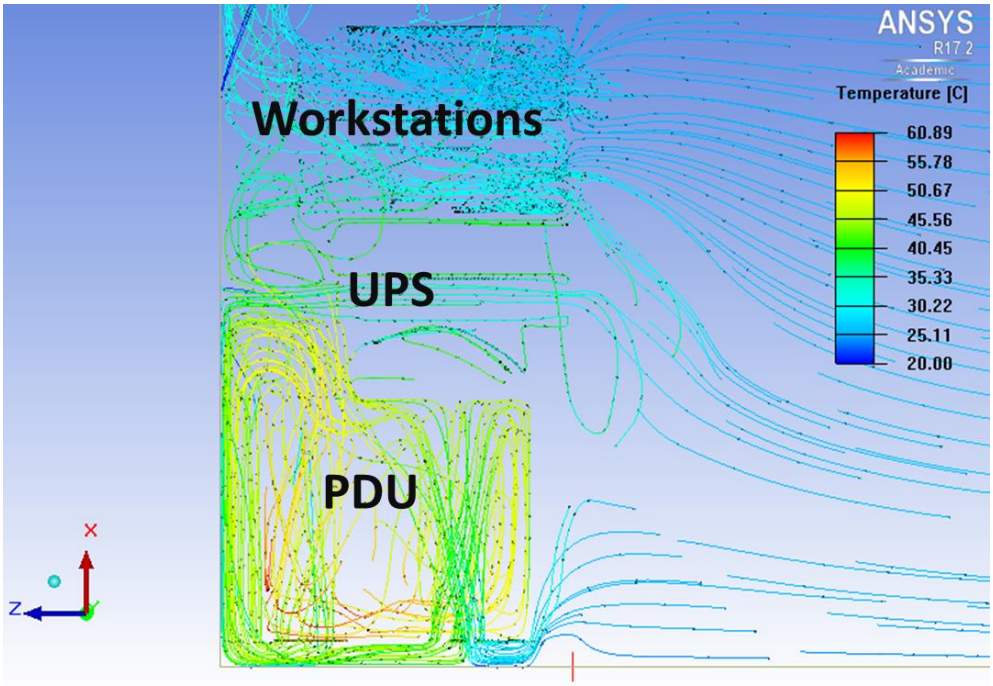

Figure 4.33. Airflow distribution on the lower part of the cabinet center plane (y = 0.255m)

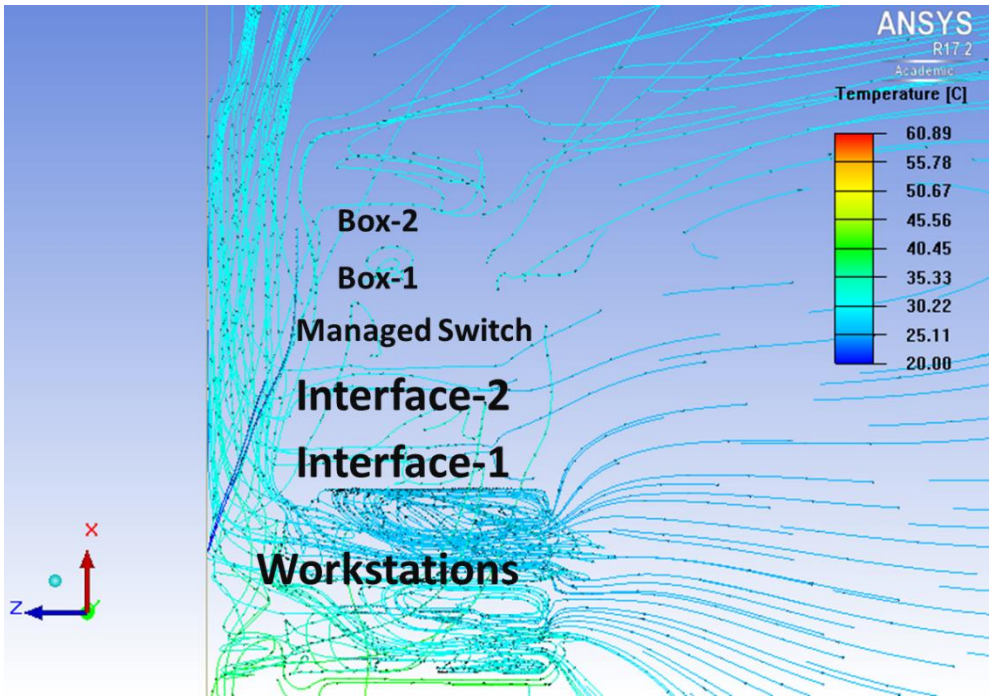

Figure 4.34. Airflow distribution on the upper part of the cabinet center plane (y = 0.255m)

As figure shows, the directions of vectors are all towards cabinet on the front plane, as expected. It can be concluded that preventing the leakage using blanking panels leads to a more uniform airflow on the front plane of the cabinet, which reduces the hot air recirculation and, hence, the temperatures overall.

In this chapter, a mesh independent numerical cabinet model is created and validated using experimental data. The effects of cable model are investigated by comparing models with and without cables. Then, the effects of blanking panels are observed by placing thin plates in between components to prevent leakages due to the absence of cables. Results show that blanking panels are viable options to prevent leakages through the front plane of the cabinet and hot air recirculation which leads to overheating.

CHAPTER 5

FRONT COVER PATTERNS

5.1. Front Cover Details

Initial experiments and modeling are done without any front cover to be able to compare with the effects of having one. These results are compared to two covers with different perforation patterns with the rest of the cabinet being the same as before. A front cover may be needed to create a cage for reducing electromagnetic interference.

A front cover may also be compulsory to have to block the heat and airflow out of front plane of the cabinet, if there is such a requirement. However, presence of a front cover may lead to hotspots itself, in case hot air fails to leave the cabinet and starts to recirculate (Capozzoli & Primiceri, 2015), (Artman et al., 2002). Therefore, it is important to see the effects of having one with different openness rations.

The first modeled front cover has a slot-like pattern as shown in Figure 5.1 and Figure 5.2 with a close-up.

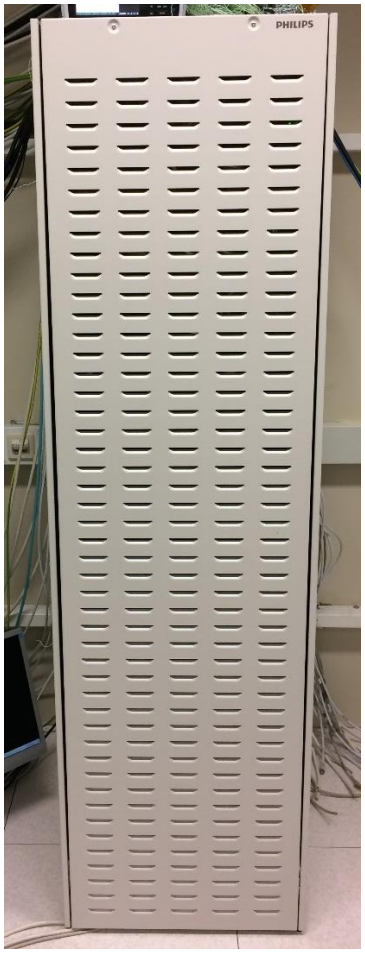

Figure 5.1. Front cover – 1

Figure 5.2. Front cover – 1 close-up

Although the perforation pattern of this front cover is not planar, it is still modeled using grille object.

The second front cover has hexagonal perforation as seen in Figure 5.3 and Figure 5.4 with a close up.

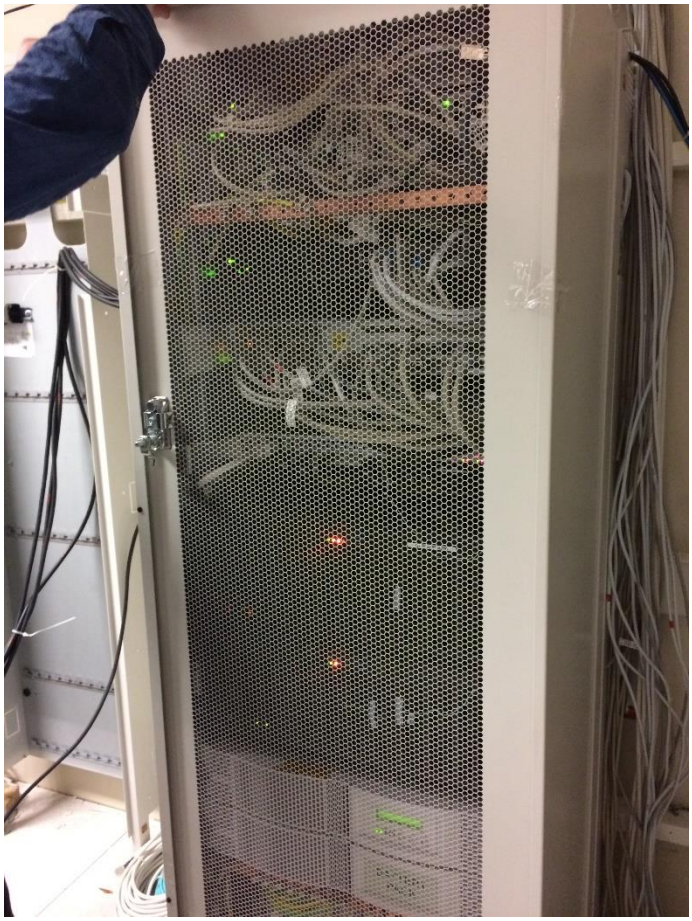

Figure 5.3. Front cover – 2

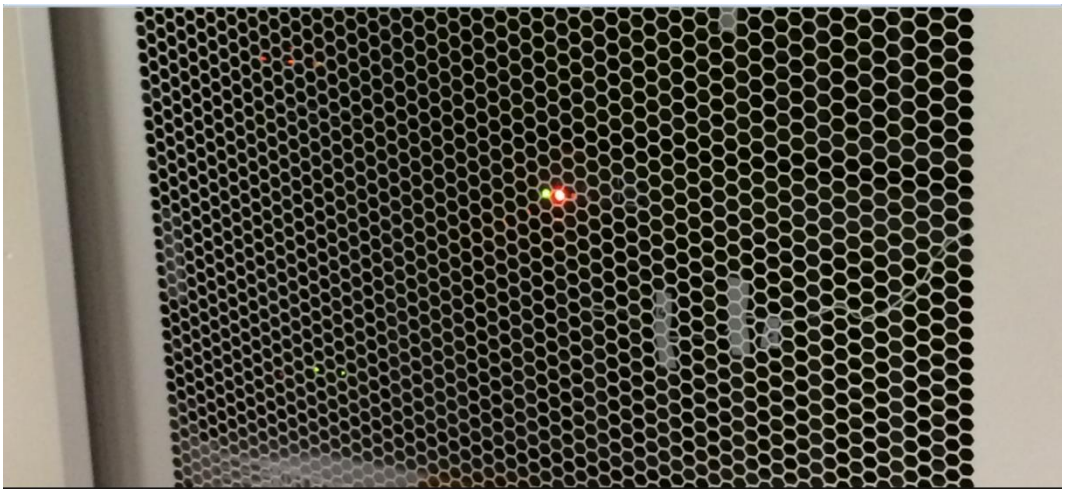

Figure 5.4. Front cover – 2 close-up

This front cover has a simple perforation pattern; therefore, it is suitable to be modeled using a “grille” object (Alkharabsheh et al., 2014). This object creates a pressure loss based on the loss coefficient calculated as Eq – 5.1 for a perforated thin vent;

$$I_c = \frac{1}{A^2}[0.707 * (1 - A)^{0.375} + 1 - A]^2 \quad (5.1)$$

where A is free area ratio. For this particular front cover, free are ratio is 85%.

The validated model is used to build upon, hence, same mesh parameters are used for both models since grille objects are planar and do not intersect with any other objects.

5.2. Results and Discussion

Temperature distribution and airflow inside cabinet are compared for both front covers. Figure 5.5, Figure 5.6 and Figure 5.7 shows the temperature distribution on xy, yz and xz planes, respectively, for 85% open front cover.

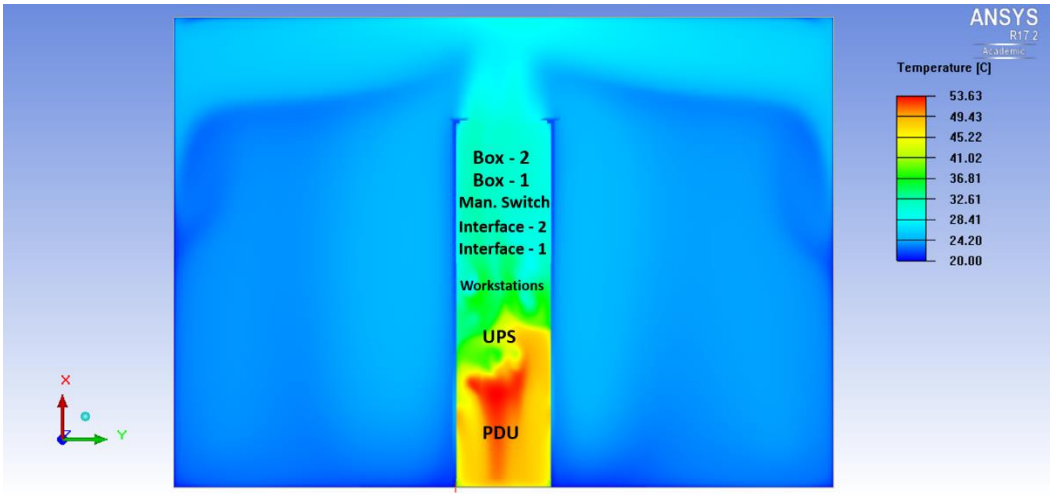

Figure 5.5. Temperature distribution on cabinet back plane for, 85% open cover (z = 0.6m)

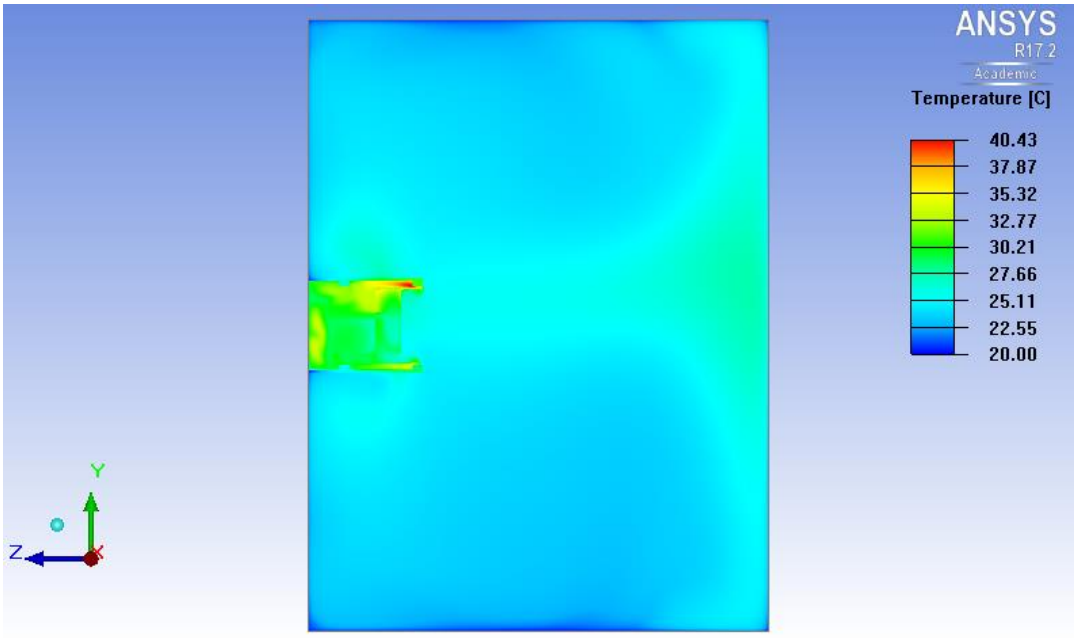

Figure 5.6. Temperature distribution on room center plane, 85% open cover (x = 1.25m)

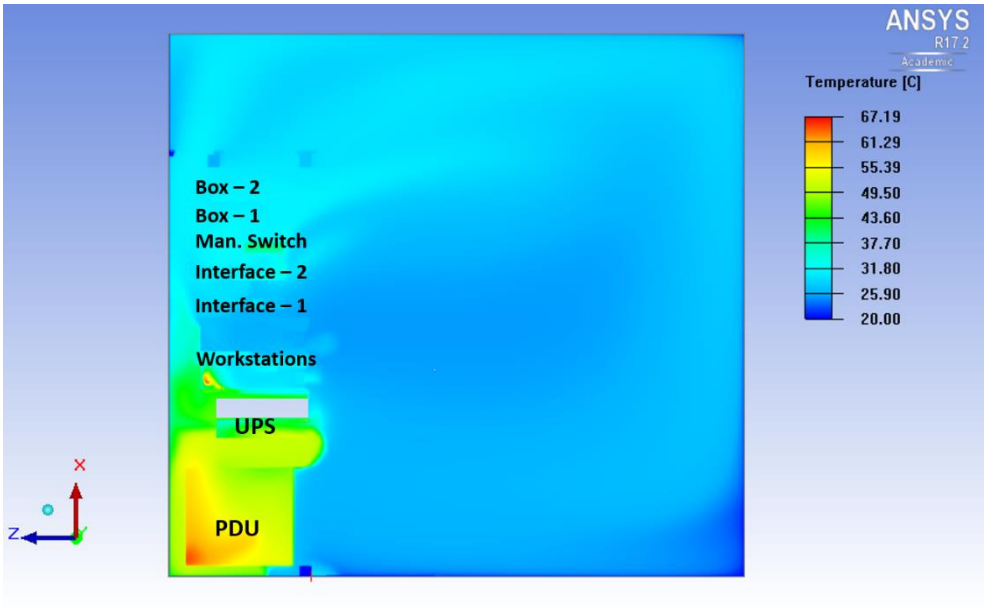

Figure 5.7. Temperature distribution on cabinet center plane, 85% open cover (y = 0.255m)

As can be seen, 85% cover has very similar temperature distribution with the validated model. Same figures are presented for 25% open front cover. Figure 5.8, Figure 5.9 and Figure 5.10, shows the temperature distribution on xy, yz and xz planes, respectively.

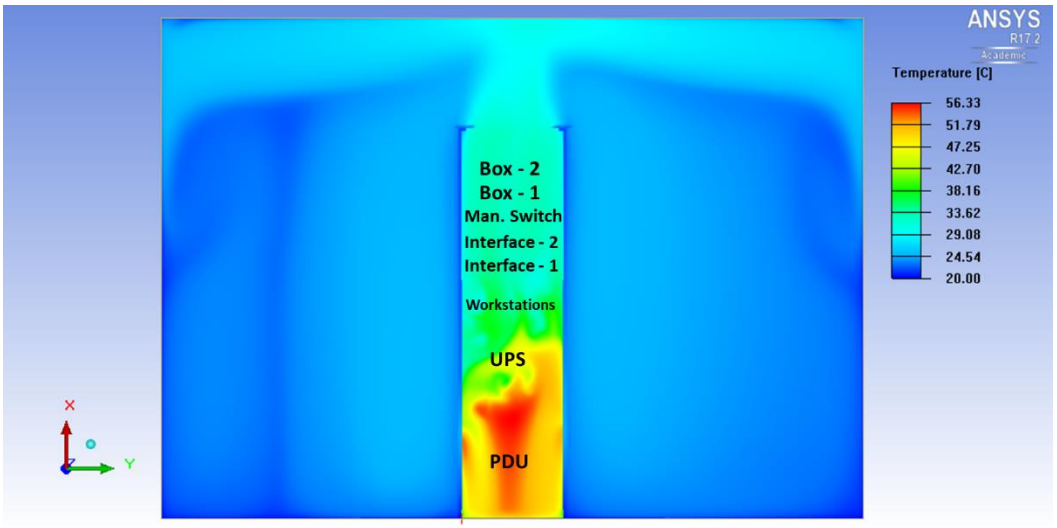

Figure 5.8. Temperature distribution on cabinet back plane, 25% open cover (z = 0.6m)

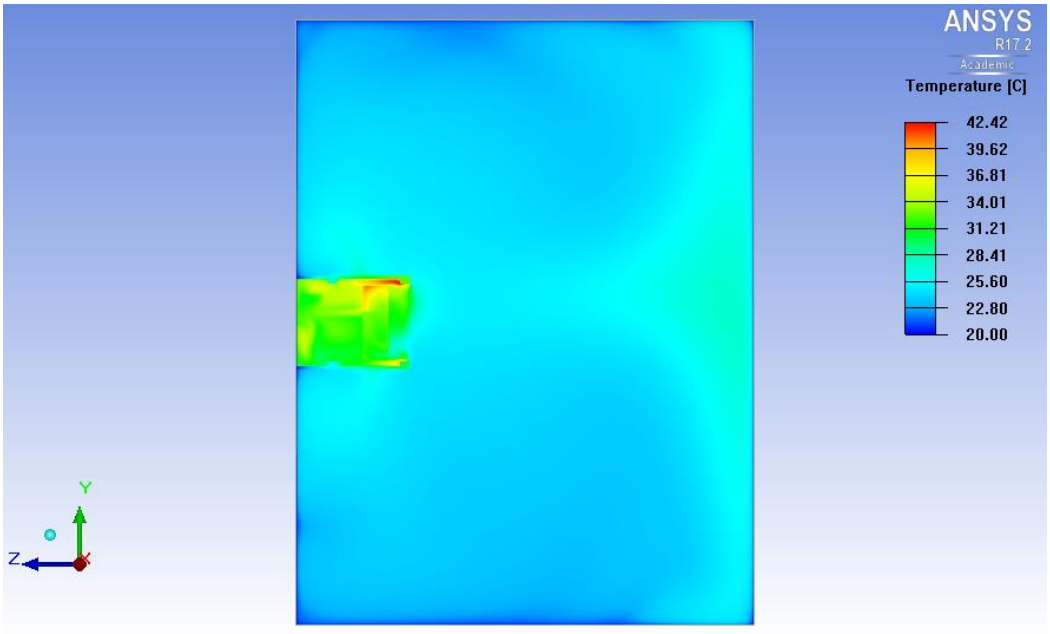

Figure 5.9. Temperature distribution on room center plane, 25% open cover (x = 1.25m)

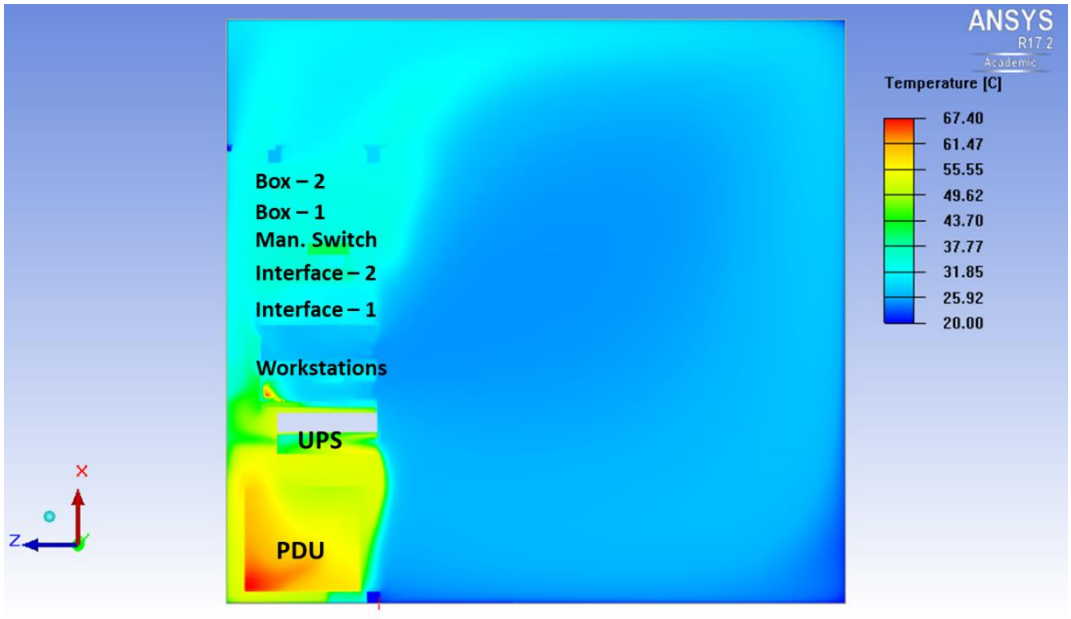

Figure 5.10. Temperature distribution on cabinet center plane, 25% open cover (y = 0.255m)

Figure 5.10 shows that temperature values are higher for 25% open front cover with a similar distribution. However, it should be noted that 25% open front cover prevents some of the leakage on the front plane, except for PDU where it increases the leakage.

A comparison of inlet and outlet temperatures for both cover patterns and validated model without a front cover is made and presented in Figure 5.11.

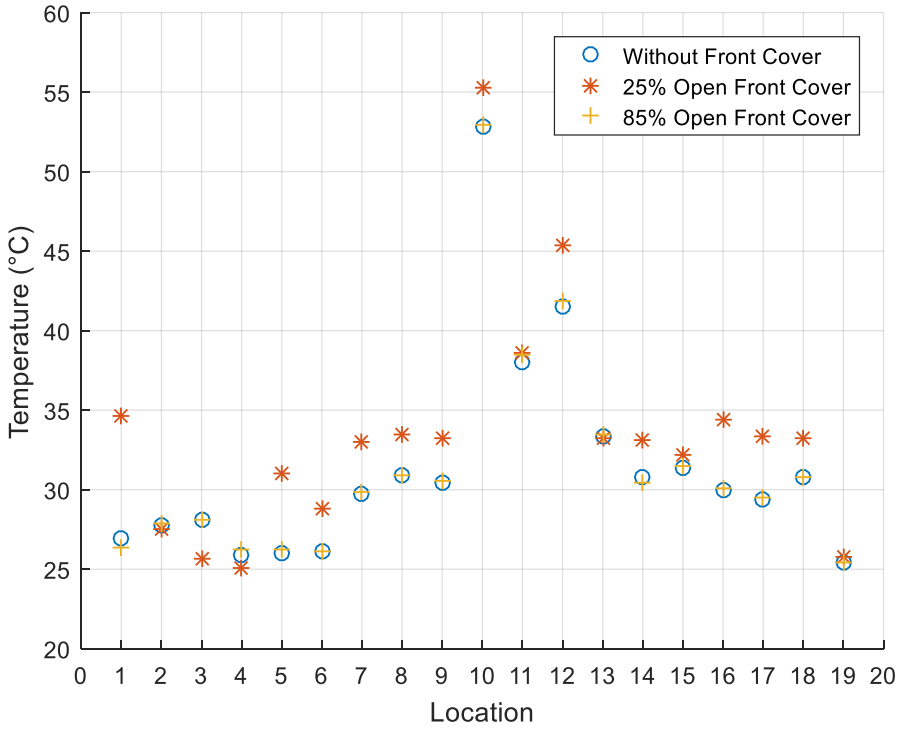

Figure 5.11. Temperature comparison of all models

As can be seen, 25% open front cover leads to higher temperatures on inlet and outlet of the components, except for workstation inlets. This can be explained by the lack of leakage from the workstations to the front plane.

85% open front cover follow very similar temperature values with validated model without a front cover. This means that 85% open front cover is suitable in case of a necessity for a front cover, as it obeys the maximum temperature limits.

Table 5.1 presents total airflow through fans for different front cover patterns.

Table 5.1. Total Airflow Through Fans for Different Patterns

	Without Front Cover	85% Open Front Cover	25% Open Front Cover
Total Airflow Through Fans (m^3/s)	0.417	0.416	0.396

Presence of 25% open cover causes a 5.47% drop in total airflow through fans inside the cabinet, whereas effect of 85% open cover is minimal. This means 25% open cover significantly reduces the ability of the cabinet to cool down, which also explains the high temperatures.

5.3. Variable Free-Area Ratio Front Cover

A new front cover pattern with variable free-area ratio is proposed. This cover is divided into segments with 1U heights, as shown in Figure 5.12, where each segment is assigned an open area ratio depending on the average z-direction velocity on that segment, where velocity values are taken from previous analysis in which no cables were present. Higher z-velocity values are assigned more open area ratios, with maximum being assigned 100% and minimum being assigned 1%, which is the minimum value that can be assigned. The rest of the system, mesh and solver parameters are the same as before.

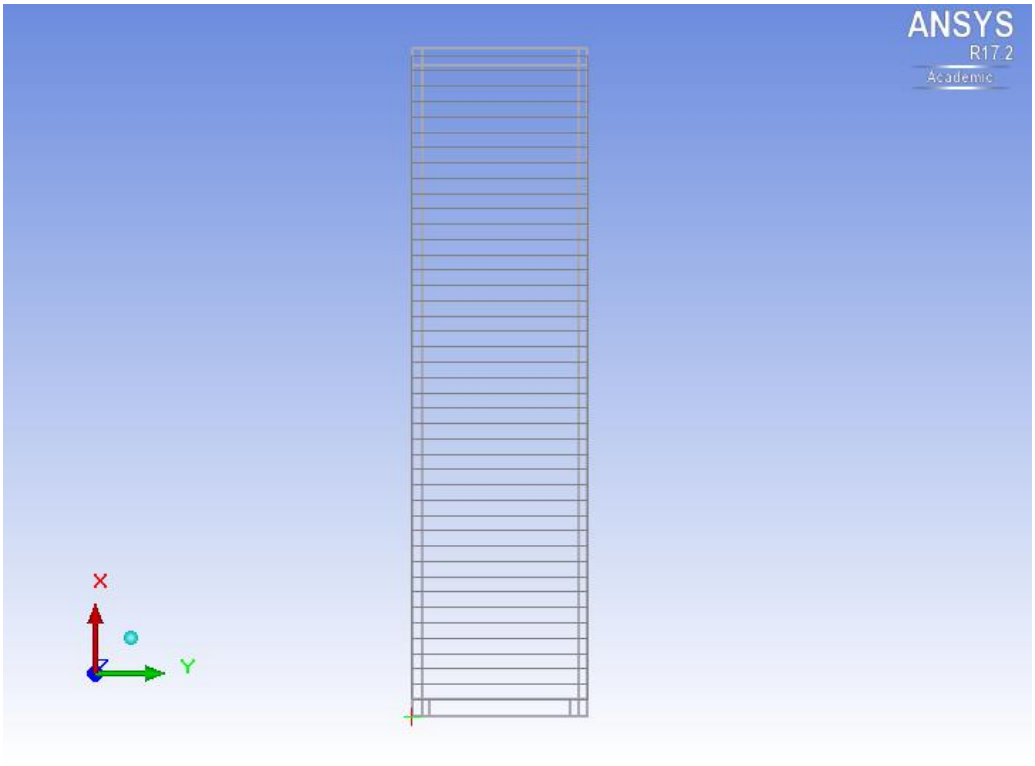

Figure 5.12. Segments with 1U height, front view

Figure 5.13, Figure 5.14 and Figure 5.15 show the temperature distribution on xy, yz and xz planes, respectively.

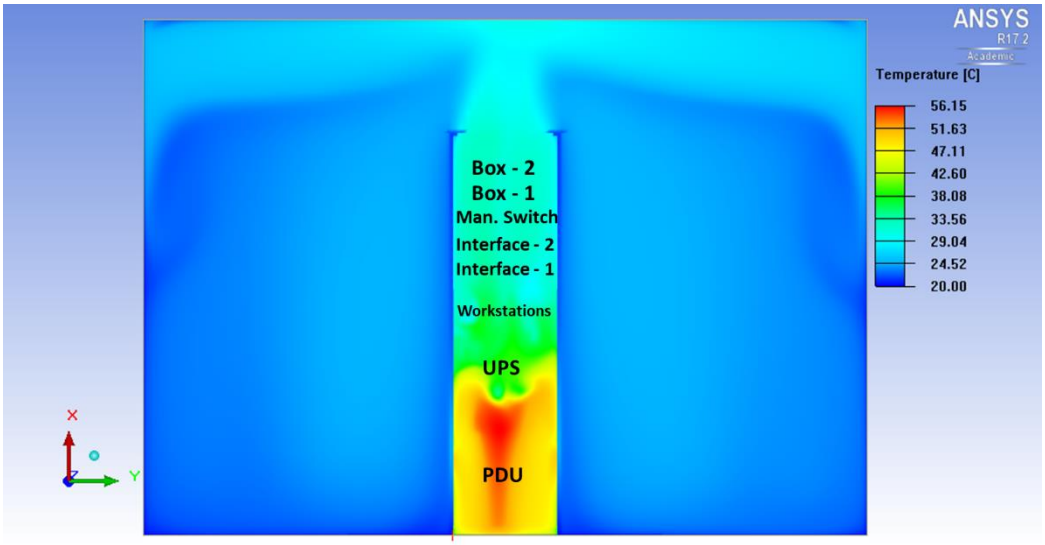

Figure 5.13. Temperature distribution on cabinet back plane, variable cover (z = 0.6m)

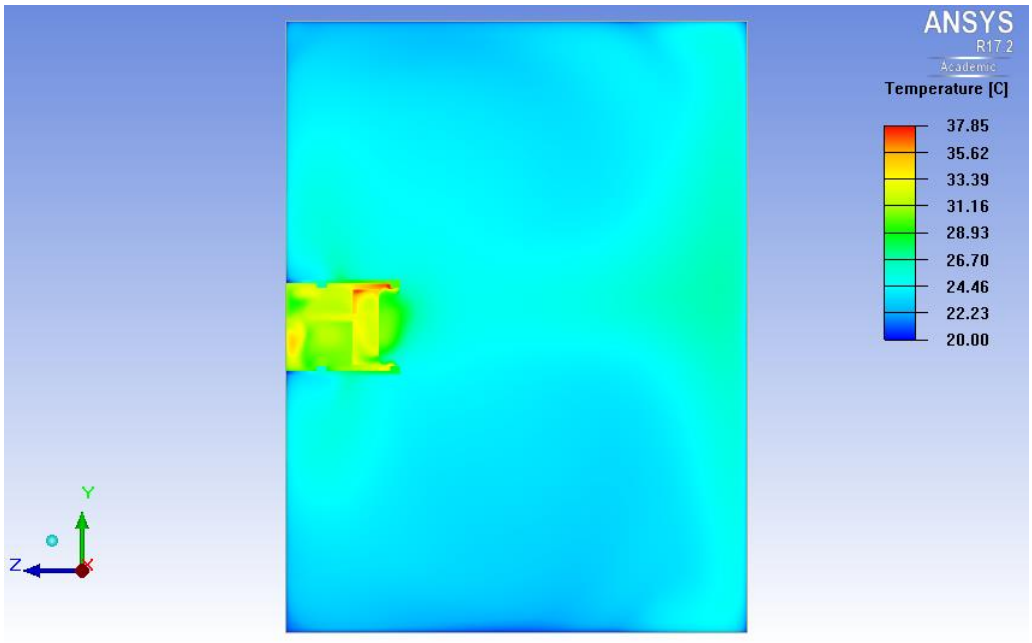

Figure 5.14. Temperature distribution on room center plane, variable cover (x = 1.25m)

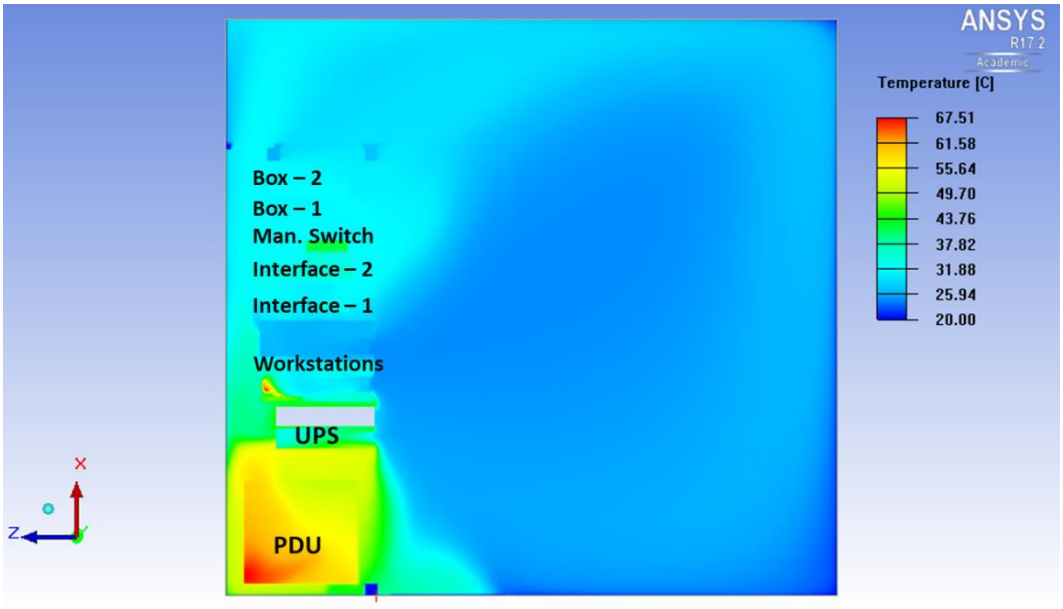

Figure 5.15. Temperature distribution on cabinet center plane, variable cover (y = 0.255m)

Figures show that variable free-area front cover fails to prevent leakages on the front plane of the cabinet and leads to hotspots in front of the PDU. Figure 5.16 presents the temperature values of components together with the model without any cables, also called model with leakage, which better visualizes the leakage through PDU.

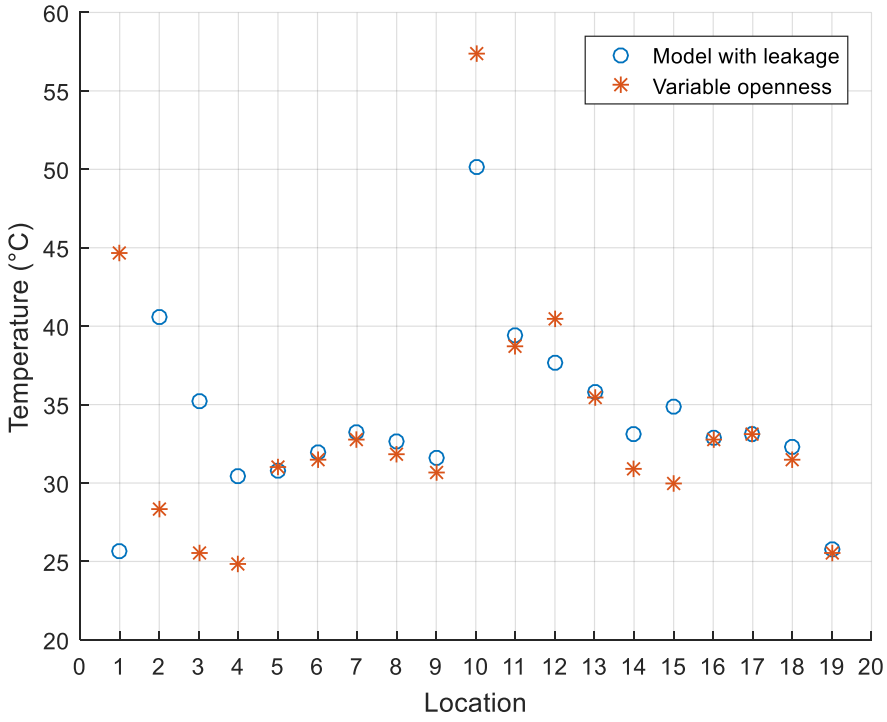

Figure 5.16. Comparison of model with leakage and variable free-area cover

As can be seen, PDU inlet is way over the temperature limit, which is 30 °C, which also causes a higher temperature on the PDU outlet. The rest of the temperatures are either better than the model with leakage, or very close. To better understand the high PDU temperatures, particle traces are presented in Figure 5.17.

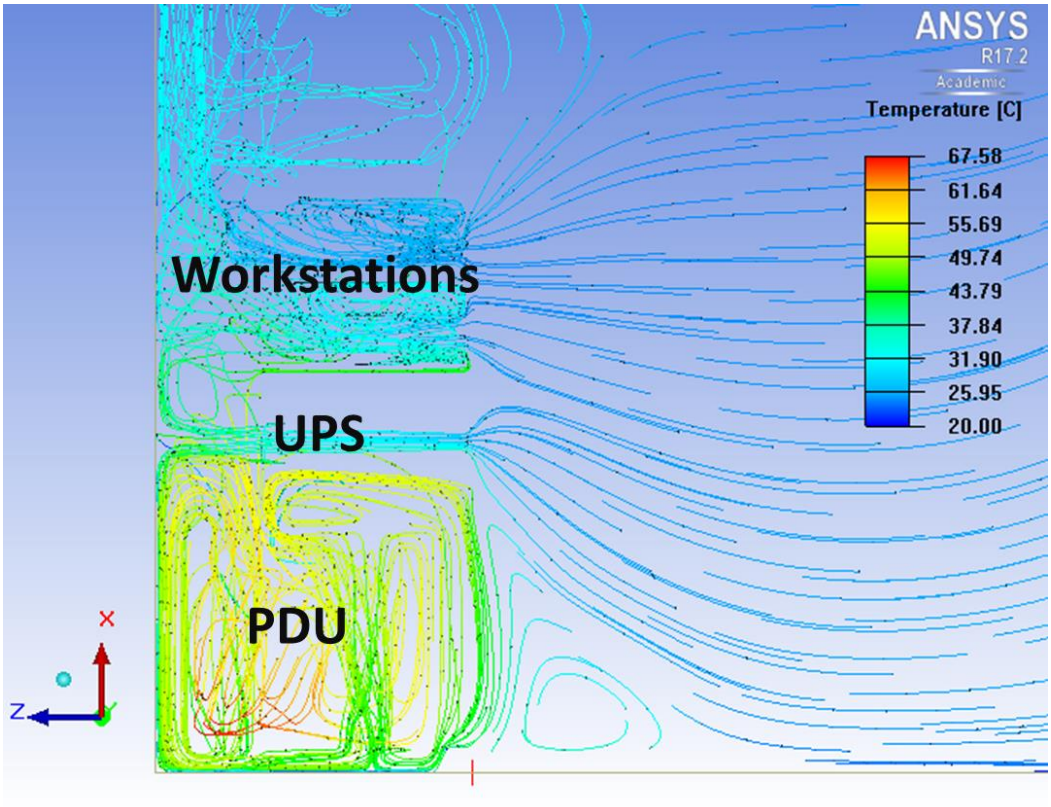

Figure 5.17. Particle traces on lower part of the cabinet center plane (y = 0.255m)

As figure clearly shows, hot air leaving PDU comes back to the front plane through the area in between PDU and UPS, and goes back to the inlet, heating both the inlet and outlet of PDU. This means that a front cover with variable free-area ratio alone cannot be a viable solution for the cabinet with leakage. The hot airflow leaving the PDU must be redirected towards the cabinet outlet either with blanking panels or cables, latter being an imperfect solution. Therefore, another model with same front cover and a blanking panel only on the outlet of the PDU is investigated. Figure 5.18 shows the temperature distribution on xz plane.

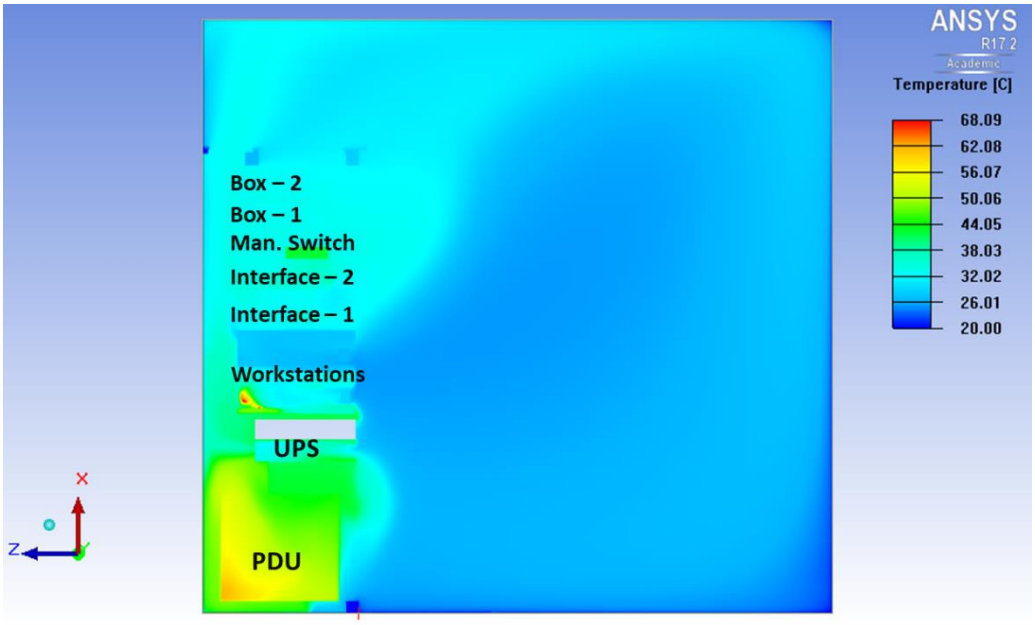

Figure 5.18. Temperature distribution on cabinet center plane for variable free-area front cover and only one blanking panel (y = 0.255m)

As it can be seen, leakage that causes a hotspot on the PDU inlet is greatly reduced as hot air leaving PDU is redirected by the blanking panel. This can be better understood with particle traces shown in Figure 5.19.

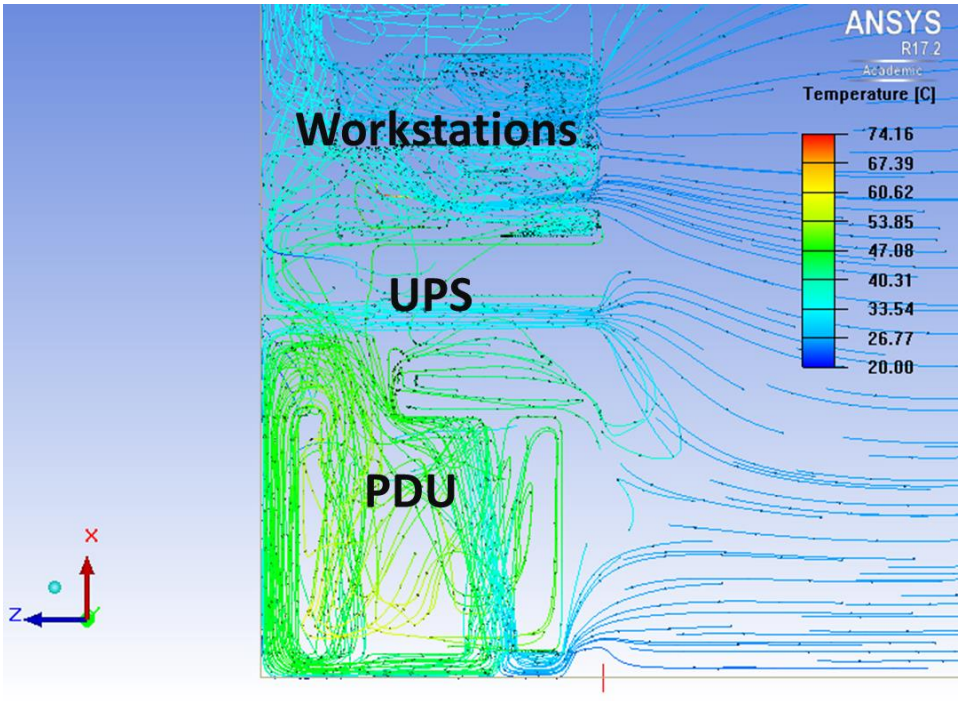

Figure 5.19. Particle traces on cabinet center plane for variable free-area front cover and only one blanking panel (y = 0.255m)

Figure 5.19 clearly shows that the air coming to the PDU inlet is all from the room rather than the PDU outlet. Figure 5.20 shows the comparison of 19 temperature values for both models.

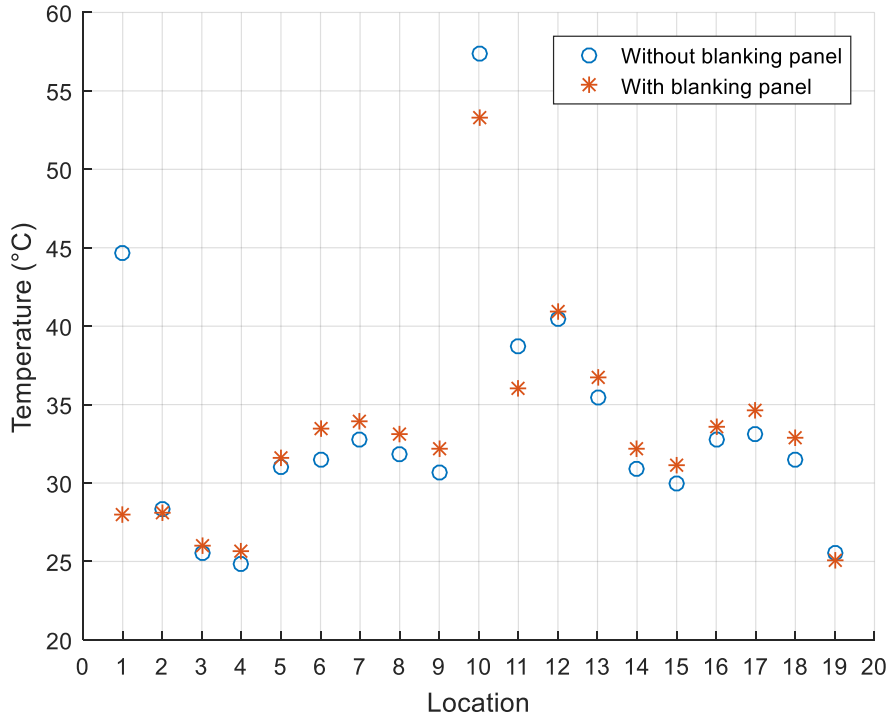

Figure 5.20. Comparison of temperatures for variable free-area front cover model with and without blanking panel

As it can be seen, using a blanking panel on the outlet of the PDU reduced both the inlet and outlet temperatures of PDU. On the rest of the system, model with blanking panel results in close temperature values with model without one, without a significant difference. Therefore, it can be concluded that variable free-area front cover should be used with a solution that redirects the PDU outlet air, such as a blanking panel used here.

Figure 5.21 shows the solutions that obey the temperature limits all together to provide a better perspective.

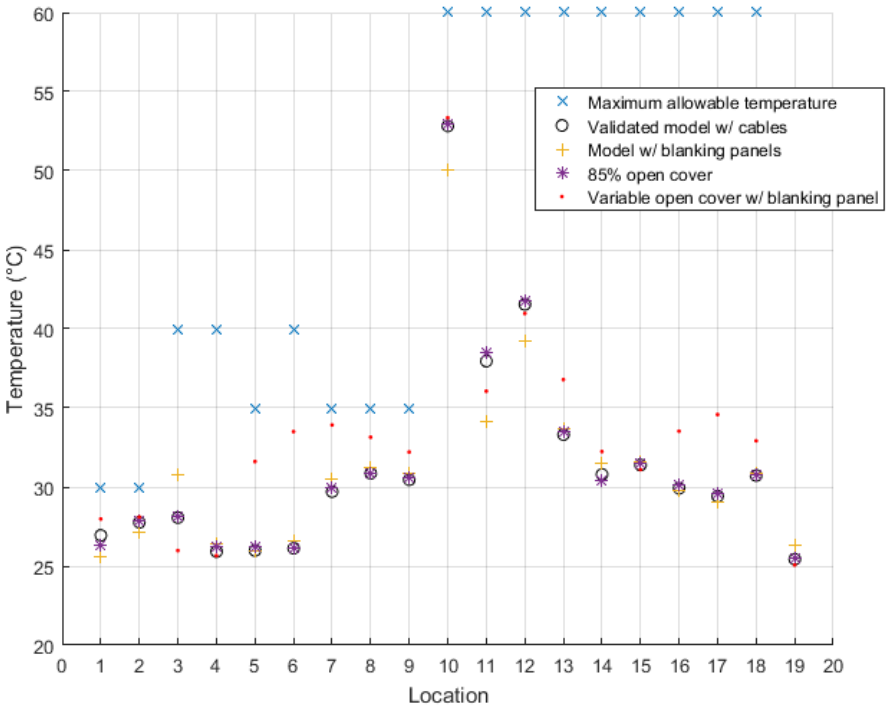

Figure 5.21. Models that obey temperature limits

In this chapter, different front covers with different free-area ratios are computationally modeled and analyzed. Results show that 85% open cover and variable free-area ratio front cover with a blanking panel are viable options.

CHAPTER 6

CONCLUSION AND FUTURE WORK

In this thesis, thermal management of an industry standard cabinet populated with components with difference geometries and heat dissipation values is analyzed. Experimental measurements are done without a front cover to make sure every component obeys its own temperature limit. Measurements show that all components obey their limits; however, in certain applications, a front cover may be necessary; therefore, a CFD model of the cabinet is created to observe different solutions. This CFD model is validated using the 19 experimental temperature data collected and a mesh independent solution is obtained. The effects of natural convection and lumped modeling is observed by changing the solution parameters and geometries. Results show that natural convection effects are insignificant, which is supported by hand calculations, and lumped modelling cannot be used as it misses the temperature variation on the Workstation – 1 outlet.

Then, the effects of cables are investigated by building a model without any cable geometries. The importance of this model is that in a real-life case, cables may be configured in such a way that they are perfectly out of the path of the airflow. Results show that absence of cables leads to leakage through the front plane of the cabinet, which in turn leads to higher temperatures for all components except for PDU. As UPS inlet temperature is above the limit, this model is not a viable option, and solutions must be provided to prevent such temperatures. One solution is using blanking panels, which is an industry-wide application. These panels are placed in between the components to prevent leakages. Results show that usage of blanking panels is a viable option to prevent leakages as all temperatures are below the limits.

Next, effects of different front cover free-area ratios are investigated by placing 25% and 85% open front covers, or grilles, on the front plane of the validated model. The rest of the solution domain and parameters are left the same as the validated model.

Results show that 25% open front cover produces high temperature values on most of the locations, even exceeding the limit on PDU inlet, which prevents it from being a viable front cover. On the other hand, 85% front cover produces similar results to the validated model, which is without a front cover. Therefore, it is below the temperature limits on all locations and can be used as a front cover solution.

A front cover with variable free-area ratio is proposed as a solution to the model with leakages. This front cover is divided into segments of 1U height and free-area ratios are input depending on the mean velocity in z-direction, or normal to the front cover. These velocity values are taken from the model with leakages. Results show that although variable open front cover produces better or close temperature values, on PDU inlet and outlet it creates hotspots that lead to PDU inlet being above the limit. This is due to the recirculation of hot air leaving the PDU, which goes to the PDU inlet rather than cabinet outlet, as it is not redirected by anything such as cables or blanking panels. Therefore, proposed cover with variable free-area ratio is not a viable solution alone. To prevent the hot air recirculation, same cover with only one blanking panel in between PDU and UPS is tested. Results show that usage of this blanking panel leads to a better temperature on the PDU inlet and brings it down below the limit.

In conclusion, for the healthy operation of an electronics cabinet, necessary measurements should be done to make sure components operate below their temperature limits. This study shows that a cabinet without any solution to prevent leakages, such as cables or blanking panels, cannot operate reliably. It is also shown that 25% open cover cannot be used, whereas 85% open cover can be. Lastly, the front cover with variable free-area ratio can be used only together with a blanking panel to redirect the hot air on PDU outlet.

Future work for this study includes testing of multiple cabinets together inside a room and testing of different cooling solutions such as usage of air conditioners.

REFERENCES

Alkharabsheh, S., Sammakia, B., Murray, B., Shrivastava, S., & Schmidt, R. (2014). Experimental characterization of pressure drop in a server rack. In *Thermomechanical Phenomena in Electronic Systems - Proceedings of the Intersociety Conference* (pp. 547–556). Orlando, FL, USA: IEEE. https://doi.org/10.1109/ITHERM.2014.6892329

ANSYS. (2012). *ANSYS Icepak User's Guide* (Vol. 15).

ANSYS. (2016). *ANSYS Fluent Theory Guide*. *Computer Communications* (Vol. 17.0). https://doi.org/10.1016/0140-3664(87)90311-2

Artman, P., Moss, D., & Bennett, G. (2002). *Rack Impacts on Cooling for High Density Servers*. *Dell Enterprise Systems*.

Bergman, T. L., Lavine, A. S., Incropera, F. P., & dewitt. (2011). *Fundamentals of Heat and Mass Transfer*. *Journal of Experimental Psychology: General* (7th ed.). Hoboken, NJ: John Wiley and Sons.

Caceres, C., Ortega, A., Silva-Llanca, L., Jones, G. F., & Sapia, N. (2018). Thermal and Exergy Analysis in UPS and Battery Rooms by Numerical Simulations. In *Proceedings of the 17th InterSociety Conference on Thermal and Thermomechanical Phenomena in Electronic Systems, ITherm 2018* (pp. 521–529). San Diego, CA, USA: IEEE. https://doi.org/10.1109/ITHERM.2018.8419512

Capozzoli, A., & Primiceri, G. (2015). Cooling systems in data centers: state of art and emerging technologies. *Energy Procedia*, *83*, 484–493. https://doi.org/10.1016/j.egypro.2015.12.168

Cengel, Y. A. (2003). *Heat Transfer A Practical Approach* (2nd ed.). Mcgraw-Hill.

Choi, J., Kim, Y., Sivasubramaniam, A., Srebric, J., Wang, Q., & Lee, J. (2007). Modeling and managing thermal profiles of rack-mounted servers with ThermoStat. In *Proceedings - International Symposium on High-Performance Computer Architecture* (pp. 205–215). Pheonix, AZ, USA. https://doi.org/10.1109/HPCA.2007.346198

Dang, C., Jia, L., & Lu, Q. (2017). Investigation on thermal design of a rack with the pulsating heat pipe for cooling CPUs. *Applied Thermal Engineering*, *110*, 390–398. https://doi.org/10.1016/j.applthermaleng.2016.08.187

Gao, C., Yu, Z., & Wu, J. (2015). Investigation of airflow pattern of a typical data center by CFD simulation. *Energy Procedia*, *78*, 2687–2693. https://doi.org/10.1016/j.egypro.2015.11.350

Ghosh, R., Sundaralingam, V., & Joshi, Y. (2012). Effect of rack server population on temperatures in data centers. In *InterSociety Conference on Thermal and Thermomechanical Phenomena in Electronic Systems, ITHERM* (pp. 30–37). San Diego, CA, USA: IEEE. https://doi.org/10.1109/ITHERM.2012.6231410

Hermansen, K. A. (2011). *Validation Of Simplified Rack Boundary Conditions For Numerical Data Center Models*. University of Colorado.

Idel'chik, I. E. (1960). *Handbook of Hydraulic Resistance*. Florida: CRC Press.

Liang, T. S., & Hung, Y. M. (2010). Experimental investigation on the thermal

performance and optimization of heat sink with U-shape heat pipes. *Energy Conversion and Management*, *51*(11), 2109–2116. https://doi.org/10.1016/j.enconman.2010.03.003

Nelson, G. (2007). *Development of an experimentally-validated compact model of a server rack: Master Thesis*. Georgia Institute of Technology.

Pandiyan, V. (2012). *Development of Detailed Computational Flow Model of High End Server and Validation Using Experimental Methods*. The University of Texas at Arlington.

Radmehr, A., Karki, K. C., & Patankar, S. V. (2007). Analysis of Airflow Distribution Across a Front-to-Rear Server Rack. In *Proceedings of the ASME InterPACK '07 Conference*. Vancouver, BC, Canada. https://doi.org/10.1115/IPACK2007-33574

Rambo, J., & Joshi, Y. (2005). Thermal Performance Metrics for Arranging Forced Air Cooled Servers in a Data Processing Cabinet. *Journal of Electronic Packaging*, *127*(4), 452–459. https://doi.org/10.1115/1.2056575

Rasmussen, N. (2009). Improving Rack Cooling Performance Using Airflow Management ™ Blanking Panels. *APC White Paper*.

Strong, L., Karki, K. C., & Merchant, B. T. (2009). *Two-Dimensional Computational Fluid Dynamics Analysis of Blanking Panel Solutions* (Vol. 57).

Tan, S., Toh, K., & Wong, Y. (2007). Server-Rack Air Flow And Heat Transfer Interactions In Data Centers. In *Proceedings of the ASME InterPACK '07 Conference* (pp. 1–5). Vancouver, BC, Canada. https://doi.org/10.1115/IPACK2007-33672

Zhang, X., VanGilder, J. W., Iyengar, M., & Schmidt, R. R. (2008). Effect of rack modeling detail on the numerical results of a data center test cell. In *11th Intersociety Conference on Thermal and Thermomechanical Phenomena in Electronic Systems* (pp. 1183–1190). Orlando, FL, USA. https://doi.org/10.1109/ITHERM.2008.4544395

APPENDICES

A. Details of CPU Package and GPU

Figure 0.1 and Figure 0.2 present the detailed models of CPU and GPU, respectively.

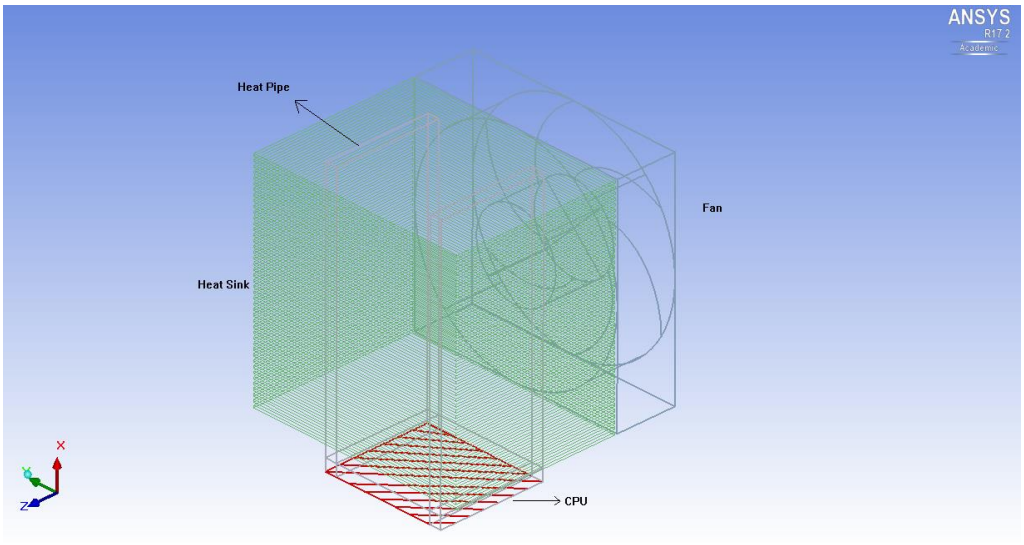

Figure 0.1. Details of CPU package

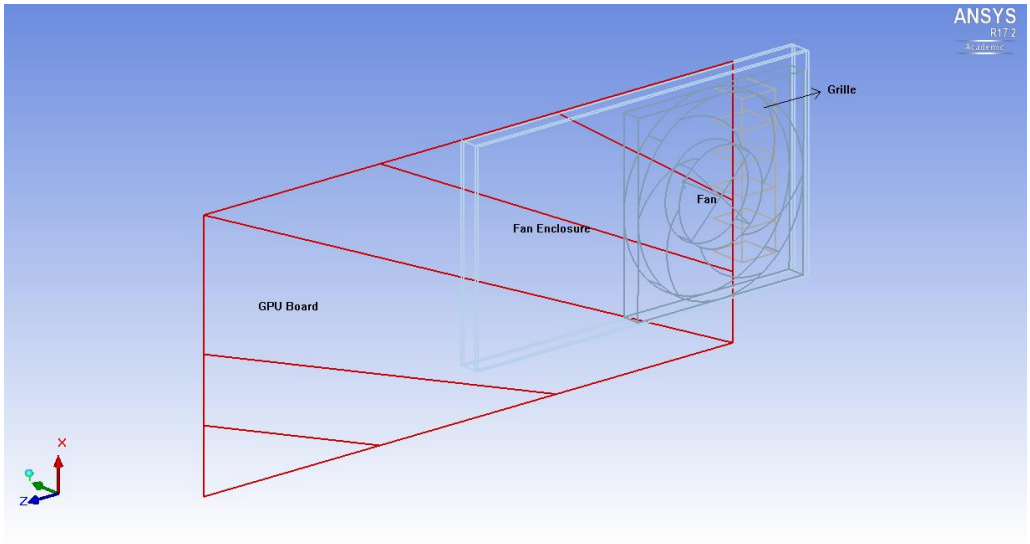

Figure 0.2. Details of GPU

B. Workstation Mesh Independence

Three different mesh configurations with different number of elements are compared to establish a mesh independent solution.

Figure 0.3 shows the reference line that lies on the motherboard and passes through the CPU-2. This line is chosen as temperatures vary significantly along CPUs. Three different mesh configurations with different number of meshes, namely 2465480, 2911094 and 3304824 are chosen. All the other parameters are the same for all configurations.

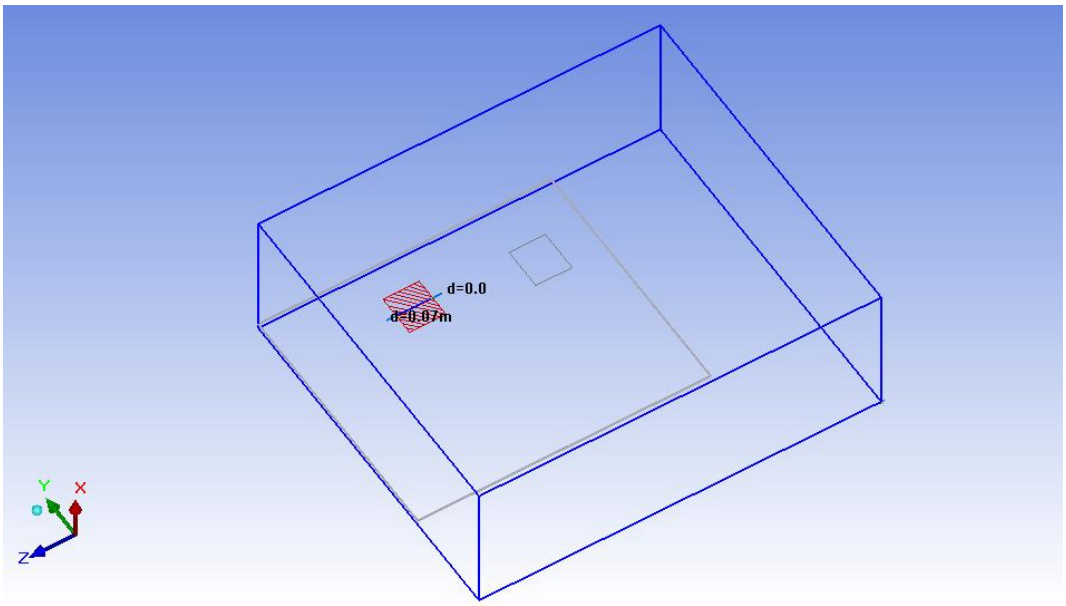

Figure 0.3. Reference Line Chosen for Mesh Independence Analysis

Figure 0.4 shows the temperature distribution along the reference line for different mesh configurations.

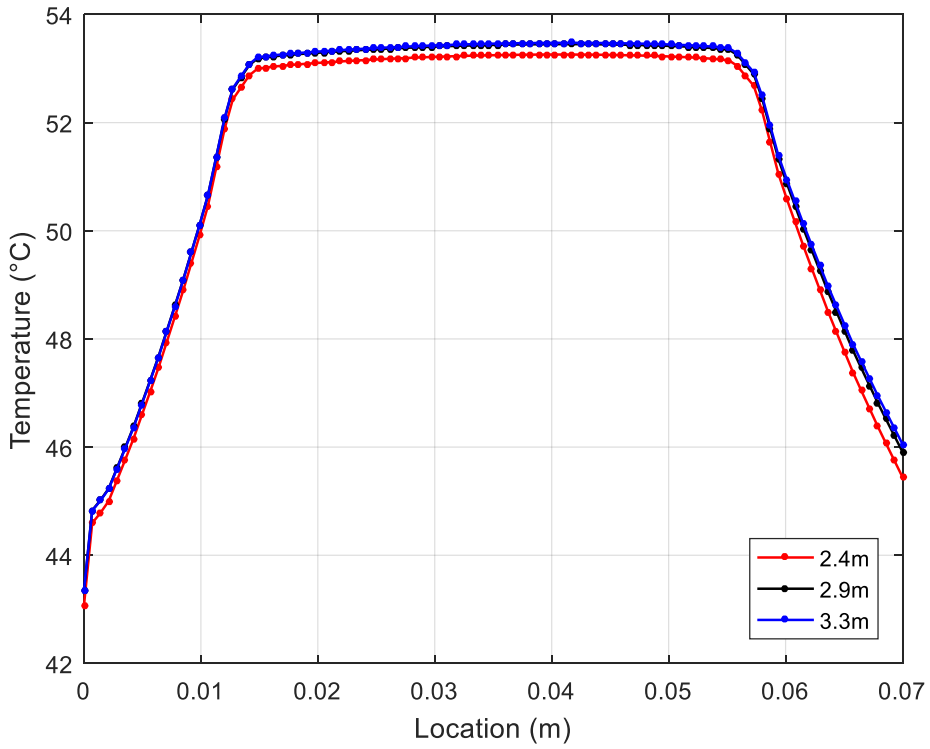

Figure 0.4. Temperature distribution for different meshes

As it can be seen, largest difference occurs at the extremes of the reference line, where 2.4m mesh separates from other two. 2.9m and 3.3m meshes are almost exactly the same, even at the extremes.

However, another comparison is made on different locations inside the Workstation – 1 to see the effect of coarser mesh. For this analysis, temperatures of 7 locations are compared; CPU-1, CPU-2, GPU-1, GPU-2, PCIe-1, outlet temperatures on fan outlet and grille outlet, as shown in Figure 0.5.

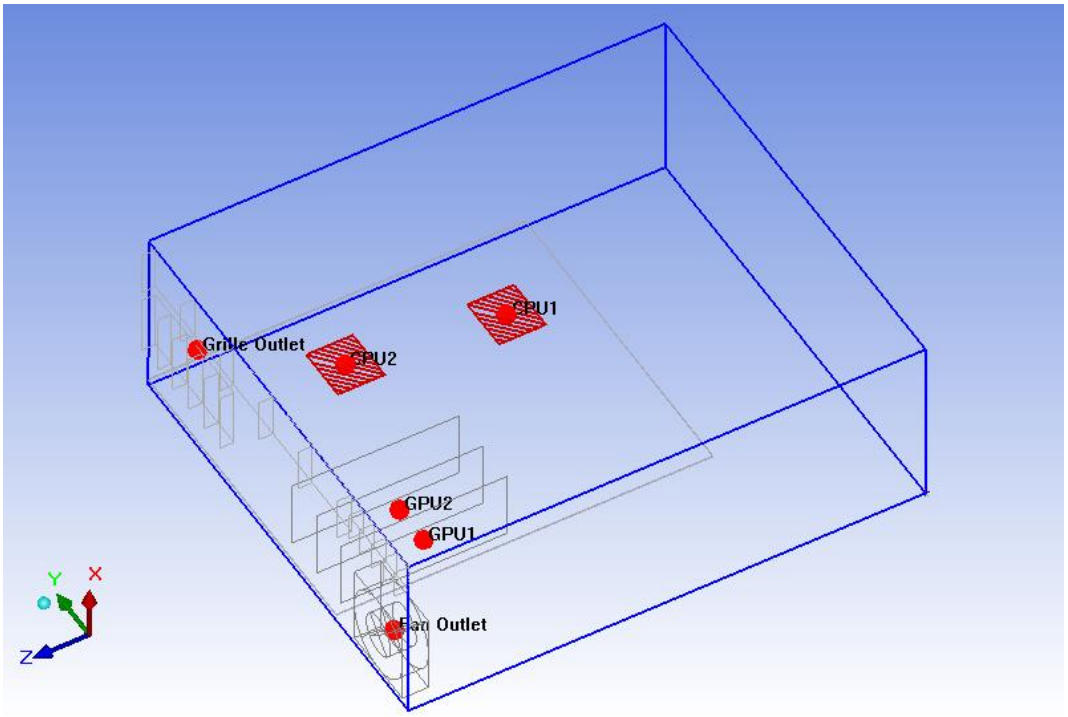

Figure 0.5. Temperature measurement locations

Table 0.1 shows the temperatures for both mesh configurations. Note that all surfaces of an object are combined together for a single average temperature value except for Fan Outlet and Grille Outlet, where a single point is used instead of a surface average.

Table 0.1. *Temperatures for different locations*

Location	2.4m (℃)	2.9m (℃)	3.1m (℃)
CPU-1	46.8	46.8	46.8
CPU-2	51.6	51.8	51.8
GPU-1	54.6	54.7	54.6
GPU-2	50.7	51.3	51.5
PCIe-1	37.0	38.2	37.7
Fan Outlet	30.1	30.2	30.3
Grille Outlet	32.4	32.3	32.4

To be able to compare the temperature difference between the two solutions, a dimensionless temperature variable θ_t is defined as;

$$\theta_t = \left(\frac{T - T_{min}}{T_{max} - T_{min}}\right) \tag{0.1}$$

where T is the measured temperature value, T_{min} is defined as inlet temperature 25 ℃, T_{max} is defined as maximum operating temperature of CPUs, that is 87 ℃. Every measurement is made dimensionless via Eq – 0.1 and percent difference between them is calculated thereafter. Table 0.2 shows the dimensionless temperature values.

Table 0.2. *Dimensionless temperatures for different locations*

Location	2.4m	2.9m	3.1m
CPU-1	0.35	0.35	0.35
CPU-2	0.43	0.43	0.43
GPU-1	0.48	0.48	0.48
GPU-2	0.41	0.42	0.43
PCIe	0.19	0.21	0.21
Fan Outlet	0.08	0.08	0.08
Grille Outlet	0.12	0.12	0.12

When two mesh configurations of 2.4m and 2.9m are compared, it can be seen that largest difference occurs at PCIe at 8.7%. However, outlet temperatures are nearly the same with 1% difference. Therefore, 2.4m mesh is deemed sufficient for this model.